CIVIL ENGINEERING STUDIES

ELASTO-PLASTIC ANALYSIS OF THREE-DIMENSIONAL STRUCTURES USING THE ISOPARAMETRIC ELEMENT

by

AJAYA K. GUPTA
BIJAN MOHRAZ
WILLIAM C. SCHNOBRICH

UNIVERSITY OF ILLINOIS
URBANA, ILLINOIS
AUGUST, 1971

ELASTO-PLASTIC ANALYSIS OF THREE-DIMENSIONAL STRUCTURES USING THE ISOPARAMETRIC ELEMENT

by

AJAYA K. GUPTA

BIJAN MOHRAZ

WILLIAM C. SCHNOBRICH

UNIVERSITY OF ILLINOIS
URBANA, ILLINOIS

August, 1971

ERRATA

The following are corrections to be incorporated into this report:

Page	Location	Error	Correction
35	line 7	Eq. 2.1	Eq. 3.1
54	last line	vessle	vessel
55	line 14	Fig. 9b	Fig. 10
61	line 11	angel	angle
83	Fig. 5(b)	$u_3^t = -u_3^b$	$u_3^t = u_3^b$
89	Fig 12(b) upper right corner	x_2	x_1
107	vertical axis		q/q_y
121	line 1	Appendix B	APPENDIX B
126	line 1	Appendix C	APPENDIX C

ACKNOWLEDGMENTS

TABLE OF CONTENTS

LIST OF TABLES

LIST OF FIGURES

Chapter 1

INTRODUCTION

1.1 General

In addition to the elastic response of a structure to service
load conditions, the behavior of the structure when stressed beyond its
elastic range and the determination of its ultimate load capacity are
important aspects which must be studied for an efficient and economical
design of the structure. For instance, in case of the nozzle opening in
a shell, a highly localized stress concentration exists in the vicinity
of the junction. Obviously, the zone of stress concentration is first
to reach yielding. If the load on the structure is increased, an inelastic
behavior results near the junction. For a more efficient and economical
design of such a structure, a small inelastic zone can frequently be
tolerated without endangering the safety and performance of the structure.

The concept of inelastic analysis has been applied successfully
in the limit analysis of framed structures. Various methods have been
used for the nonlinear analysis of problems in continuum mechanics. Hodge
and White[1] analyzed the thick circular cylinder under uniform internal
pressure using the finite difference equivalent of the governing equations.
They assumed that the material of the structure followed the von Mises
yield criterion. Koiter[2] solved the same problem in closed form using
Tresca's yield criterion. Method of successive approximation has been used
in conjunction with the finite-difference and the integral equation tech-
niques by several investigators for solving the temperature gradient pro-
blems of the flat plate, thin circular shell, long solid cylinder and the

1

the rotating disk.[3,4,5] Similar methods have been applied by Davis[6] and Tulsa[7] in the analysis of uniformly stressed infinite plate with circular hole.

A general method of elasto-plastic analysis of plane strain problems was suggested by Argyris, Kelsey and Kamel,[8] using the finite element method. Later, Argyris[9] indicated that a similar technique could be employed for three-dimensional problems using tetrahedron elements. Swedlow, Williams and Yang[10] used the finite element method to obtain solutions for elasto-plastic plates. Marcal and Pilgrim[11] analyzed the elastic-plastic shells of revolution using a stiffness approach. Ueda and Matsuishi[12] solved the elasto-plastic buckling of plates by the finite element method. Popov, Khojasteh-Bakht and Yaghmai[13] studied the bending of circular plates with elastic-perfectly plastic material, and extended the method to strain-hardening material.[14] Khojasteh-Bakht[15] has also analyzed the elasto-plastic shells of revolution under axisymmetric loading. The tension cutoff phenomenon or rocks has been considered by Zienkiewicz, Valliappan and King[16] using the finite element method. A quadratic programming approach for solving nonlinear structural problems has been proposed by Maier,[17] and later extended to allow for large displacements.[18]

The lumped parameter method has also been employed for the solution of the inelastic problems. Lopez and Ang[19] used the method for the analysis of elasto-plastic plates. Shoeb and Schnobrich[20] used a similar approach for analyzing elasto-plastic shell structures. Galloway and Ang[21] solved plane problems by using a generalized lumped paremeter model. Mohraz, Schnobrich and Echeverria Gomez[22] applied the lumped parameter approach to study crack development in a prestressed concrete reactor vessel.

Although much has been done in the inelastic analysis of struc-
tures, almost every investigator has avoided its application to real three-
dimensional problems. In many engineering problems, a state of plane stress
or strain can be assumed to exist and the problem can be solved as though
it were two-dimensional. Using suitable assumptions, plates and shells
are analyzed as two-dimensional problems. Axisymmetric solids represent
another class of problems which has been treated successfully as two-
dimensional.

The two-dimensional idealization makes the problem simpler and
much more economical to solve. Nevertheless, there are engineering pro-
blems which cannot be idealized as two-dimensional without distorting the
behavior of the structure. For instance, gravity dams have been frequently
analyzed as plane strain problem. Although such an analysis gives an ac-
curate estimate of displacements and stresses in the interior portions of
the dam, it cannot predict the behavior of the structure near the abutments.
Prestressed concrete reactor vessels have been analyzed as axisymmetric
structures. However, for access to the enclosed space of the vessel, open-
ings are provided in various locations. A three-dimensional analysis is
needed for obtaining solutions to such structures. Underground tunnels
have been successfully analyzed as plane strain problems, although their
behavior near the ends remains largely unexplained by such an analysis. In
these cases as in many others, it is necessary that one consider the true
three-dimensional aspects of the problem, in order to have a better insight
into the behavior of the structure.

Due to lack of suitable closed form solution for three-dimensional
problems, one is forced to employ a numerical approach. Among the various
numerical methods which can be used for three-dimensional problems, the

more common are the finite difference method; its counterpart, the lumped
parameter or analog model; and the finite element method. Both the finite
difference and the lumped parameter methods become too cumbersome for three-
dimensional problems, especially for irregular shaped boundaries. In addi-
tion, a variable grid which is necessary for obtaining accurate solutions
in regions of high stress concentration, presents considerable difficulty
both in the formulation and programming of the methods.

The finite element method which has been applied extensively to
problems of stress analysis during the past decade is well suited for model-
ing irregular shaped boundaries. The formulation and programming of the
method should not present any difficulty for the three-dimensional analysis.

1.2 Object and Scope

The objective of the present study is to develop an analytical
procedure for the analysis of three-dimensional structures with elasto-
plastic material behavior.

The finite element method, in conjunction with the three-dimensional
isoparametric element, is used in the study. In the range of plastic be-
havior, an initial stress approach is used for the analysis. The initial
stress field within the element is defined by a stress interpolation approach.

Although the method of analysis is general, for the purpose of il-
lustration, elastic isotropic material properties are used in the example
problems. In the plastic range, linear strain-hardening is assumed. The
von Mises yield criterion with the assumption that the material strain
hardens isotropically is applied. The assumption of isotropic strain harden-
ing is applicable only when the loading is monotonic.

The applicability of the proposed procedure is illustrated by presenting numerical examples and comparing them with existing solutions wherever possible.

1.3 Notations

All the symbols have been defined where they appear first in the text. The following summarizes the main symbols used. Two prefixes have been employed to denote increments, viz., d and Δ. Whereas d represents an infinitesimal increment, Δ is used to denote finite increments.

a_i	a vector of arbitrary constants in the constant strain displacement field, Eq. 2.3
a_i^m	value of a_i at the element node m
A	area of a given surface
b_{ij}	an array of coefficients of global coordinates in the constant strain displacement field, Eq. 2.3
c^r	a column array of polynomial functions of isoparametric coordinates used in Eq. 2.10
c^{mr}	value of c^r at the element node m
D	a specified domain, such as a given volume, area or length
D^{rm}	inverse of the array c^{mr}
E	modulus of elasticity
$E_{ijk\ell}$	material property tensor

$f(\xi)$, $f(\xi_1,\xi_2)$ $f(\xi_1,\xi_2,\xi_3)$	functions of isoparametric coordinates in one, two and three dimensions, respectively; used as integrands for numerical integration, Eq. 2.50-2.52
f^i, f^{ij}, f^{ijk}	values of $f(\xi)$, $f(\xi_1,\xi_2)$ and $f(\xi_1,\xi_2,\xi_3)$ at the Gaussian quadrature points (n^i), (n^i,n^j) and (n^i,n^j,n^k), respectively
F	nodal load vector for the structure
$\overline{F}$	nodal load vector for the unconstrained structure
$\Delta F''$	incremental initial load vector
$\Delta^i F''$	incremental initial load vector for the ith iteration
g^S	a column array of exponential functions of the isoparametric coordinates used in Eq. 2.25
G^{mS}	value of g^S at the node m
H^{Sm}	inverse of the array G^{mS}
k_r	stiffness matrix of the element r
k_{ij}^{mn}	element stiffness matrix in index notation (see foot note on p. 25)
K	structural stiffness matrix
$\overline{K}$	the stiffness matrix for the unconstrained structure
N^m	shape function at the element node m

P_i^m — generalized load at the element node m in direction i

$\Delta P_i^{m\,\prime\prime}$ — incremental initial load at the element node m in direction i

q_i — applied distributed load in direction i

Q_i^A — concentrated load applied at a point A in direction i

s — scale factor applied to a given loading system to initiate yielding in the structure

S_{ij} — deviatoric stress tensor

T — geometric transformation matrix relating the displacement vectors of the unconstrained and the constrained structures, respectively, Eq. 2.58

u_i — displacement at any point within an element in direction i

u_i^m — displacement at the element node m in direction i

u_i^t, u_i^b — displacements at the top and bottom faces in a plate, respectively

U — structural displacement vector

$\bar{U}$ — displacement vector for the unconstrained structure

ΔU — incremental displacement vector for the structure

$\Delta^\circ U$ — approximate value of the incremental displacement vector given by Eq. 3.47

$\Delta^i U$	i^{th} correction in the incremental displacement vector
V	volume of a given solid domain
W_{ext}, W_{int}	work done by external and internal forces, respectively
W^P	work done through a plastic deformation
x_i	global cartesian coordinates
x_i^m	global cartesian coordinates at the element node m
z	strain-hardening coefficient
Z_{ijk}^m	geometric array relating the strain tensor ε_{ij} and the nodal displacements u_k^m, Eq. 2.34
α^r	a column array of coefficients of the poly-nomial functions used in Eq. 2.10
β	a constant coefficient used in Eq. 2.17
γ^s	a column array of coefficients of the exponential functions used in Eq. 2.25
Γ	an expression defined by Eq. 3.9
δ	a prefix denoting first variation of a function
δ_{ij}	Kronecker delta
ε_{ij}	total strain tensor

ϵ'_{ij} elastic strain tensor

ϵ''_{ij} plastic strain tensor

ϵ total uniaxial strain

ϵ_e elastic uniaxial strain

ϵ_p plastic uniaxial strain

n^i position constant for the Gaussian quadrature point i

κ yield function

$d\lambda$ an incremental constant of proportionality, used in Eq. 3.2

Λ Lamé's constant

μ modulus of rigidity

ξ_i isoparametric coordinates at any point within an element

ξ_i^m isoparametric coordinates at the element node m

ρ^i weight coefficient for the Gaussian quadrature point i

σ_{ij} stress tensor

$d\sigma_{ij}, \Delta\sigma_{ij}$ incremental stress tensor

$d\sigma'_{ij}, \Delta\sigma'_{ij}$ incremental elastic stress tensor

$d\sigma_{ij}^{''}, \Delta\sigma_{ij}^{''}$ incremental initial stress tensor

$d\bar{\sigma}_{ij}^{''}, \Delta\bar{\sigma}_{ij}^{''}$ incremental pseudo initial stress tensor

$d\bar{\sigma}_{ij}^{m''}, \Delta\bar{\sigma}_{ij}^{m''}$ incremental pseudo initial stress tensor at the element node m

σ_e effective stress

σ_e^m effective stress at the element node m

σ_c loading stress as defined by Eq. 3.34

σ_c^+ loading stress at the end of a loading increment

σ_c^m loading stress at the element node m

σ_y uniaxial yield stress

ϕ a function representing a component of coordinates, displacements, stresses, etc.

ϕ^m value of ϕ at node m

ϕ^{AB} value of ϕ along the edge AB

$\Delta^{AB}\phi$ departure of ϕ^{AB} from the linear response defined by ϕ^A and ϕ^B

Ψ loading function

Ω an expression defined by Eq. 3.11

Chapter 2

FINITE ELEMENT METHOD FOR THREE-DIMENSIONAL PROBLEMS

2.1 General

The finite element method is an approximate method of analysis in which the structure is idealized by subdividing it into a number of subregions referred to as elements. On the basis of an assumed displacement field defined in terms of displacements at selected nodal points, the stiffness properties of individual elements are evaluated and assembled to give the total stiffness of the structure expressible in terms of those nodal displacements. This results in a set of simultaneous equations which, upon solution, give the desired displacements and stresses throughout the structure. The accuracy of the solution depends upon the adequacy of the structural idealization, if any is involved, and the generality of the assumed displacement field for the element.

It is desirable that the element properties be such that they do not violate the compatibility between adjacent elements, although noncompatible elements have been used successfully for solutions to bending problems.[23] Recently some study has been given to relaxing the compatability criterion even in direct stress problems in order to retain simple elements for three-dimensional problems. These studies are still indecisive.

In the idealization of a continuum by finite elements, the element sizes should be small in regions of high stress gradients in order to minimize the violation of local equilibrium. In general, the accuracy of the solution will improve with an increase in the number of elements. Another and frequently better way for improving the accuracy of the solution is to increase the number of degrees of freedom per element. This

improvement can be achieved by either of two ways. One approach is to define more variables such as the first and the higher derivatives of the displacement at each node (higher nodal valency). A second approach is to define additional intermediate, edge and/or internal, nodes in the element. The latter approach, although it possesses a lower nodal valency, allows a more systematic and gradual increase in the order of the assumed displacement field than does the use of corner derivatives. There is a limit in the extent one can go in either approach however, because of the computational complexity involved in using such higher order elements. Argyris' Lumina[24] and Hermes[25] elements are examples of the higher order elements obtained by including intermediate nodes and defining derivatives of the displacements at the corner nodes, respectively. The displacement fields in the two elements are defined by using Lagrangian and Hermitian interpolation functions respectively. The use of Lagrangian rather than Hermitian interpolation function allows more flexibility of choice.

The first suggestion for the use of the finite element analysis of three-dimensional solids was made by Martin[26] and independently by Gallagher, et al.,[27] both of whom proposed a four-node tetrahedron element which is, in fact, a three-dimensional counterpart of the original constant strain triangle used in two-dimensional stress analysis. Later, Argyris[28-31] developed a refined element, a ten-node tetrahedron, which is the counterpart of the two-dimensional linear strain triangle. Melosh[32] has also proposed an element in the form of a rectangular prism. The isoparametric family of hexahedron elements, which has been developed by Ergatoudis, et al., [33-36] is a rather recent and very remarkable contribution to the three-dimensional analysis.

Melosh's rectangular prism is, in fact, a special form of the hexahedron elements belonging to the wider isoparametric family of elements.

In selection of an element, therefore, the choice lies between the constant strain and the higher order tetrahedrons, and the isoparametric element. The tetrahedron element has found wide application in the analysis of the three-dimensional solids to this date. It is simple (at least to the extent of the constant strain tetrahedron), and it satisfies all the conditions of monotonic convergence--including compatibility, the states of rigid body motion and constant strain. However, it possesses the disadvantage of not conforming to the curved boundaries. In such cases, the boundary is approximated by several small flat triangular faces of the tetrahedron. Such an idealization unnecessarily increases the number of unknown displacements. As will be discussed later, the isoparametric element has the capability of conforming to curved boundaries more closely. In addition, Clough[37] has shown that an eight node isoparametric hexahedron is more "flexible" than any eight node hexahedron assembly of tetrahedrons. Since the process of discretization partially constrains the continuum by using finite degrees of freedom (making it less flexible), a comparatively flexible element is more desirable. The isoparametric element is also "isotropic" in the sense that it does not have preferential directions as an assembly of tetrahedrons would inevitably have.[37]

It can be noted here that it is possible to develop a tetrahedron element with curved faces.[38] However, the formulation is at least as complicated as that for the isoparametric element. The features of flexibility and isotropy would still be lacking. In addition, extra effort is needed for assembling the tetrahedrons into hexahedrons.

With the present-day knowledge of finite element, it can be concluded that the isoparametric element is a very suitable element for the analysis of three-dimensional structures.

2.2 The Isoparametric Element

In three dimensions, the basic shape of the isoparametric element is a hexahedron consisting of eight corner nodes and straight edges. The general shape of each face is a hyperbolic paraboloid surface, Fig. 1. The higher order elements, with curved boundaries, if desired, can be obtained by including intermediate nodes on the edges, Figs. 2 and 3.

In general, the formulation of the isoparametric element can be described as follows:

1. Using Lagrangian interpolation, it is possible to pass a $(n-1)$ degree curve through n given points on any edge of the isoparametric element. Thus, two corner nodes define a straight line; addition of one intermediate node makes it quadratic (parabolic); and two intermediate nodes similarly make the edge a cubic curve.

2. A set of local curvilinear coordinates, designated as the isoparametric coordinates, ξ_i, are established such that each of the curved faces of the element can be defined by an equation $\xi_i = \pm 1$, where $i = 1, 2, 3$. An explicit transformation relationship between global cartesian coordinates and the isoparametric coordinates is achieved by using Lagrangian interpolation functions, designated here as "shape functions." Using the index notation and employing the summation convention

$$x_i = N^m x_i^m \qquad\qquad (2.1)$$

where

x_i =   global coordinates (i = 1,2,3)

N^m =   shape function at node m

x_i^m =   coordinates at node m

(Superscripts and subscripts are used to denote the node

number and the direction of coordinates, respectively.

Therefore, x_i^m represents the coordinate at node m in the

direction i; e.g., x_2^{10} denotes the y-coordinate at node 10.)

Since each shape function N^m in Eq. 2.1 is a Lagrangian

interpolation function, it has a value of unity at node m

and is zero at all other nodes.

3. The displacement field in the element is defined in terms

of the nodal displacements by using the same interpolation

functions. Thus,

$$u_i = N^m u_i^m \qquad\qquad (2.2)$$

where

u_i =   displacements at any point in the element

u_i^m =   displacement at node m in direction i

Since both the global coordinates and the displacements

are expressed in terms of the same parameters (shape func-

tions), the element has been designated as the "Iso-Parametric"

element.

2.3 Compatibility and Convergence

For a solution to converge monotonically to the true solution, it is nec-

essary that the displacements be continuous across the interfaces between adjacent

elements. This condition is satisfied, if the displacement of any point on an edge between the adjacent elements is uniquely defined in terms of the displacements of the nodal points along that boundary line, and that the boundaries of the adjacent elements fit with each other before any deformation has taken place. Since the displacements and the coordinates along the edge of an element are functions of the nodal displacements and the nodal coordinates, Eqs. 2.2 and 2.1, respectively, the compatibility of the displacement between adjacent elements is satisfied.

Other conditions for convergence, i.e., the state of rigid body motion and constant strain, are in fact implicitly insured in the isoparametric formulation. This can be verified by showing that a displacement field of the form

$$u_i = a_i + b_{ij}x_j \qquad (2.3)$$

is admissible in the displacement field as defined by Eq. 2.2. In Eq. 2.3 a_i and b_{ij} are arbitrary constants. At node m, Eq. 2.3 gives

$$u_i^m = a_i^m + b_{ij}x_i^m \qquad (2.4)$$

where, each a_i^m has the same value as a_i in Eq. 2.3. Substituting Eq. 2.4 into Eq. 2.2, one obtains

$$u_i = a_i^m N^m + b_{ij}N^m x_j^m \qquad (2.5)$$

If the displacement field given by Eq. 2.3 is admissible, Eq. 2.5 must be identical to Eq. 2.3. This can be shown by proving that the following are identities:

$$a_i = N^m a_i^m \tag{2.6a}$$

$$x_i = N^m x_i^m \tag{2.6b}$$

Equation 2.6b is identical to Eq. 2.1. In order to prove that Eq. 2.6a is also an identity, a linear transformation of coordinate system x_i into another cartesian coordinate system $\overline{x}_i$ is considered.

$$x_i = \overline{x}_i + a_i \tag{2.7a}$$

At node m, Eq. 2.7a gives

$$x_i^m = \overline{x}_i^m + a_i^m \tag{2.7b}$$

Substituting Eqs. 2.7a and 2.7b into Eq. 2.1, one obtains

$$\overline{x}_i + a_i = N^m (\overline{x}_i^m + a_i^m)$$

or $\tag{2.8}$

$$a_i = N^m a_i^m + (N^m \overline{x}_i^m - \overline{x}_i)$$

Since the isoparametric coordinate system is unique to a given element, Eq. 2.1 holds for any global coordinate system, hence,

$$\overline{x}_i = N^m \overline{x}_i^m \tag{2.9}$$

Substitution of Eq. 2.9 into Eq. 2.8 gives

$$a_i = N^m a_i^m$$

which is the same as Eq. 2.6a. If Eq. 2.6a is written in ordinary notation, one obtains $\Sigma N^m = 1$, with summation extended over all the nodes.

2.4 Generation of Polynomial Shape Functions

For various elements suitable polynomial which satisfy the necessary conditions of continuity can be written by including only the terms which give the appropriate variation along the sides of the elements. For example, considering the linear element, Fig. 1, one can write

$$\phi = \alpha^1 + \alpha^2 \xi_1 + \alpha^3 \xi_2 + \alpha^4 \xi_3 + \alpha^5 \xi_1 \xi_2 + \alpha^6 \xi_2 \xi_3 + \alpha^7 \xi_3 \xi_1$$

$$+ \alpha^8 \xi_1 \xi_2 \xi_3 = \alpha^r c^r \tag{2.10}$$

where

ϕ = a component of the global coordinate or the displacement vector at any point in the element

α^r = constant coefficients

c^r = functions of isoparametric coordinates, ξ_i; thus, $c^1 = 1$, $c^2 = \xi_1$, . . ., $c^8 = \xi_1 \xi_2 \xi_3$

Evaluating Eq. 2.10 at node m, one obtains

$$\phi^m = C^{mr} \alpha^r \tag{2.11}$$

where

C^{mr} = c^r at node m

Equation 2.11 can be solved to obtain

$$\alpha^r = D^{rm} \phi^m \tag{2.12}$$

Substitution of Eq. 2.12 into Eq. 2.10 yields

$$\phi = D^{rm} c^r \phi^m$$

or $\hspace{9cm}$ (2.13)

$$\phi = N^m \phi^m$$

where N^m is the required shape function given by

$$N^m = D^{rm}{}_c{}^r \hspace{7cm} (2.14)$$

In many cases, it is possible to write these functions by inspection and on the basis of the fundamental property of the shape functions which has been stated in Section 2.2, i.e., the shape function for the node m, N^m, is unity at node m and zero at all other nodes. Thus, for an eight node element

$$N^m = \frac{1}{8} (1+\xi_1^m \xi_1)(1+\xi_2^m \xi_2)(1+\xi_3^m \xi_3) \hspace{4cm} (2.15)$$

in which ξ_i^m is the value of ξ_i at node m.

2.5 Higher Order Elements

As it has been indicated in Section 2.2, the isoparametric family of elements consists of various orders of elements beyond the linear 8 node hexahedron. A higher order element is obtained by including intermediate nodes on the edges. For instance, a "quadratic element" consists of eight corner nodes and twelve intermediate nodes (one on each edge), Fig. 2a. A "cubic element" is obtained by including twenty-four intermediate nodes-- two on each edge, Fig. 2b, and so on. The foregoing examples, however, are special cases of the general isoparametric element in which it is possible to assign any order of response to individual edges, Fig. 3.

Figure 4 shows a typical edge, AB, under various degrees of responses. When there are only two corner nodes, A and B, the response is

linear, Fig. 4a. Addition of an intermediate node results in both a parabolic edge and displacement field. A set of shape functions, quadratic in the isoparametric coordinate along AB, say ξ_1, can be formulated for corner nodes A and B, and the intermediate node 1. This, however, would mean that everytime an additional intermediate node is introduced on any edge, a new set of shape functions must be used for the corner nodes. This difficulty is overcome by defining the quadratic response on the edge as the departure from linearity, thus retaining the linear response defined by the corner nodes.

$$\phi^{AB} = N^A \phi^A + N^B \phi^B + \Delta^{AB}\phi \qquad (2.16)$$

where

$$\phi^{AB} = \text{a component of coordinate or displacement vector,}$$
$$\text{evaluated on edge AB}$$

$$N^A, N^B = \text{linear shape function for the corner nodes A and B}$$

$$\phi^A, \phi^B = \text{values of } \phi^{AB} \text{ at node A and B, respectively}$$

$$\Delta^{AB}\phi = \text{the quadratic departure of } \phi^{AB} \text{ from the linear re-}$$
$$\text{sponse defined by the corner nodes}$$

On the basis of known characteristics of $\Delta^{AB}\phi$, i.e., it is quadratic, and vanishes at A and B ($\xi_1 = \pm 1$), one can write

$$\Delta^{AB}\phi = \beta (1 - \xi_1^2) \qquad (2.17)$$

where

$$\beta = \text{an unknown coefficient which is to be determined for the}$$
$$\text{edge under consideration}$$

For the corner node A on the edge AB, Eq. 2.15 becomes

$$N^A = \frac{1}{8}(1+\xi_1^A\xi_1)(1+\xi_2^A\xi_2)(1+\xi_3^A\xi_3) \tag{2.18}$$

Also on the edge AB

$$\xi_2 = \xi_2^A = \pm 1$$

$$\xi_3 = \xi_3^A = \pm 1 \tag{2.19}$$

Substitution of Eq. 2.19 into Eq. 2.18 gives

$$N^A = \frac{1}{2}(1+\xi_1^A\xi_1) \tag{2.20a}$$

Similarly,

$$N^B = \frac{1}{2}(1+\xi_1^B\xi_1) \tag{2.20b}$$

At the intermediate node 1, $\phi^{AB} = \phi^1$, and $\Delta^{AB}\phi = \Delta^{AB}\phi^1$. Substituting $\xi_1 = 0$ into Eq. 2.17 and Eqs. 2.20 one obtains

$$\Delta^{AB}\phi^1 = \beta$$

$$N^A = N^B = \frac{1}{2} \tag{2.21}$$

Substituting for N^A, N^B and $\Delta^{AB}\phi$ into Eq. 2.16 and solving for β results in

$$\beta = \phi^1 - \frac{1}{2}(\phi^A + \phi^B) \tag{2.22}$$

The term β can be defined as the modified value of ϕ^1 and denoted by $\bar{\phi}^1$. Equation 2.16 now becomes

$$\phi^{AB} = N^A\phi^A + N^B\phi^B + \bar{N}^1\bar{\phi}^1 \tag{2.23}$$

where $\bar{N}^1$ is the shape function for the modified nodal value $\bar{\phi}^1$ and is written

on the basis of Eq. 2.17 as

$$\overline{N}^1 = \frac{1}{4} (1-\xi_1^2)(1+\xi_2^{AB}\xi_2)(1+\xi_3^{AB}\xi_3) \tag{2.24}$$

It can be seen that by substituting $\xi_2 = \xi_2^{AB}$ and $\xi_3 = \xi_3^{AB}$ for the edge AB in Eq. 2.24, $\overline{N}^1 = (1-\xi_1^2)$, which is in agreement with Eq. 2.17.

More intermediate nodes can be introduced on the same edge in order to define a higher degree of response. Figure 4c, for instance, represents a cubic response on the edge AB, which has two intermediate nodes 1 and 2. If there are I intermediate nodes defined on the same edge, Fig. 4d, the degree of response would be (I+1). Equation 2.16 can again be used to define the total response on the edge. The term $\Delta^{AB}\phi$ represents the departure of degree (I+1) from linearity. In a manner similar to Eq. 2.17, it can be written as

$$\Delta^{AB}\phi = (1-\xi_1^2)(\gamma^1+\gamma^2\xi_1+\gamma^3\xi_1^2+ \ldots +\gamma^I\xi_1^{I-1}) =\gamma^S g^S \tag{2.25}$$

The superscripts on ξ_1 in the above expression represent exponential powers, γ^S's are a set of I unknown coefficients for the edge, and g^S's are I functions of ξ_1. The isoparametric coordinates for each of the I intermediate nodes can be substituted in Eq. 2.25. Thus,

$$\Delta^{AB}\phi^m = G^{ms}\gamma^S \tag{2.26}$$

where, $\Delta^{AB}\phi^m$ and G^{ms} are the values of $\Delta^{AB}\phi$ and g^S at the mth intermediate node, respectively. Solution of Eq. 2.26 for γ^S gives

$$\gamma^S = H^{sm} \Delta^{AB}\phi^m \tag{2.27}$$

Since the set of ϕ-values of I-intermediate nodes are replaced by the same

number of $\bar{\phi}$-values in Eq. 2.25, as before, $\bar{\phi}^m$'s are designated as the modified ϕ-values. The terms $\overline{N}^m$ are the shape functions corresponding to each of the $\bar{\phi}^m$-values, Eqs. 2.25, 2.26. It can be seen from Eq. 2.26 that on edge AB, $(\xi_2 = \xi_2^{AB}, \quad \xi_3 = \xi_3^{AB})$, $\overline{N}^m = g^m$, which is in conformity with Eq. 2.24.

It should be noted here, that arrays G^{mn} and H^{mn}, Eqs. 2.26 and 2.27 are constant for a given number of intermediate nodes and they are independent of the position or direction of the edge. It is, therefore, possible to compute and store them at the beginning of the program for future use.

2.6 The Element Stiffness Matrix

With the given displacement field for the element, Eq. 2.2, it is possible to obtain the stiffness matrix using the principle of virtual displacement and the constitutive relations of the continuum.

In a cartesian space, the strain tensor is given by

$$\varepsilon_{ij} = \frac{1}{2} \left(\frac{\partial u_i}{\partial x_j} + \frac{\partial u_j}{\partial x_i} \right) \tag{2.32}$$

Differentiating Eq. 2.2 and substituting into Eq. 2.32, one obtains

$$\varepsilon_{ij} = Z^m_{ijk} u^m_k \tag{2.33}$$

in which

$$Z^m_{ijk} = \frac{1}{2} \left(\delta_{ik} \delta_{j\ell} + \delta_{i\ell} \delta_{jk} \right) \frac{\partial N^m}{\partial x_\ell} \tag{2.34}$$

where, δ_{ik} is the Kronecker delta.

The shape functions N^m, are expressed in terms of the isoparametric coordinates. In order to evaluate their derivatives with respect to the global coordinates, one needs the transformation relationship between the

cartesian and the isoparametric coordinates. This relationship can be obtained by differentiating Eq. 2.1 with respect to ξ_j.

$$\frac{\partial x_i}{\partial \xi_j} = \frac{\partial N^m}{\partial \xi_j} x_j^m \qquad (2.35)$$

The required transformation array $\frac{\partial \xi_j}{\partial x_i}$ is obtained by inverting the Jacobian matrix $\frac{\partial x_i}{\partial \xi_j}$, Eq. 2.35. The global derivatives of the shape functions N^m, Eq. 2.34, can be evaluated now by

$$\frac{\partial N^m}{\partial x_i} = \frac{\partial N^m}{\partial \xi_j} \frac{\partial \xi_j}{\partial x_i} \qquad (2.36)$$

The stresses are related to strains by

$$\sigma_{pq} = E_{pqij} \varepsilon_{ij} \qquad (2.37)$$

where E_{pqij} is the material property tensor.

If the element is given a virtual displacement δu_k^m, the corresponding change in strain can be computed from Eq. 2.33.

$$\delta \varepsilon_{ij} = Z_{ijk}^m \delta u_k^m \qquad (2.38)$$

The internal work associated with the virtual displacement is

$$\delta W_{int} = \int_V \sigma_{ij} \delta \varepsilon_{ij} \, dV \qquad (2.39)$$

and the external work of the nodal forces through the nodal virtual displacements is

$$\delta W_{ext} = P_i^m \delta u_i^m \qquad (2.40)$$

For a system in equilibrium $\delta W_{int} = \delta W_{ext}$. Equations 2.33, 2.34, and 2.37 to 2.40 give

$$P_i^m = k_{ij}^{mn} u_j^n \tag{2.41}$$

in which k_{ij}^{mn} is the element stiffness matrix[*] which is given by

$$k_{ij}^{mn} = \int_V E_{ikj\ell} \frac{\partial N^m}{\partial x_k} \frac{\partial N^n}{\partial x_\ell} \, dV \tag{2.42}$$

where

$$dV = dx_1 dx_2 dx_3 = \left| \frac{\partial x_i}{\partial \xi_j} \right| d\xi_1 d\xi_2 d\xi_3 \tag{2.43}$$

For the elastic isotropic material, the material property tensor $E_{ikj\ell}$ can be expressed explicitly in terms of the Lamé's constant Λ, and the modulus of rigidity μ.

$$E_{ikj\ell} = \Lambda \delta_{ik} \delta_{j\ell} + \mu(\delta_{ij}\delta_{k\ell} + \delta_{i\ell}\delta_{jk}) \tag{2.44}$$

Substituting Eq. 2.44 in Eq. 2.42 one obtains

$$k_{ij}^{mn} = \int_V \Lambda \frac{\partial N^m}{\partial x_i} \frac{\partial N^n}{\partial x_j} + \mu \left(\frac{\partial N^m}{\partial x_k} \frac{\partial N^n}{\partial x_k} \delta_{ij} + \frac{\partial N^m}{\partial x_j} \frac{\partial N^n}{\partial x_i} \right) \, dV \tag{2.45}$$

A numerical integration scheme for computing the stiffness matrix is given in Section 2.8. It was found during the study that the index notation formulation of the stiffness matrix results in an economic organization of computation. In addition, in case of homogeneous material in which the terms of material property tensor are independent of position coordinates, a further reduction in computer time is achieved by taking the material property tensor $E_{ikj\ell}$ outside of the integral sign, Eq. 2.42. A more detailed discussion on this subject is given in Appendix A.

---

[*] Since k_{ij}^{mn} is a four-dimensional array, it cannot be defined by the term "matrix." Nevertheless, the term "stiffness matrix" is conventionally used to define a relationship between the nodal forces and the nodal displacements, and is used in the study.

2.7 The Generalized Loads

In the discrete formulation of continuum problems, the applied loads must be transferred to nodal points, where the displacements are defined. This transformation is best achieved by using an energy approach similar to that used for obtaining the element stiffness properties. The nodal loads so obtained are referred to as the generalized loads.

The applied loads may either be concentrated loads acting at any point, or they may be distributed over a continuous domain, such as a volume, an area or a length.

2.7.1 Concentrated Loads

The equavalent nodal loads resulting from a concentrated load Q_i^A acting at point A ($\xi_i = \xi_i^A$) are obtained by equating the work of both the nodal and the concentrated loads through a virtual displacement. Thus,

$$P_i^m \, \delta u_i^m = Q_i^A \, \delta u_i^A = Q_i^A \, N^m(\xi_i^A) \, \delta u_i^m \qquad (2.46)$$

where

$$P_i^m = \qquad \text{desired generalized load}$$

$$\delta u_i = \qquad \text{virtual displacement field}$$

The term $N^m(\xi_i^A)$ represents the value of N^m at point A. Since, δu_i and thus δu_i^m are arbitrary displacements, Eq. 2.46 yields

$$P_i^m = Q_i^A \, N^m(\xi_i^A) \qquad (2.47)$$

2.7.2 Distributed Loads

In a procedure similar to that for the concentrated loads, for a distributed load of intensity q_i acting on a domain D, the equivalent nodal

loads are obtained from

$$P_i^m = \int_D q_i N^m dD \qquad (2.48)$$

As an example, for the case where the load is distributed over a face of the element, the domain D is replaced by the area A. Equation 2.48 becomes

$$P_i^m = \int_A q_i N^m dA \qquad (2.49)$$

2.8 The Numerical Integration

If performed manually, the computation of both the element stiffness matrix k_{ij}^{mn}, Eq. 2.42, and the generalized loads, P_i^m, Eq. 2.48, is a prohibitive task. As an alternative, various computations can be performed with the help of a computer. In this situation, the integration involved in computation of those quantities must be performed numerically.

There are many approaches available for numerical integration. Their detailed description can be found in the standard books on numerical analysis.[39,40] Zienkiewicz[41] has selected two of them as the most useful in the finite element formulation, the Gaussian quadrature formula and the Newton-Cotes quadrature formula. Ergatoudis,[33] however, has pointed out that the former is about three times as efficient as the latter. Therefore, in the present study, the Gaussian quadrature formula has been used.

Using the Gaussian quadrature formula, one can exactly integrate a polynomial $f(\xi)$ of degree $(2n-1)$ as a weighted means of its particular values at n specified points. The expression can be written as

$$\int_{-1}^{+1} f(\xi)d\xi = \rho^i f^i \qquad (2.50)$$

where

ρ^i = the weighting coefficients, and

f^i = the value of function $f(\xi)$ at n specified points ($\xi = \eta^i$)

In two dimensions, the integral becomes

$$\int_{-1}^{+1} \int_{-1}^{+1} f(\xi_1, \xi_2) d\xi_1 d\xi_2 = \rho^i \rho^j f^{ij} \qquad (2.51)$$

and in three dimensions, it is

$$\int_{-1}^{+1} \int_{-1}^{+1} \int_{-1}^{+1} f(\xi_1, \xi_2, \xi_3) d\xi_1 d\xi_2 d\xi_3 = \rho^i \rho^j \rho^k f^{ijk} \qquad (2.52)$$

The ρ^i and η^i values for different orders of Gaussian quadrature are readily obtainable.[39,40]   In the present study, as was also found by other investigators,[37] integration carried with the 4th order Gaussian quadration is considered to be sufficiently accurate to handle all problems.

2.9 The Load-Displacement Equations for the Structure

In the displacement method of finite element analysis, the problem always reduces to the solution of a set of simultaneous equations, referred to as the load-displacement equation. In matrix notation,

$$KU = F \qquad (2.53)$$

where

K = the nonsingular structural stiffness matrix

U = the vector of unknown displacements, and

F = the nodal load vector

Solution of Eq. 2.53 yields the unknown displacements U, which upon substitution into the strain-displacement relation, Eq. 2.33, and subsequent use

of stress-strain relation, Eq. 2.37, gives the desired stresses.

Various steps in arriving at Eq. 2.53 are discussed in the following sections.

2.9.1 Assembling the Structural Stiffness Matrix

The structural stiffness matrix is obtained on the basis of the principle of virtual displacement. The total virtual work done on the structure consists of the virtual work contributions of the individual elements. The structural stiffness matrix is obtained by summing up the stiffness matrices of the contributing elements. Thus,

$$\overline{K} = \sum_{r=1}^{M} k_r \qquad (2.54)$$

where

$\overline{K}$ = the stiffness matrix of the unconstrained structure

k_r = the stiffness matrix of the element r

M = the total number of elements

The stiffness matrix obtained in Eq. 2.54 is used to obtain the load-displacement relationship for the unconstrained structure.

$$\overline{K}\,\overline{U} = \overline{F} \qquad (2.55)$$

where $\overline{U}$ and $\overline{F}$ are the vectors of nodal displacements and loads, respectively, for the unconstrained structure.

Without any constraints, a structure is free to undergo rigid body motion; therefore, there is no unique solution to Eq. 2.55. Mathematically, this phenomenon manifests itself by the singular nature of the stiffness matrix $\overline{K}$. Nevertheless, all stable structures are provided with enough displacement constraints to prevent rigid body motion. A nonsingular stiffness

matrix K can be obtained from the singular stiffness matrix $\overline{K}$ by incorporating those constraints in a manner explained in the next section.

2.9.2 Displacement Constraints

Some of the constraints envisaged in the preceding section can be in the form of zero nodal displacements in given global directions at certain joints. If there are no other constraints, the nonsingular stiffness matrix K can be obtained from the assembled stiffness matrix $\overline{K}$, Eq. 2.54, by omitting the rows and the columns corresponding to the constrained displacements.

Another type of constraint often encountered is in the form of a set of explicit relationships between two displacements, say $\overline{U}_1$ and $\overline{U}_2$, such as

$$\overline{U}_1 = C \, \overline{U}_2 \qquad (2.56)$$

where C is a known constant. For instance, constraints defined by Eq. 2.56 exist when the displacements are zero in the direction normal to a boundary which is inclined to the specified coordinate axes, Fig. 5a. If the boundary is parallel to x_3 axis and makes an angle θ with the x_1 axis, then $C = \cot \theta$, in Eq. 3.56, where $\overline{U}_1$ and $\overline{U}_2$ now represent the displacements in x_1 and x_2 directions, respectively, at a node on the boundary.

In the case of a medium thick plate subjected only to lateral load, Fig. 5b, denoting the displacements in x_1, x_2, x_3 directions by u_1, u_2, u_3, respectively, and using superscripts t and b to denote the top and bottom layers, the following relationships are easily obtained:

$$u_1^t = -u_1^b$$

$$u_2^t = -u_2^b \qquad (2.57)$$

$$u_3^t = u_3^b$$

Equations 2.57 are also of the type of Eq. 2.56.

With the given constraints, in general, a relationship between the displacement vectors of the unconstrained and the constrained structure can be written as

$$\overline{U} = TU \qquad (2.58)$$

where T is a geometric transformation matrix. On the basis of the principle of contragradience,[42]

$$F = T^T \overline{F} \qquad (2.59)$$

Substituting Eq. 2.58 into Eq. 2.55, and substituting the resultant expression for $\overline{F}$ into Eq. 2.59, one obtains

$$F = (T^T \overline{K} T) U \qquad (2.60)$$

Comparison of Eq. 2.53 and 2.60 yields

$$K = T^T \overline{K} T \qquad (2.61)$$

which is the desired expression for the nonsingular structural stiffness matrix.

In most cases, the geometric transformation matrix T of Eq. 2.58 is only sparsely filled. Computations for Eq. 2.61 can, therefore, be

organized economically without actually performing direct matrix multipli-
cation.

2.9.3 Solution of the Load-Displacement Equations

As has been mentioned earlier in this section, in the displacement
method of finite element analysis, the problem always reduces to the solution
of a set of simultaneous equations, Eq. 2.53. Invariably, an efficient
method of solving equations takes into account the symmetry and the banded
nature of the stiffness matrix. In the present study, only the upper tri-
angular portion of the stiffness matrix is considered, and a variable band
width approach has been followed. The resulting banded upper triangular
matrix has been stored in a column array in order to economize the storage
requirement. The solution of the equations is based on the Gaussian elimin-
ation method.[43]

The method of solution followed in this study is quite efficient
for solving a banded set of equations. However, in three-dimensional pro-
blems the band width of the individual equations tends to be very large,
thus requiring a large storage. In addition, one has to operate on many
zero terms within the band, which adds to the cost of equation solving. The
frontal method[44] is an improvement in this respect. In this method, only
that part of the stiffness matrix which corresponds to the current active
variables in the "front" is stored in core, thus making a substantial saving
on the core requirement. In general, the size of the front is smaller than
the band width of the equations, which in effect, eliminates a good number
of zeroes from the process of computation. This results in economy of the
computer time. On the other hand, the frontal method uses several input-
output operations. For this reason, in many problems, a straight, variable

band width approach (used in this study) may prove to be more economical.

Several other methods have been used for the solution of simultaneous equations. The so-called "square-root method"[45] is one which has been used extensively. The method consists of decomposing the stiffness matrix into a product of a lower triangular matrix and an upper triangular matrix. A similar method has been used in the general purpose finite element program NASTRAN.[46]

Chapter 3

PLASTIC ANALYSIS

3.1 General

As is well known in the elastic deformation, strains are related to stresses by a holonomic relationship. An elastic process is also reversible. On the contrary, the phenomenon of plastic deformation implies that the state of strain is not uniquely determined by the state of stress--it is path dependent. Also, the process of plastic deformation is irreversible. This means that the work done during a plastic action cannot be recovered.

Most materials behave elastically up to a certain stage of loading, beyond which plastic deformations take place. In a uniaxial state of stress, the stage at which yielding starts can be determined easily from the experimental stress-strain curve. In multiaxial state of stress, however, there are infinite number of possible combinations of stresses at which yielding starts. A unified basis of establishing all such combinations is known as the yield criterion. Another necessary consideration in constructing a plasticity theory is the incremental relationship between stresses and strains in the plastic range. Both the yield criterion and the plastic incremental stress-strain relationship are discussed in the following section.

3.2 The Yield Criterion and the Flow Rule

The yield criterion is described by a hypersurface (designated as the yield surface) in six-dimensional stress space.[47]

$$\Psi(\sigma_{ij}) = \kappa \qquad\qquad\qquad (3.1)$$

where

Ψ = the loading function, and

κ = the yield function or the work-hardening function

For a given previous deformation history, $\Psi(\sigma_{ij})$ is a function of the current state of stress and κ is a constant. If the state of stress is such that it lies on the yield surface described by Eq. 2.1, initiation of plastic deformation can take place.

For a perfectly plastic material, the yield surface, Eq. 3.1, remains constant. However, for a strain hardening material, the yield surface must change with continued straining beyond the initial yield. This phenomenon is incorporated in Eq. 3.1 by allowing both Ψ and κ to be functions of the state of stress and the plastic deformation history. Thus, every time yielding takes place, κ takes on a new value. If the material is unloaded and then loaded again, additional yielding does not take place unless the current value of κ has been exceeded.

As has been mentioned earlier, in general, Ψ is the function of both, the state of stress and the deformation. A good deal of analytical simplification is achieved by neglecting the Bauschinger effect,[48] assuming that the material strain hardens isotropically. Such an assumption is approximately true if the load is applied monotonically.[49] It should be noted that a basic assumption in the plastic analysis is that the loading function $\Psi(\sigma_{ij})$ exists.

Various incremental stress-strain equations, or the so-called flow rules have been suggested for analysis in the plastic range.[47] Most

of them implicitly assume that the infinitesimal stresses and strains are related linearly. A unified approach for arriving at the incremental stress-strain equation, as presented by Drucker,[50] is followed here.

Drucker postulated the implications of work hardening and the ideally plastic material, and established that the plastic strain increment, $d\varepsilon_{ij}''$, is proportional to the stress gradient of the yield surface.

$$d\varepsilon_{ij}'' = d\lambda \frac{\partial \Psi}{\partial \sigma_{ij}} \tag{3.2}$$

where

$d\lambda$ = a positive incremental constant of proportionality

Equations 3.1 and 3.2 form the basis of the development of the method of plastic analysis discussed in the following sections.

3.3 Incremental Stress-Strain Equation

In the plastic range, the relationship between stresses and strains is nonlinear and also path dependent (see the preceding two sections). In order to perform a plastic analysis, the loading path is discretized into several linear load steps. The increments in stresses and strains for each step are then related by the rate constitutive laws. The assumption is that the extension of the linearized steps is small so that the change in stresses during a particular step can be regarded as infinitesimal and Eq. 3.2, which is true for infinitesimal increments of stresses and strains, can be employed for small finite increments.

The total strain increment $d\varepsilon_{ij}$ is the sum of the increments in elastic and plastic strains $d\varepsilon_{ij}'$ and $d\varepsilon_{ij}''$, respectively.

$$d\varepsilon_{ij} = d\varepsilon_{ij}' + d\varepsilon_{ij}'' \tag{3.3}$$

The relationship between stresses and elastic strains is given by Eq. 2.37 which is modified for incremental stresses and elastic strains as

$$d\sigma_{ij} = E_{ijk\ell} \, d\varepsilon_{k\ell}^{i} \qquad (3.4)$$

Substituting $d\varepsilon_{k\ell}^{i}$ from Eq. 3.3 into Eq. 3.4 and subsequently making use of Eq. 3.2, one obtains

$$d\sigma_{ij} = E_{ijk\ell} \, d\varepsilon_{k\ell} - d\lambda \, E_{ijk\ell} \frac{\partial \Psi}{\partial \sigma_{k\ell}} \qquad (3.5)$$

It has been stated in Section 3.2 that the yield function κ, Eq. 3.1, is a function of the state of stress and the plastic deformation path. For many materials an equivalent statement is that the yield function is a function of the plastic work W^P. Thus,

$$\kappa = \kappa(W^P) \qquad (3.6)$$

where

$$dW^P = \sigma_{ij} \, d\varepsilon_{ij}^{\,\prime\prime} \qquad (3.7)$$

Obviously, even for those materials which satisfy Eq. 3.6, the yield function continues to be a function of the state of stress and the plastic deformation path since W^P is a function of the state of stress and of this path, Eq. 3.7.

Making use of Eqs. 3.2, 3.6 and 3.7, the complete differential of Eq. 3.1 can be written as

$$\frac{\partial \Psi}{\partial \sigma_{ij}} \, d\sigma_{ij} = \Gamma d\lambda \qquad (3.8)$$

where

$$\Gamma \quad = \quad \frac{d\kappa}{dW^P} \frac{\partial \Psi}{\partial \sigma_{ij}} \sigma_{ij} \tag{3.9}$$

Substituting Eq. 3.5 into Eq. 3.8 and solving for the incremental constant of proportionality, $d\lambda$, one obtains

$$d\lambda \quad = \quad \Omega \; E_{ijk\ell} \frac{\partial \Psi}{\partial \sigma_{ij}} d\varepsilon_{k\ell} \tag{3.10}$$

where

$$\Omega \quad = \quad (\Gamma + E_{ijk\ell} \frac{\partial \Psi}{\partial \sigma_{ij}} \frac{\partial \Psi}{\partial \sigma_{k\ell}})^{-1} \tag{3.11}$$

Substitution of Eq. 3.10 into Eq. 3.5, gives

$$d\sigma_{ij} \quad = \quad d\sigma_{ij}' - d\sigma_{ij}'' \tag{3.12}$$

in which

$$d\sigma_{ij}' \quad = \quad E_{ijk\ell} \; d\varepsilon_{k\ell} \tag{3.13}$$

$$d\sigma_{ij}'' \quad = \quad \Omega \; E_{ijk\ell} \; E_{pqrs} \frac{\partial \Psi}{\partial \sigma_{k\ell}} \frac{\partial \Psi}{\partial \sigma_{rs}} d\varepsilon_{pq} \tag{3.14}$$

The tensor $d\sigma_{ij}'$ represents the elastic increment in stresses corresponding to the total strain increment $d\varepsilon_{ij}$. The tensor $d\sigma_{ij}''$ is designated as the incremental "initial stress" tensor in analogy to the initial strains. Equation 3.14 holds good only when the incremental stress tensor lies outside the yield surface.

In the "initial" stress approach, discussed later in this chapter, Eqs. 3.12 to 3.14 form the basis of the computations.

3.4 Application to von Mises Yield Criterion

Various yield criteria have been proposed for plastic analysis

of solids having different material properties.[47] The von Mises yield criterion explains the behavior of a wide class of ductile materials very closely. The Prandtl-Reuss equations form the flow rule associated with the von Mises yield criterion.

For the von Mises yield criterion, Eq. 3.1 reduces to

$$\frac{3}{2} S_{ij} S_{ij} = \sigma_e^2 \tag{3.15}$$

in which

$$\Psi(\sigma_{ij}) = \frac{3}{2} S_{ij} S_{ij} \tag{3.16}$$

and

$$\kappa = \sigma_e^2 \tag{3.17}$$

where S_{ij} is the deviatoric stress tensor and is given by

$$S_{ij} = \sigma_{ij} - \frac{1}{3} \sigma_{kk} \delta_{ij} \tag{3.18}$$

It is seen from Eq. 3.15 that for a uniaxial state of stress, where the only nonzero component of stress tensor is σ_{11}, one obtains

$$\sigma_{11} = \sigma_e \tag{3.19}$$

By the analogy represented by Eq. 3.19, σ_e is designated as the effective stress (equivalent to the uniaxial state of stress).

Differentiating Eq. 3.16 with respect to σ_{ij}, one obtains

$$\frac{\partial \Psi}{\partial \sigma_{ij}} = 3 S_{ij} \tag{3.20}$$

Substitution of Eq. 3.20 into Eq. 3.2, yields

$$d\varepsilon_{ij}'' = 3 S_{ij} d\lambda \tag{3.21}$$

It is assumed that the plastic work done by the stresses σ_{ij} through the plastic strain increment $d\varepsilon_{ij}''$ is equal to the work done by the effective stress σ_e through equivalent plastic strain increment $d\varepsilon_p$ in a uniaxial state of stress. Thus,

$$dW^P = \sigma_{ij}\, d\varepsilon_{ij}'' = \sigma_e\, d\varepsilon_p \tag{3.22}$$

Substituting Eq. 3.21 into Eq. 3.22 and solving for $d\lambda$, one obtains

$$d\lambda = \frac{1}{2}\frac{d\varepsilon_p}{\sigma_e} \tag{3.23}$$

Substitution of Eq. 3.23 into Eq. 3.21 gives

$$d\varepsilon_{ij}'' = \frac{3}{2}\frac{d\varepsilon_p}{\sigma_e} S_{ij} \tag{3.24}$$

Equations 3.21 and 3.24 are known as the Prandtl-Reuss equations.

Using Eqs. 3.22 and 3.24, it can be shown that

$$d\varepsilon_p = \sqrt{\frac{2}{3}\, d\varepsilon_{ij}''\, d\varepsilon_{ij}''} \tag{3.25}$$

In a uniaxial system, Eq. 3.25 reduces to

$$d\varepsilon_p = d\varepsilon_{11}'' \tag{3.26}$$

which is in agreement with the prior statement about the definition of the equivalent plastic strain increment.

Equations 3.17 and 3.22 give

$$\frac{d\kappa}{dW^P} = 2\frac{d\sigma_e}{d\varepsilon_p} \tag{3.27}$$

It is assumed that the material has a bilinear stress-strain relationship in uniaxial state of stress, Fig. 6. Thus,

$$\sigma_e = \sigma_y + \frac{zE}{1-z}\varepsilon_p \tag{3.28}$$

where z is the strain hardening coefficient. Differentiating Eq. 3.28 with respect to ε_p, one obtains

$$\frac{d\sigma_e}{d\varepsilon_p} = \frac{z\,E}{1-z} \tag{3.29}$$

Substituting Eq. 3.29 into Eq. 3.27 and substituting the resulting expression together with Eq. 3.20 into Eq. 3.9, one gets

$$\tau = 4\,\sigma_e^2\,\frac{z\,E}{1-z} \tag{3.30}$$

Substitution of Eqs. 2.44, 3.20 and 3.30 into Eq. 3.10 yields

$$\Omega = \frac{1}{4\sigma_e^2}\left(\frac{z}{1-z}\,E + 3\mu\right)^{-1} \tag{3.31}$$

Substituting Eqs. 3.13, 3.20 and 3.31 into Eq. 3.14 one obtains

$$d\sigma_{ij}'' = \left(1 + \frac{z\,E}{3(1-z)\mu}\right)^{-1} S_{ij}\,\frac{d\sigma_e}{\sigma_e} \tag{3.32}$$

where

$$d\sigma_e = \frac{3}{2\sigma_e}\,E_{ijk\ell}\,S_{ij}\,d\varepsilon_{k\ell} \tag{3.33}$$

It should be noted that Eqs. 3.32 and 3.33 are applicable only when Eq. 3.15 is satisfied in the beginning of the increment, i.e., when the state of stress lies on the yield surface. Also $d\sigma_e$ should always be positive or zero.

The loading function, as defined by Eq. 3.16, is quadratic in stresses. For the sake of convenience in forthcoming discussion, a "loading stress"

$$\sigma_c = \sqrt{\Psi(\sigma_{ij})} = \sqrt{\frac{3}{2}\,S_{ij}\,S_{ij}} \tag{3.34}$$

is defined, which varies linearly with the linear change in stresses. Equation 3.15, which defines the yield surface, can be rewritten as

$$\sigma_c = \sigma_e \tag{3.35}$$

In case the state of stress does not lie on the yield surface (i.e., Eqs. 3.15 or 3.35 are not satisfied), at the beginning of the load increment, the change in loading stress is computed using an equation similar to Eq. 3.33

$$d\sigma_c = \frac{3}{2\sigma_e} E_{ijk\ell} S_{ij} d\varepsilon_{k\ell} \tag{3.36}$$

An incremental pseudo initial stress field is obtained by substituting $d\sigma_c$ for $d\sigma_e$ in Eq. 3.32. Thus,

$$d\bar{\sigma}_{ij}'' = (1 + \frac{z E}{3(1-z)\mu})^{-1} S_{ij} \frac{d\sigma_c}{\sigma_e} \tag{3.37}$$

The actual values of incremental initial stresses $d\sigma_{ij}''$ are obtained on the basis of the state of stress in the beginning and the end of the load increment. If σ_c is the loading stress at the beginning of the load increment and σ_c^+ is the loading stress at the end of the increment, three cases arise.

1. $\sigma_c^+ < \sigma_e$

No plastic deformation has taken place, therefore,

$$d\sigma_e = 0$$
$$\tag{3.38}$$
$$d\sigma_{ij}'' = 0$$

2. $\sigma_c^+ > \sigma_e$ and $\sigma_c = \sigma_e$

The plastic deformation has occurred during the complete

loading increment. In this case,

$$d\sigma_e = d\sigma_c$$

$$d\sigma_{ij}'' = d\bar{\sigma}_{ij}''$$

(3.39)

3. $\sigma_c^+ > \sigma_e$ and $\sigma_c < \sigma_e$

Only part of loading increment has caused plastic deformations. Since a linear problem is solved for each loading increment, one can write

$$d\sigma_e = d\sigma_c - (\sigma_e - \sigma_c)$$

$$d\sigma_{ij}'' = \frac{d\sigma_e}{d\sigma_c} d\bar{\sigma}_{ij}''$$

(3.40)

Equations 3.34 to 3.40 are used in applying the initial stress approach to the isoparametric element. The significance of the above treatment becomes more obvious in Section 3.7.

3.5 Method of Analysis

As has been mentioned in Section 3.3, an incremental loading approach must be used for the analysis in the plastic range of material behavior. The incremental equations in the preceding two sections are written in differential notations which imply that the increments are infinitesimally small. However, in practice one must use finite increments. It is assumed that the relationships, which are true for infinitesimal increments, can be applied for small finite increments. In order to distinguish between the infinitesimal increments and the finite increments, the differential operator "d" will be replaced by "Δ" in the further

treatment. For instance, $\Delta\sigma_{ij}$ will denote a finite increment in the stress tensor σ_{ij}.

One of the earlier methods which follows the incremental loading approach is the "initial strain" method.[51] An elastic problem is solved for each increment of loading. An estimate of the plastic strain for the loading increment is made and this assumed plastic strain is treated as the initial strain. A loading system "equivalent" to the initial strain is evaluated and is applied on the structure in order to solve another elastic problem. The iterative process consists of determining the initial strains, evaluating the equivalent loading and solving the elastic problem. The convergence is assumed to have been reached once the initial strains become negligible within a given tolerance.

A serious drawback of the initial strain method is that it applies only to materials showing a pronounced degree of strain hardening. When the strain hardening is either very small or zero, very large plastic strains are caused by small increments of loads, resulting in a poor convergence.

Another approach to the finite element incremental plastic analysis is the quadratic programming method.[17,18] The incremental problem is solved "exactly" in a finite number of iterations for both work hardening and perfectly plastic behavior. However, computer programs for large scale quadratic programming problems are not readily available. Moreover, the application to finite element models with nonconstant stresses and strains in each element presents some complications.

A third incremental method of plastic analysis is the tangent stiffness method.[52,53] In this method, at any loading step, the incremental stress-strain relationship is used to determine the stiffness

matrix of the element which has undergone a plastic deformation. Such a stiffness matrix is designated as the "tangent stiffness matrix." For each loading increment, an elastic problem is solved using the tangent stiffness matrix of the structure. For elements which have undergone further plastic deformation, the state of stress in the element and thus, the incremental stress-strain relation for the element have changed. A new tangent stiffness matrix is evaluated and the problem is resolved. This process is continued for each loading increment until the structure becomes very flexible due to widespread plastic deformations in critical zones such that the displacements become unbounded.

Since, for each loading increment, a new stiffness matrix is computed for the element which has undergone plastic deformation, the equilibrium equations at every joint which is incident on that element must be modified. Both the recomputation of the element stiffness matrix and modifications of equilibrium equations constitute a major computational effort, especially for the three-dimensional isoparametric element. For this reason, a more economical method of incorporating the plastic material behavior, the initial stress method[54] is considered in this study.

In this method of analysis, for each loading increment, the problem is solved elastically. If any point has undergone plastic deformation during the loading increment, the increments of stresses and strains at that point will not satisfy the incremental stress-strain relationship, Eq. 3.12.[*] In order to satisfy Eq. 3.12, a set of stresses $\Delta\sigma_{ij}''$, Eq. 3.14, are calculated and subtracted from the elastically evaluated stress increment, Eq. 3.13. In analogy to the initial strains, the stresses $\Delta\sigma_{ij}''$ can

---

[*] The equations referred to here should be considered as applied to finite increments.

be called incremental "initial stresses." Equilibrium is restored by applying a set of loads on the structure equivalent to the incremental initial stresses. A new elastic problem is then solved with the new loading. An iterative scheme is used which consists of evaluating the initial stresses, applying the equivalent set of loads on the structure and carrying a new elastic analysis. The iterative process is continued until the set of loads equivalent to the computed incremental initial stresses become sufficiently small.

Figure 7 shows the graphical representation of the initial stress method on a two-dimensional stress plane.

The initial stress method is economical since the original stiffness matrix of the structure is not changed during the analysis. The Gaussian elimination procedure for reducing the stiffness matrix of the structure to an upper triangular matrix coefficient is performed only once. As opposed to the initial strain method, this method can be applied to materials with zero or small strain hardening, since for any state of strain the state of stress is uniquely defined.

3.6 The Incremental Load-Displacement Relationship

An incremental load-displacement relationship can be developed in conjunction with the initial stress method of plastic analysis discussed in the preceding section. The incremental strain-displacement relationship can be written on the basis of Eq. 2.33.

$$\Delta \varepsilon_{ij} = Z^m_{ijk} \Delta u^m_k \tag{3.41}$$

The incremental stress-strain relationship is given by Eq. 3.12; it can be rewritten with the help of Eq. 3.13 as

$$\Delta\sigma_{ij} = E_{ijk\ell} \ \Delta\varepsilon_{k\ell} - \Delta\sigma_{ij}^{''} \tag{3.42}$$

The incremental load-stress relationship is obtained from Eq. 3.41, using the principle of contragradience.[42]

$$\Delta P_k^m = \int_V Z_{ijk}^m \ \Delta\sigma_{ij} \ dV \tag{3.43}$$

Combining Eqs. 3.41 to 3.43, one obtains the desired incremental load-displacement relationship for an element

$$\Delta P_i^m = k_{ij}^{mn} \ \Delta u_j^n - \Delta P_i^{m''} \tag{3.44}$$

where k_{ij}^{mn} is the elastic stiffness matrix, Eq. 2.42, and

$$\Delta P_i^{m''} = \int_V Z_{jk\ell}^m \ \Delta\sigma_{jk}^{''} \ dV \tag{3.45}$$

The vector $\Delta P_i^{m''}$ is designated as the incremental initial load vector.

The incremental load-displacement relationship can be obtained by proper summation of Eq. 3.44 over all the elements in a manner similar to that discussed in Section 2.9. Using matrix notation

$$\Delta F = K \ \Delta U - \Delta F^{''} \tag{3.46}$$

The vector $\Delta F^{''}$ in Eq. 3.46 denotes the incremental initial load vector for the structure.

Equation 3.46 represents a set of nonlinear simultaneous equations. The nonlinearity stems from the fact that the incremental initial load vector $\Delta F^{''}$ is a function of the state of stress which in general does not remain constant during a loading increment.

For a given loading increment, Eq. 3.46 can be solved using a modified Newton-Raphson approach.[42] First, an approximate value for the incremental displacement vector $\Delta^\circ U$ is obtained by solving the linear equation

$$\Delta F = K \Delta^\circ U \qquad (3.47)$$

Using the approximate value of the incremental displacement vector $\Delta^\circ U$, an initial load vector $\Delta^\circ F''$ is calculated (see Eqs. 3.44 and 3.46). A linear system of equations,

$$\Delta^\circ F'' = K \Delta^1 U \qquad (3.48)$$

is solved for a set of corrections $\Delta^1 U$ in the incremental displacement vector. An incremental initial load vector $\Delta^1 F''$ is computed and another set of equations similar to Eq. 3.48 is solved. At the ith iteration, the field equation can be written as

$$\Delta^{i-1} F'' = K \Delta^i U \qquad (3.49)$$

The iterations are terminated when the incremental initial load vector $\Delta^i F''$ has become sufficiently small. The total increment in the displacement vector is given by

$$\Delta U = \sum_{r=0}^{i} \Delta^r U \qquad (3.50)$$

The same procedure is followed for the analysis of other loading increments.

Figure 8 illustrates the Newton-Raphson method schematically for a uniaxial loading.

3.7 Application to the Isoparametric Element

The iterative scheme, as explained in the preceding section, can be applied to any finite element provided a suitable way of defining the incremental initial stress field $\Delta\sigma_{ij}''$ is available. In a partially yielded element, the elasto-plastic boundary divides the element into two portions. The value of $\Delta\sigma_{ij}''$ will be zero in the unyielded portion and it will have a nonzero value in the portion which has been yielded.

The initial stress field is used in Eq. 3.45 in order to compute the equivalent nodal loads. In the isoparametric element, the volume integral on the right-hand side of Eq. 3.45 is evaluated numerically. Therefore, it is sufficient to know the value of $\Delta\sigma_{ij}''$ at the points of integration only. In order to compute the value of $\Delta\sigma_{ij}''$ at any point using the incremental form of Eq. 3.14, one needs to know both the current state of stress and the state of stress at the beginning of the loading increment. This means that the stresses must be computed at each point of integration within an element and stored for future use for each loading increment.

Computing and storing stresses for several points of integration in each element is an expensive process. Moreover, the stress field which, in this case, is defined as a function of nodal displacements within an element, is not continuous across the element boundaries. This may force some of the element boundaries to become the elasto-plastic boundaries in the continuum. Therefore, in view of these drawbacks, a "stress-interpolation" approach is employed.

In the stress-interpolation approach, it is assumed that the averaged nodal stresses are reasonably accurate representations of the state of stress at those points. It is further assumed that any stress

field can be defined as an interpolation of averaged nodal stresses in an element. Thus, a stress field can be defined as

$$\phi = N^m \phi^m \tag{3.51}$$

where

ϕ = a component of the stresses

ϕ^m = value of ϕ at the element node m

N^m = interpolation function for node m, same as the shape function used in Eq. 2.1

The state of stress is examined at each node in order to determine whether it has undergone a plastic deformation during a particular loading increment. An element is partially or fully plastic if some or all the nodes in the element have undergone a plastic deformation. For a plastic element, the incremental pseudo initial stresses are calculated at each node of the element using Eq. 3.37. The incremental pseudo initial stress field in the element is then defined according to Eq. 3.51.

$$\Delta\bar{\sigma}_{ij}^{\,\prime\prime} = N^m \Delta\bar{\sigma}_{ij}^{\,\prime\prime} \tag{3.52}$$

Similarly, the loading stress σ_c and the effective stress σ_e at any point within the element are obtained from

$$\sigma_c = N^m \sigma_c^m \tag{3.53}$$

$$\sigma_e = N^m \sigma_e^m \tag{3.54}$$

Once the incremental pseudo initial stresses, the loading stresses and the effective stresses have been computed at the integration points, Eqs. 3.52 - 3.54, the incremental initial stresses for these points can be obtained from Eqs. 3.38 - 3.40.

Having determined the incremental initial stresses at the integration points, the computation of incremental initial loads and the iterative solution of the resulting set of equations is carried out in the manner explained in Section 3.6.

3.8 Summary of the Plastic Analysis

The initial stress method has been used for analyzing the structure in the plastic range. The fundamental approach of the method has been outlined in Section 3.5. The nonlinear set of load-displacement equations has been obtained in Section 3.6. It is shown that the iterative procedure followed in the initial stress method is a modified Newton-raphson method for solving nonlinear simultaneous equations. The method is adaptable to any finite element provided a procedure is set up to define the incremental initial stress field within the element. A stress interpolation scheme is suggested in Section 3.7 for applying the method to the isoparametric element.

The computational procedure for carrying out the plastic analysis using the initial stress method is summarized below.

1. Initiation of yielding

   a. Apply the specified set of loads and determine σ_{ij} and ε_{ij}

   b. Calculate the loading stress σ_c for all the nodes. Obtain the highest value of σ_c, say $\sigma_{c/max}$. The scale factor s to initiate yielding is

$$s = \frac{\sigma_y}{\sigma_{c/max}}$$

c. Apply the scale factor to the applied loads, displacements, strains and stresses in order to determine their state at the initiation of yielding

2. Elasto-plastic analysis

a. Apply a specified fraction of the yield load as the next loading increment. Compute $\Delta\sigma'_{ij}$ and $\Delta\varepsilon_{ij}$ at all the nodes on the basis of an elastic analysis

b. Add $\Delta\sigma'_{ij}$ and $\Delta\varepsilon_{ij}$ to existing values of σ_{ij} and ε_{ij}, respectively, to obtain the current values of σ_{ij} and ε_{ij}

c. Compute the current value of the loading stress σ_c^+ and examine the state of plastic deformation at all the nodes

d. Compute the incremental pseudo initial stresses at all the nodes of the elements which have partially or fully yielded

e. Compute the incremental initial stresses $\Delta\sigma''_{ij}$ at the joints which have yielded and subtract them from the current state of stress

f. Compute the incremental initial load vector for the structure. There are three possible cases:

1) If the elements of the load vector are sufficiently small, the convergence has been achieved. Proceed with the next loading increment at step 2a

2) If the elements of the load vector are large and the specified number of iterations have not been exceeded,

carry out an elastic analysis with the initial loads.
Compute $\Delta\sigma_{ij}'$ and $\Delta\varepsilon_{ij}$. Proceed with step 2b.

3) If the loads are large but the specified number of
iterations have been exceeded, it can be assumed
that the convergence cannot possibly be achieved,
and the ultimate load has been exceeded. The
computations are terminated at this point.

Chapter 4

NUMERICAL RESULTS

4.1 General

As has been mentioned in Chapter 1, the objective of the present study is to develop a method for analyzing three-dimensional elasto-plastic structures. The finite element method of analysis, used in the present study, has been outlined in Chapter 2. A method for incorporating plastic analysis into the three-dimensional finite element has been presented in Chapter 3.

A critical examination of the method has been made from two aspects, the adequacy of the discretized model representation of the medium, and the applicability of the method of incorporating plastic analysis. Various problems have been solved in the elastic range of material behavior to examine and to demonstrate the adequacy of the finite element model. The method is then applied to solve elasto-plastic problems in order to establish the suitability of the model and the method described in Chapter 3 for obtaining solutions in plastic range.

4.2 Elastic Solutions

A variety of problems have been solved in the elastic range. Simple one and two-dimensional structures have been considered in order to compare the numerical results with the existing solutions. The hollow circular cylinder and the beam are the one-dimensional problems presented here. The rectangular plate, the Boussinesq problem and the axisymmetric pressure vessle are examples of the two-dimensional structures used in

the study. The general applicability of the model to three-dimensional structures has been demonstrated by analyzing the end slab for a pre-stressed concrete reactor vessel. This slab is a thick circular plate. A number of penetrations in the form of circular openings pass through the slab.

4.2.1 Hollow Circular Cylinder

A hollow circular cylinder with a 10-in. internal radius and a 1-in. shell thickness has been analyzed for an internal pressure of 100 psi. Due to symmetry the problem is reduced to that of a pie-shaped segment with an internal angle of 10 degrees, Fig. 9. The segment is divided into four elements. The material has a Poisson's ratio $\nu = 0$. (the analytical solution is independent of the Poisson's ratio). The radial and the circumferential stresses σ_r and σ_θ, respectively, obtained from the three-dimensional finite element solution are given in Fig. 9b. Also shown are the theoretical curves[55] given by the elasticity solution. The agreement is excellent, except at the boundaries. There, as is often true, the averaged nodal stresses are not sufficiently representative of the state of stress.

4.2.2 Beam

Elastic solutions were obtained for beams with three different thickness to span ratios. The beams are designated as EB-1, EB-2 and EB-3. The dimensions, the loading, the properties of the beams, and comparison of various solutions are given in Table 1. Each element has an intermediate node in the longitudinal and the transverse directions. Due to the flexible nature of shallow and medium thick beams, and also due to

the wide disparity in the bending, compressive and the shear stiffnesses, it was found that the solutions obtained using single precision calculations (IBM 360/75 computer) were in error. Therefore, all the beams were analyzed using double precision and a marked improvement was observed.

There are two types of classical solutions which are available for beams, viz., the simple beam solution using Bernoulli's assumption which neglects the effect of shear stresses and the normal stresses, and the theory of elasticity solution in which the beam is treated as a plane stress problem.[35] The difference in the two solutions is not very marked in the case of the beams solved in the present study. However, it can be seen from Table 1 that the numerical results of the present study lie between the two solutions. In fact, the theory of elasticity solution is exact, and the slight discrepancy in the numerically obtained results can be attributed to the finite degrees of freedom used in the finite element solutions.

4.2.3 Plate

Strictly speaking the laterally loaded plate is a three-dimensional problem of continuum mechanics. Kirchoff's assumptions make it possible, however, to treat it as a plane stress problem. A normal to the plate surface is assumed to remain normal, straight and unstrained after deformation. The plane stress assumption in effect neglects the effect of shear stresses and the transverse stresses. The discrepancy due to this assumption is negligible for medium thick and thin plates. Reissner's plate theory does take into account the effect of shear stresses and thus, is a better approximation to the real situation.

A simply supported square plate (span = 8 in., thickness = 1 in.) subjected to uniformly distributed lateral load of 1 psi is selected as the test case. Since the 8-node element can be shown to function in an excessively stiff fashion, intermediate nodes are used on both the internal and external edges. In the three-dimensional analysis, three boundary conditions are required on each edge (as also in the Reissner's plate theory), whereas an analysis based on Kirchoff's assumptions demands only two boundary conditions. The boundary conditions for a simply supported plate can be summarized as follows:

Kirchoff's Plate Theory

$$w = 0$$
$$M_n = 0 \tag{4.1}$$

Three-dimensional Analysis and the Reissner's Plate Theory

Case a

$$w = 0$$
$$M_n = 0 \tag{4.2}$$
$$\theta_{nt} = 0$$

Case b

$$w = 0$$
$$M_n = 0 \tag{4.3}$$
$$M_{nt} = 0$$

Here

w = the lateral displacement

M_n = bending moment in the plane normal to the boundary

θ_{nt} = twist along the boundary

M_{nt} = twisting moment along the boundary

It should be noted here that the Kirchoff's plate theory does not distinguish between cases a and b.

The finite element solutions obtained for case a in the present study, together with the corresponding solutions based on Kirchoff's plate theory[56] and Reissner's plate theory,[57] are given in Table 2. It is observed that the maximum bending stress is equal to one for Reissner's plate theory and that the central deflection is closer to that obtained for Reissner's theory than Kirchoff's theory. As can be seen from the results for 2 x 2 and 4 x 4 girds, the tendency is that the central deflection may eventually converge to that for Reissner's plate theory as the grid is refined.

A more detailed convergence study was made using the boundary conditions of case b. The results are given in Table 3. The maximum bending stress does not change (within three significant figures obtained) as the grid is refined. Nevertheless, the central deflection increases slightly as the grid is refined. A plot of the central deflection versus the inverse of the number of elements, Fig. 11, suggests that the central deflection should converge to 207.15/E. This is very close to the value of central deflection obtained for the 6 x 6 grid. It should be noted that the value of central deflection obtained for a 2 x 2 grid is only 2.5 percent less than the "converged" value. This indicates that even a

2 x 2 grid is a reliable model when judged on the basis of the engineering accuracy usually desired. As should be expected, due to the effect of shear stresses, the results obtained for the present study are slightly higher than those obtained by Kirchoff's plate theory.

The foregoing solutions for the plate were obtained using 20-node elements (8 corner nodes, 12 intermediate nodes--one on each edge). Such a model make it possible to solve plate problems without making any simplifying assumptions. If the intermediate nodes in the direction of the thickness are omitted, one of Kirchoff's assumptions, i.e., the normals remain straight after deformation is satisfied. The other two assumptions, the normals remain normal and unstrained cannot be applied to the three-dimensional element in its present form. The 16-node element that results from dropping the intermediate nodes at mid-depth was used to solve the same plate problem (case b). The results obtained by using the element and the 20-node element, together with the results obtained by Kirchoff's plate theory for Poisson's ratios of 0.0 and 0.3, are given in Table 4. It should have been expected that the central deflection for the 16-node element would be between that obtained for the 20-node element and Kirchoff's plate theory. On the contrary, for a Poisson's ratio of 0.3, the central deflection obtained for the 16-node element is nearly 5 percent less than that for Kirchoff's plate theory. No improvement is achieved by refining the grid.

For the 16-node element, the computed values of σ_z, for nonzero values of Poisson's ratio were grossly in error (they were very close to the applied external stresses in the case of 20-node element). The error is even more pronounced for higher Poisson's ratios. Even though the effect of shear stresses tend to make the plate more flexible, it can be

shown that the error in σ_z results in a stiffer plate and therefore, in smaller displacements.

Whereas the preceding explanation seems to be satisfactory, it does not support the use of 16-node element in the plate analysis. Only a 20-node three-dimensional isoparametric element can be used for this purpose. A better alternative is to use the superparametric element,[58] which is formulated on the basis that a state of plane stress exists in the plate (or shell).

4.2.4 Boussinesq Problem

The Boussinesq problem, solved in the present study, consists of a semi-infinite body subjected to a normal concentrated load on the boundary. Using Saint-Venant's principle,[55] the stress distribution in the neighborhood of the concentrated load can be determined by considering a finite portion of the semi-infinite body. The body thus considered can be of any shape. In the present analysis two shapes, a rectangular prism and a cylinder, are considered. Due to symmetry, only one-fourth of the prism is considered, Fig. 12a. In the case of the cylinder, an axial pie-shaped segment with a small internal angle (10 degrees) is analyzed, Fig. 12b. The finite element grids for the two idealized structures are shown in Figs. 12c and 12d, respectively.

A plot of vertical stresses at various depths obtained from the finite element solution together with the analytical curves[55] are shown in Fig. 13. Even with the steep gradient of displacements and stresses near the axis of the concentrated load, and the relatively small number of elements used in the idealization of the problem, the agreement between the numerical results and the analytical solution is fairly good. A

direct comparison of displacements is not possible since a correction is required to account for the fact that the base of the region does not extend to infinity.[41]

4.2.5 Axisymmetric Pressure Vessel

Pressure vessels and concrete reactor vessels are used for storing gas, and housing of nuclear reactors. Various kinds of vessels have been employed in practice. The one analyzed for the present study consists of a cylindrical barrel enclosed by thick flat slabs.

A section of the pressure vessel together with the finite element grid used in the analysis are shown in Fig. 14. Since the vessel is axisymmetric, only a pie-shaped sector with an internal angel of 10 degrees is considered. The numerical results obtained by the present study are compared with those obtained by Mohraz and Schnobrich,[59] Figs. 15, 16, and 17. In general, the agreement is excellent. The dimensions, the material properties and the loading are also given in the figure.

4.2.6 Prestressed Reactor Vessel with Circular Openings in the Slabs

The axisymmetric pressure vessel solved in Section 4.2.5 is an idealized representation of the pressure vessels used in practice. As mentioned in Chapter 1, for access to the enclosed space of the vessel, openings are provided in various locations. The vessel analyzed here consists of the same structural elements as the one solved in the preceding section, except that it has circular openings in the top slab, Fig. 18. The loading consists of an internal pressure of 3000 psi, a longitudinal prestressing load of 26,000 psi distributed over the top of the cylinder, and a circumferential prestressing load of 1200 psi applied around the

outer surface. The stiffness of the prestressing cables have been neglected since its effect on the stress distribution in the slabs is negligible. Since this example was selected to be similar to a specimen from a test series,[60] and since those test specimens had a cover over the penetrations to prevent pressure leaking out or even into the openings, the example presented here also has such a lid or cover over the hole. The internal pressure on that lid over the opening is transferred to the edge of the opening as a line load. However, it was found during the study that a line load on the edge of the free surface (i.e., the cylindrical surface of the opening) is non-unique in the sense that the same set of generalized loads can be obtained through other distribution of loads. This can be explained with the aid of Fig. 19b which shows an enlarged view of an element at the opening. The line load applied on the edge AB is transformed into general-ized loads at the nodes on the edge. The same set of generalized loads can be obtained for both a linearly distributed normal load on the face ABCD, and a linearly distributed tractive load (shear) on the face ABFE. The non-uniqueness in loading results in a numerical solution which does not satisfy the free stress condition on the cylindrical boundary. To overcome the situation, the edge load is distributed uniformly on the bottom faces of the elements around the opening, for example, on the face ABCD of the element shown in Fig. 19b. In this manner, a much better satisfaction of the stress boundary condition is achieved.

The distribution of radial stress as calculated by the present finite element solution is shown in Fig. 20 for stress at the top and bot-tom of the slab for two different section lines, one through the hole and the other midway between holes, with and without openings. A similar plot for the circumferential stress is presented in Fig. 21. At points of

discontinuity along a radial line passing through the center of the opening, the radial stresses become negligible (nearly zero) and the circumferential stresses tend to be very large (theoretically, they can be infinite). As should be expected, the radial stress approaches infinity at the inside junction of the slab to the cylinder. In Fig. 21, it is seen that the circumferential stresses "oscillate" in a region near the opening. This phenomenon is due to the readjustment of stresses around the opening, and the resulting inability of the neighboring regions to take sufficient stress in the circumferential direction. Figure 22 shows the distribution of tangential stress around the opening. It should be noted that all the curves in Figs. 20, 21, and 22 have been obtained by "smoothing" the points given by the numerical solution.

One of the purposes of analyzing the prestressed reactor vessel with openings in the end slab is to show the applicability of the three-dimensional isoparametric element to a real three-dimensional problem. Although comparison of results was not possible because of the unavailability of an existing solution, the plausible nature of results for this problem and the close agreement with the existing solutions for other problems, substantiate the adequacy of the model.

4.3 Elasto-Plastic Solutions

As in the case of elastic solutions, the first few problems solved in the elasto-plastic range are those for which there are existing solutions, and therefore, a comparison can be made. The thick hollow circular cylinder, the beam, and the circular plate are problems in this category. A thick circular plate with openings is the three-dimensional problem solved.

4.3.1 Thick Hollow Circular Cylinder

A hollow circular cylinder with internal and external radii of
10 in. and 20 in., respectively, has been analyzed under increasing inter-
nal pressure. As in the case of the elastic analysis (Section 4.2.1)
only a pie-shaped segment is considered. Eight elements, each with inter-
mediate nodes sufficient to allow a quadratic variation of displacements
in the radial direction were used.

The numerical results obtained from the present study together
with the finite difference solution[1] are shown in Figs. 23 to 25. It is
seen from the load-displacement curve, Fig. 23, that the present study
indicates a slightly stiffer structure in the plastic range than does the
corresponding finite difference solution. The distribution of radial,
circumferential, and axial stresses through the thickness for a case in
which the plasticity has propagated to a radius of 1.4 times the internal
radius is shown in Fig. 24. This case corresponds to an internal pressure
of 1.57 times the pressure corresponding to the initiation of yielding.
The variation of radial and circumferential stresses at a section 1.4 times
the internal radius is shown in Fig. 25 for an increasing internal pres-
sure.

Even with eight elements, the agreement between the results of
the present study and those obtained using finite differences, as is evi-
dent in Fig. 23 to 25, is very good. Slight discrepancy between two solu-
tions exists at higher load levels. This discrepancy may be overcome by
using higher numbers of elements.

4.3.2 Beam

A simply supported, moderately deep beam with a 32-in. span
and a 4-in. depth has been analyzed. It is assumed that one-half of the
total uniformly distributed load has been applied on both the top and the
bottom surfaces. This makes it possible to consider only one-fourth of
the beam in the analysis, OACB in Fig. 26. This portion has been divided
into 64 elements, 16 along the half span OA, and 4 along the half depth
OB. All the elements have one intermediate node in the longitudinal direc-
tion and none in the lateral direction. As in other examples, it has been
assumed that the strain hardening coefficient is zero.

The theoretical elasto-plastic boundary (obtained by equating
the static moment and the moment of resistance of any section) for three
load levels, 1.22, 1.32 and 1.36 times the yield load, are presented in
Fig. 26. Also shown are the nodes and the element centroids which have
reached yielding according to the present study (shown by solid circles)
and those which should have yielded but did not do so (shown by solid
squares). For a load level of 1.22 times the yield load, all the nodes
and element centroids within the theoretical plastified region have
reached yielding. However, a few nodes and element centroids did not
reach yielding at load levels equal to 1.32 and 1.36 times the yield load.
It is seen from Fig. 26 that the discrepancy lies in the lateral direc-
tion rather than in the longitudinal direction. This means that the plasti-
fication into the depth is taking place at a slower rate, whereas the outer
fibers reach yielding almost at the same load level as that predicted by
the theoretical analysis. The reason for the disparity is that as the
plastification propagates deeper into the depth, the stress gradient along

the depth becomes very steep and the method of stress interpolation, Section 3.7, is in error. This can be explained further with the aid of Fig. 27, which shows the possible stress distributions along the depth in two elements, one adjoining the neutral axis, element I, and the other adjoining the outermost surface, element IV, during the application of a particular load step. Stress distribution 1, ABCD, is the possible stress distribution at the beginning of the load increment. It is assumed that the maximum stress AD has already reached the yield stress σ_y. Stress distribution 2, ABC'D', is obtained after carrying on an elastic analysis for the load increment. The region DED' represents the distribution of initial stress. In the stress distribution 3, ABC'ED represents the distribution of stress after the initial stress has been subtracted. However, since only the nodal stresses are stored and the stress distribution within the element is defined using the Lagrangian interpolation, the method computes the stress distribution as represented by ABC'D, which results in a "loss" of stresses shown by the triangle DC'E. The loss is more pronounced in case of element I which has a much steeper stress gradient than in case of element IV where the stress gradient is not so steep. It is apparent that the phenomenon of slow penetration of yielding through the depth is caused by the loss of stresses with the present method of interpolation. One possible solution is to use finer grid in the direction of the steep stress gradient.

Figure 28 shows the load-displacement curve for the beam under consideration. The solid curve is based upon the numerical values up to 1.4 times the yield load, beyond which the curve has been extrapolated and joined tangentially with the ideal hinge curve. It can be observed that beyond the load level of 1.4 times the yield load, the numerical results

predict that the structure is overstiff. This can again be explained on the basis of underplastification through the depth due to the stress loss discussed previously.

4.3.3 Circular Plate

A clamped circular plate (20 in. in diameter, and 1-in. thickness), subjected to a uniformly distributed lateral load has been analyzed. A Poisson's ratio of 0.24 and the strain hardening coefficient of zero have been assumed. This problem is the same as the one solved by Popov and Khojesteh-Bakht.[13] Due to the axisymmetric nature of the problem, only a pie-shaped segment is considered.

Chronologically, this problem was solved (for the present study) before studying in detail the phenomenon of the loss of stresses in the beam under steep gradient, which is characteristic of bending problems (see preceding section). The plate was divided into a relatively fewer number of elements, 5 elements in radial direction and 4 elements through the total thickness (2 elements on each side of the middle surface), Fig. 29a. With the present method of stress interpolation, this discretization is rather crude and the results can only be viewed on a qualitative basis.

Figures 29b and c show the plastified regions obtained from the nodes and the element centroids at load levels of 1.3 and 1.5 times the yield load, respectively. It is expected that the propagation of the plastic region towards the middle surface is slow and some stress losses have occurred, as in the case of the beam. The load displacement curve obtained from the present study and the corresponding one reported by

Popov and Khojesteh-Bakht[13] are shown in Fig. 30. The deviation of the two curves is noticeably marked as expected, because in the latter solution, the plate has been divided into a 20 x 40 grid (40 elements through the depth), as compared to a 5 x 4 grid in the present study. Popov and Khojesteh-Bakht have reported their results up to 1.77 times the yield load and the collapse does not take place within this range. The collapse load obtained by the present numerical solution is about 1.93 times the yield load. An approximate value for the collapse load can be obtained using the yield line theory. According to the yield line theory, the collapse load is given by

$$q_c = \frac{12m_p}{a^2} = 3 \left(\frac{h}{a}\right)^2 \sigma_y \qquad (4.12)$$

where

m_p = the fully plastic moment

h = thickness of the plate

a = radius of the plate

The load at the initiation of the yield can be obtained by applying the von Mises yield criterion to the radial and circumferential stresses at the fixed support given by Timoshenko.[54] Thus, the yield load is

$$q_y = 8.85 \frac{m_y}{a^2} = 1.48 \left(\frac{h}{a}\right)^2 \sigma_y \qquad (4.13)$$

where m_y is the yield moment. Equations 4.12 and 4.13 give

$$q_c = 2.03 q_y \qquad (4.14)$$

Despite the few number of elements used and the approximate manner in which the stress interpolation is carried out, the predicted collapse load by the present study is close to that obtained by yield

line theory. Interestingly enough, it is also closely within the concept of lower bound on the collapse load as suggested by Zienkiewicz, et al.[54]

4.3.4 Thick Circular Plate with Circular Openings

The thick circular plate with openings is an example of a three-dimensional problem. The plate solved for the present study has a radius of 14 in. and a thickness of 6 in. There are six circular openings, 2 in. in radius, with their centers placed symmetrically at a distance of 9 in. from the center of the plate, Fig. 31. The inside surface of the plate is subjected to an increasing uniformly distributed load. Due to symmetry a pie-shaped segment has been considered for the analysis.

Like in the circular plate without openings, this problem was also solved in time before carrying out the detailed study of the beam. Therefore, the finite element idealization of the structure, shown in Fig. 31, is too coarse for a plastic analysis, and the results should be viewed in a qualitative rather than quantitative manner.

Figure 32 shows the plastified regions in the structure at 1.75 and 1.95 times the yield load. The boundaries of plastified regions were drawn by enveloping the plastified nodes and element centroids obtained from the numerical solution. There are two imminent modes of failure for such a plate. One possibility is that the plate fails in flexure in a manner similar to that predicted by the yield line theory. This possibility is suggested by the spread of plastified region in the neighborhood of the support near the top and the bottom surfaces. The other possibility is a shear type failure in the neighborhood of the opening. An examination of the yielding sequence reveals that the yielding is

initiated at a point on the middle surface in the opening. At a load level equal to 1.75 times the yield load, the plastified region at the opening has penetrated deeper into the thickness than that near the support. At a load level equal to 1.95 times the yield load, the region near the opening has experienced a complete plastification through the thickness. In addition, a small zone near the center of the plate has undergone plastic action and the plastified region near the support has spread, Fig. 32. Although due to the crude idealization of the structure, one cannot ascertain the actual mode of failure, it is probable that a shear type mode of failure can develop for the problem considered.

Chapter 5

CONCLUSIONS AND RECOMMENDATIONS FOR FURTHER STUDIES

5.1 General

As has been mentioned in Section 4.1 of the preceding chapter, there are two aspects to the present study. One is to establish a suitable discrete model for the three-dimensional analysis. This is important since an appropriate model is needed to predict satisfactorily the response of the structure. The other aspect of the study is the development of a method for plastic analysis of three-dimensional structures. Both these aspects are discussed individually in the following sections.

5.2 Adequacy of the Model

The finite element method of analysis in conjunction with the three-dimensional isoparametric element has been used in this study. A measure of the adequacy of model representation of the continuum has been established by obtaining numerical solutions to a variety of problems in the elastic range of material behavior.

A fairly good degree of accuracy can be achieved in many problems even by using relatively few number of elements. As few as four elements have been used for solving the hollow circular cylinder and the plate problem. The convergence study on the plate problem reveals that the central deflection obtained by using four elements is only 2.5 percent less than the "converged" value. Even for a truly three-dimensional problem, the prestressed reactor vessel with circular openings in the slab, 48 elements were used and a satisfactory solution was obtained.

The use of intermediate nodes makes it possible to approximate the curved geometric boundaries and to idealize the regions of high stress gradient more accurately. Since the intermediate nodes can be included on any edge of the element by choice, uneconomical use of these nodes can be avoided in the regions where the curved boundaries or a sharp stress gradient do not exist. This flexibility adds to the versatility of the element.

One class of problems, in which intermediate nodes are advantageous to use, is that of bending problems. For instance, for plate bending problems, the 20-node element (8 corner nodes, 12 intermediate nodes-- one on each edge) works very efficiently. In medium thick plates, it is usually sufficient to use only one element through the thickness of the plate. A 16-node element (without intermediate nodes in the direction of the thickness) is not suitable for plate bending, when only one element is used through the thickness. This is because the values of transverse stresses obtained by such an idealization are, in general, grossly in error and result in a stiffer structure.

The axisymmetric pressure vessel and the prestressed reactor vessel with openings in the slabs are the examples of bending problems with relatively large shear stresses in the slabs. In order to obtain a more accurate distribution of shear stresses, more than one element is needed through the thickness of the slab. For such cases, it is not necessary to provide intermediate nodes in the direction of the thickness. As is well known, using less number of intermediate nodes reduces the band width.

5.3 Plastic Analysis

The initial stress method in conjunction with a Lagrangian stress interpolation approach has been used for the elasto-plastic analysis. Applicability of the method is demonstrated on the basis of the excellent agreement obtained between the numerical solution and the existing solution in case of the thick hollow circular cylinder.

For bending problems, the results obtained from the present study are not in as good an agreement with the available solutions as those for the thick hollow circular cylinder. The method does not allow the plastification to penetrate deep enough into the depth as the load is increased beyond the initiation of yielding. This is evidenced from the load-displacement curves, which show that the structure is not sufficiently flexible in the plastic range. A detailed study was made in case of a beam to determine the cause for slow penetration of the plastified region through the depth. It was found that after the structure is partially yielded, a loss of stresses takes place in the critical region as the increments of load are applied. This loss in stresses is more pronounced when the stress gradient is steep. As a possible solution of this problem, it is suggested that a finer grid should be used in the direction of the steep stress gradient.

In the case of the beam, a relatively fine grid has been used through the depth. The numerical results obtained are comparatively better in the initial stages of plastification, where the stress gradient is not so steep. However, as the plastic region penetrates into the depth, the elements near the middle surface have a very steep stress gradient and thus a large stress loss. A deep plastification through

the depth cannot be reached with the number of layers which were used in this study. A much finer grid is needed.

The circular plates (with and without openings) were analyzed before a detailed study for the stress losses was made for the beam. Therefore, the finite element grids used for these problems are rather coarse, and the results obtained can be viewed only qualitatively. Despite the crude idealization for the circular plate without openings, it is seen that the collapse load obtained numerically by the present study is very close to that computed on the basis of the yield line theory.

The present method gives a clear indication of the possible modes of failure for the thick circular plate with openings. Although the actual mode of failure cannot be ascertained with confidence due to the coarse discretization, the numerical results indicate that a shear rather than a flexural type failure is more imminent. This possibility is of particular interest because such a failure is caused by the presence of the openings and the effect of shear stresses. Therefore, an idealized analysis which would neglect either the presence of the openings or the effect of shear stresses is likely to be grossly in error.

5.4 Recommendations for Further Study

In future studies, different methods of defining the stress field within an element, which would eliminate the stress loss in the plastic range, should be investigated. One possible approach is that of defining the stresses at the integration points, Section 3.7. A drawback of such an approach will be the large amount of computational effort and input-output operation (or the core storage) involved in computing and storing

the stresses at several points of integration. It may be possible to make some savings in this respect if a lower order Gaussian quadrature can be used. This possibility should be investigated.

Other methods of elasto-plastic analysis in conjunction with the three-dimensional isoparametric element should also be investigated. The initial strain method can be used for the materials having a pronounced degree of strain hardening. The tangent stiffness method can be used for elasto-plastic materials with or without strain hardening. The use of reduced order of integration, for computing stiffness matrices, has been suggested by Zienkiewicz, Taylor and Too.[61] The concept of reduced integration in computing the tangent stiffness matrix should be studied. If this is possible, the computational effort involved in modifying the equations of equilibrium for each loading increment in the plastic range of material behavior will be greatly reduced, which may favor the use of the tangent stiffness method.

The efficiency and the versatility of the isoparametric element is well established in the elastic range of material behavior. Such a conclusion cannot be drawn for the plastic analysis. It is much simpler to apply the concepts of plastic behavior to the constant strain tetrahedron. A comparative study between the three-dimensional isoparametric element and the constant strain tetrahedron should be made to determine the relative efficiency and accuracy of these elements in obtaining solutions in the plastic range.

Table 1

Comparison of the Results of Analysis of the Simply Supported Beams

Desig- nation	h	a	q	n	Present Study		Simple Beam Theory		Theory of Elasticity[55]	
					Ew	σ	Ew	σ	Ew	σ
EB-1	1.0	40.0	40.0	10	80.0	24.0	80.0	24.0	80.1	24.0
EB-2	1.0	20.0	40.0	5	5.01	6.01	5.00	6.00	5.02	6.00
EB-3	2.0	20.0	40.0	5	0.635	1.51	0.625	1.50	0.637	1.50

h   =   thickness of the beam in inches

a   =   span of the beam in inches

q   =   load in lbs per inch

n   =   number of elements in the half span

E   =   modulus of elasticity in psi

w   =   midspan deflection in inches

ν =   Poisson's ratio = 0

σ   =   maximum bending stress at midspan in psi

Table 2

Comparison of Results of Analysis of the Simply
Supported Plate (Case a, Section 4.2.3)

Solution	Ew	
Present study, 2 x 2 grid	189	18.5
Present study, 4 x 4 grid	190	18.5
Kirchoff's Plate Theory[56]	182	18.4
Reissner's Plate Theory[57]	194	18.5

```
Span            =  8 in.
Thickness       =  1 in.
Lateral load    =  1 psi
Poisson's ratio =  0.3


E =  modulus of elasticity in psi
w =  central deflection in inches
  =  maximum bending stress at
     the center of the plate in psi
```
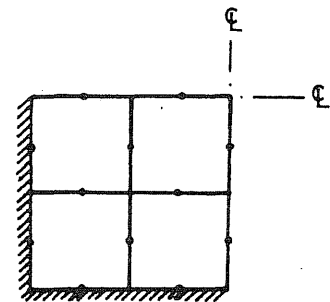

2 x 2 Grid
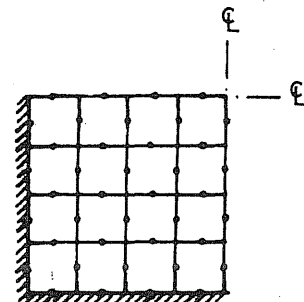
4 x 4 Grid

Table 3

Convergence Study for Simply Supported Plate (Case b, Section 4.2.3)

Present Study		Grid Size					Convergence Study,
Kirchoff's Theory[56]		2 x 2	3 x 3	4 x 4	5 x 5	6 x 6	Figure 9
Ew	182	202	205	206	206	207	207.15
σ	184	19.7	19.7	19.7	19.7	19.7	---

2 x 2 Grid   3 x 3 Grid   4 x 4 Grid   5 x 5 Grid   6 x 6 Grid

Span	= 8 in.	E =	modulus of elasticity in psi
Thickness	= 1 in.	w =	central deflection in inches
Lateral load	= 1 psi	σ =	maximum bending stress at the
Poisson's ratio	= 0.3		center of the plate in psi

Table 4

Comparison of Results of Analysis
of the Simply Supported Plate (Case b,
Section 4.2.3) using 16-Node Elements

Solution	$\nu = 0.0$		$\nu = 0.3$	
	Ew	σ	Ew	σ
Kirchoff's plate theory[56]	199	14.2	182	18.4
Present study, 20-node element, 2 x 2 grid	230	15.6	202	19.7
Present study, 16-node element, 2 x 2 grid	230	15.6	168	21.6

Span   = 8 in.
Thickness = 1 in.
Lateral load = 1 psi

E = modulus of elasticity in psi
ν = Poisson's ratio
w = central deflection in inches
σ = maximum bending stress at the
center of the plate in psi

2 x 2 Grid

Section AA
20-Node Element

Section AA
16-Node Element
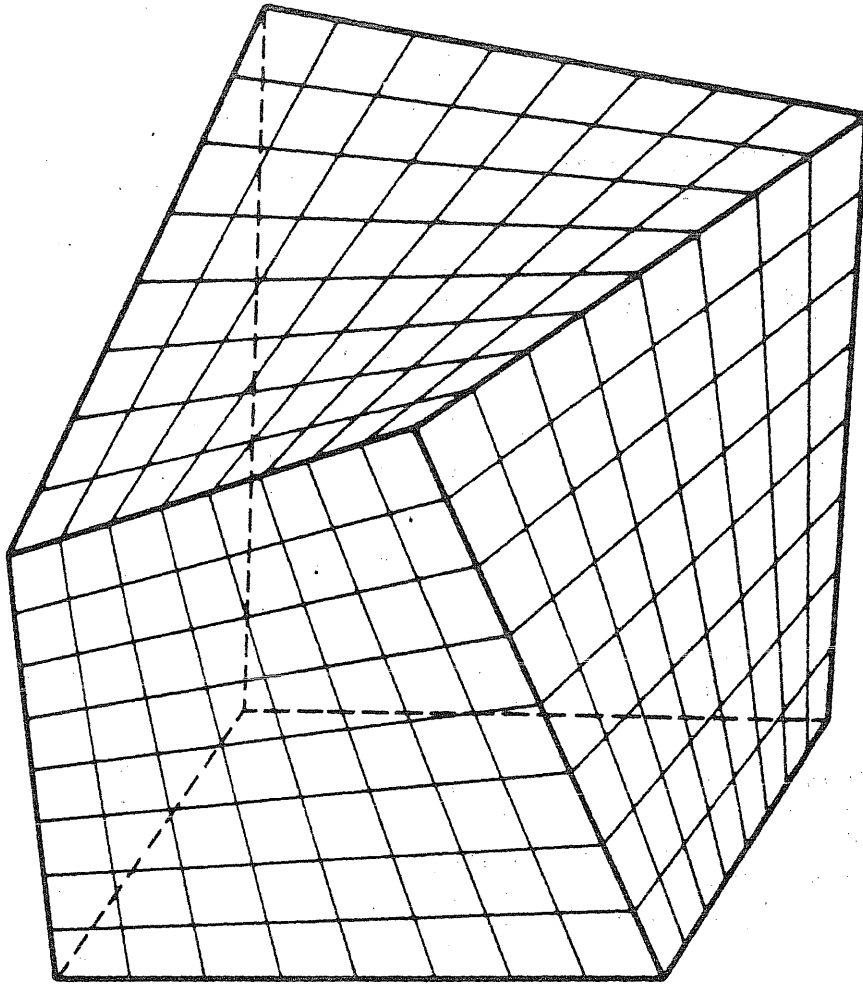
Figure 1.   Eight-Node Isoparametric Element
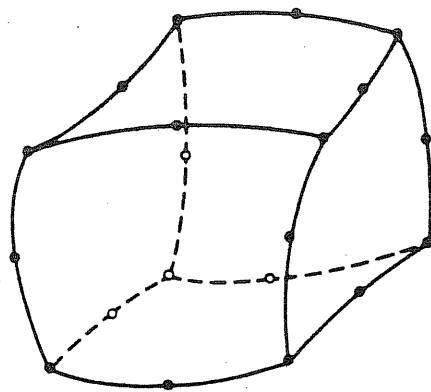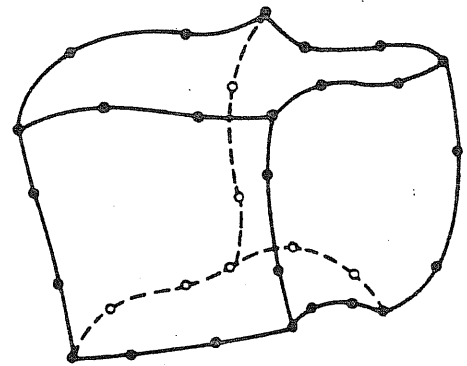
(a) 20-Node   (b) 32-Node

Figure 2.   Higher Order Isoparametric Elements
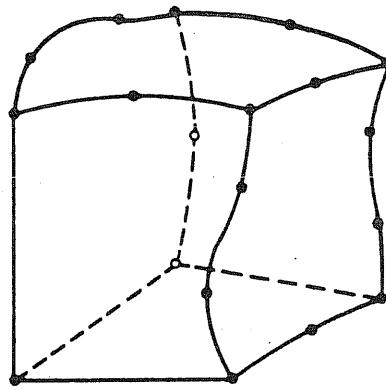
Figure 3.   A Mixed Isoparametric Element

$\xi_2 = \pm 1$, $\xi_3 = \pm 1$

(a) Linear
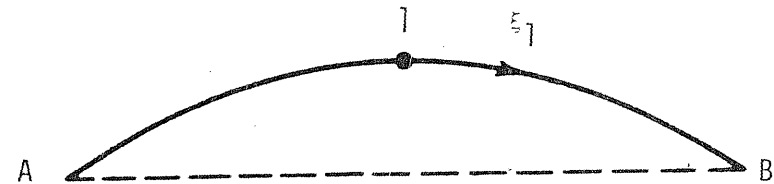
(b) Quadratic
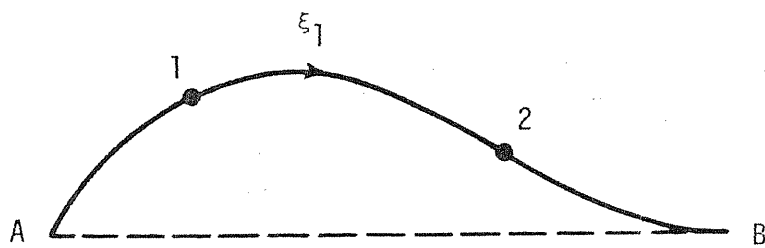
(c) Cubic
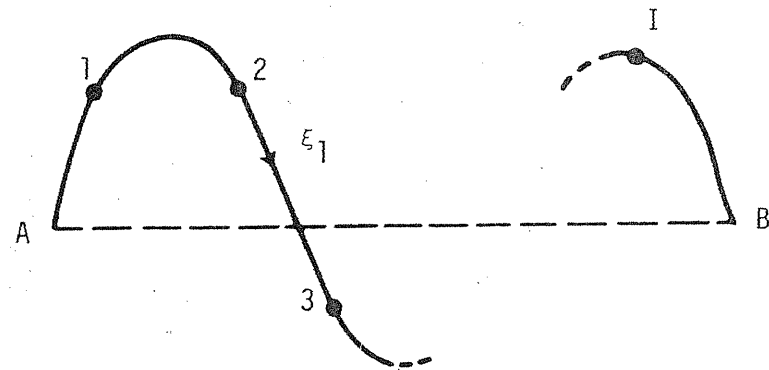
(d) I + 1 Degree

Figure 4. A Typical Edge AB Under Varying Degree of Responses

(a) Inclined Boundary

Boundary Constraint Equation

$$\overline{U}_1 = \overline{U}_2 \cot \theta$$

$$u_1^t = -u_1^b$$
$$u_2^t = -u_2^b$$
$$u_3^t = -u_3^b$$
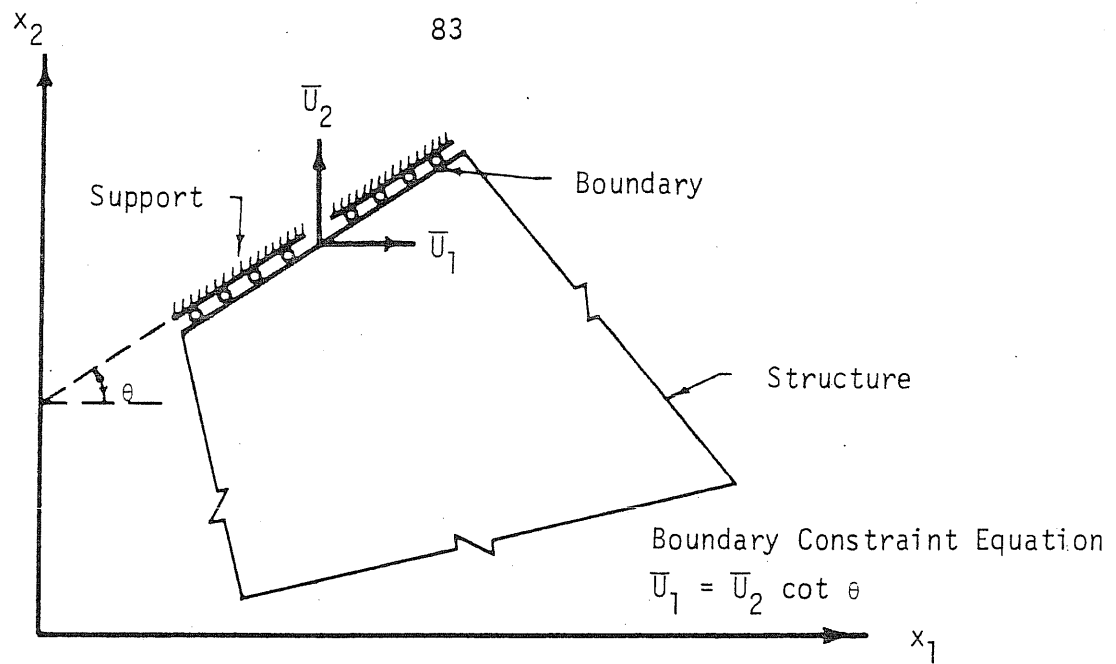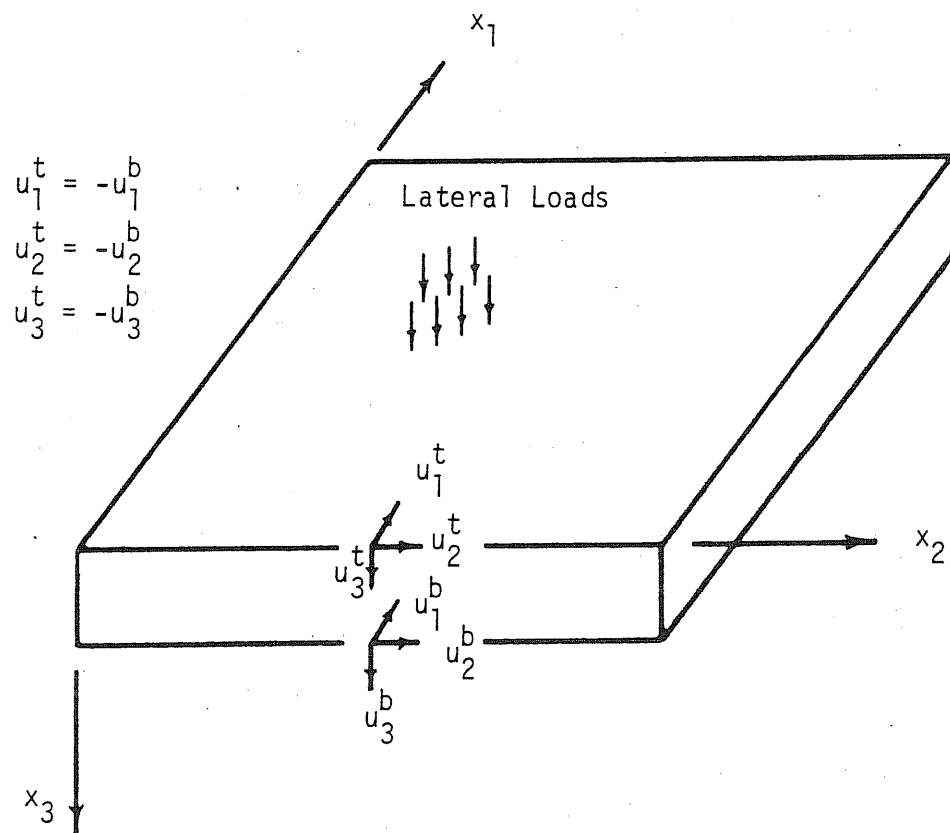
(b) Auxiliary Constraints for a Typical Plate

Figure 5.   Two Types of Displacement Constraints

$$\sigma_y = \text{yield stress}$$
$$\sigma_e = \text{effective stress}$$
$$\sigma_e = \sigma_y \text{ for } \sigma \leq \sigma_y$$
$$\sigma_e = \sigma \text{ for } \sigma > \sigma_y$$
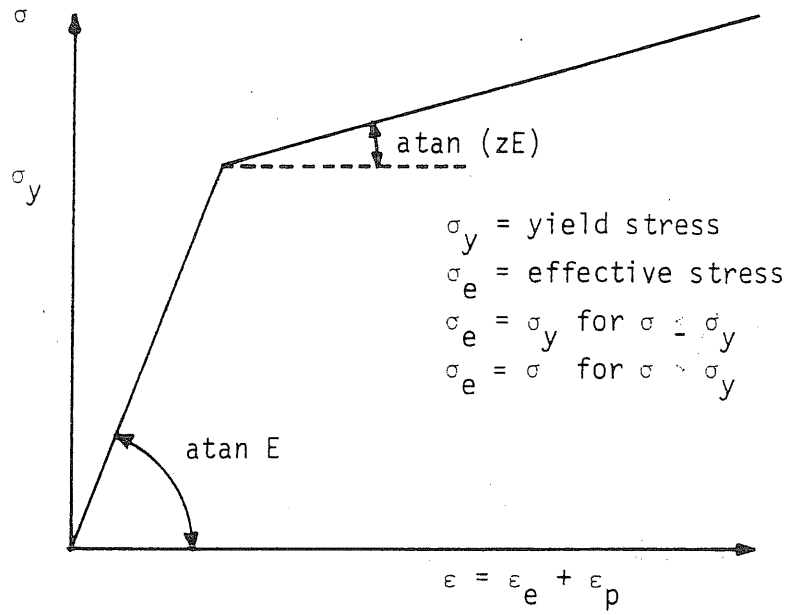
Figure 6. Bilinear Stress-Strain Curve for Uniaxial Loading
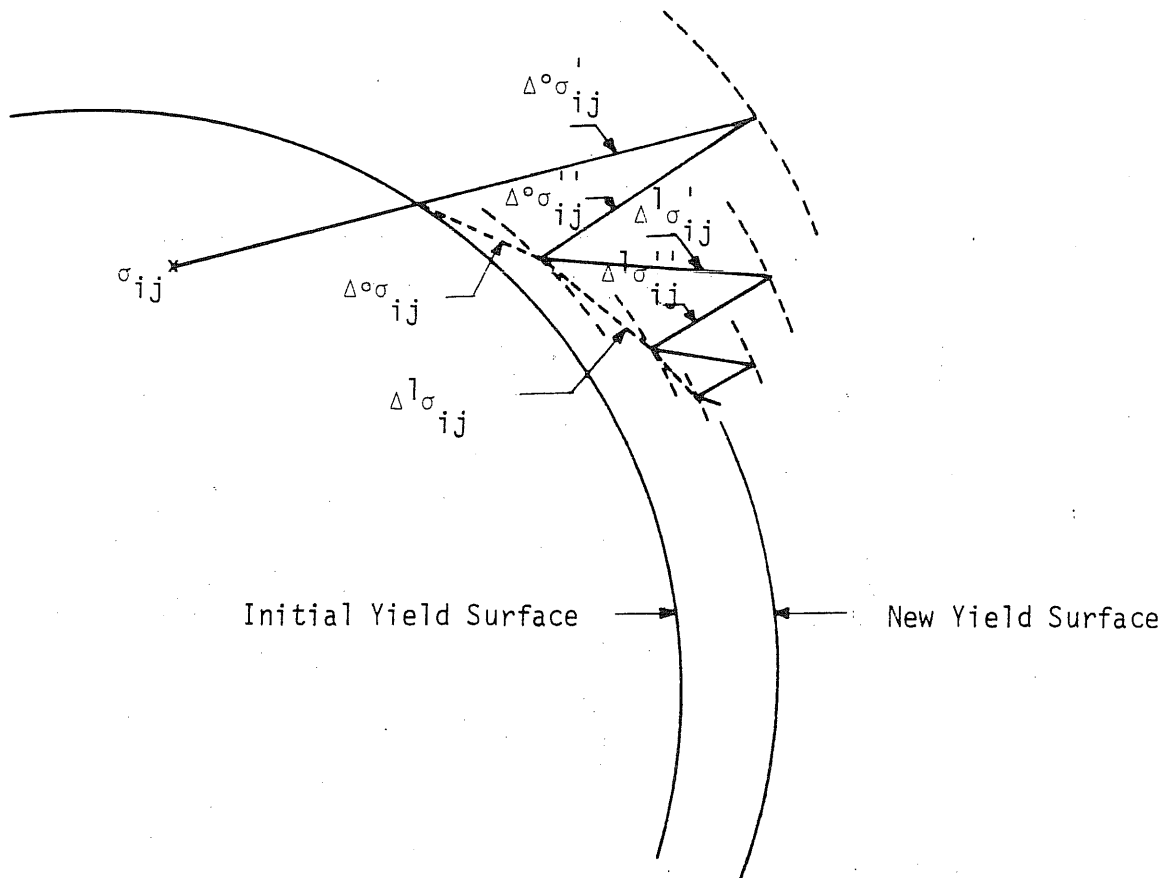
Figure 7. Graphical Representation of the Initial Stress Method
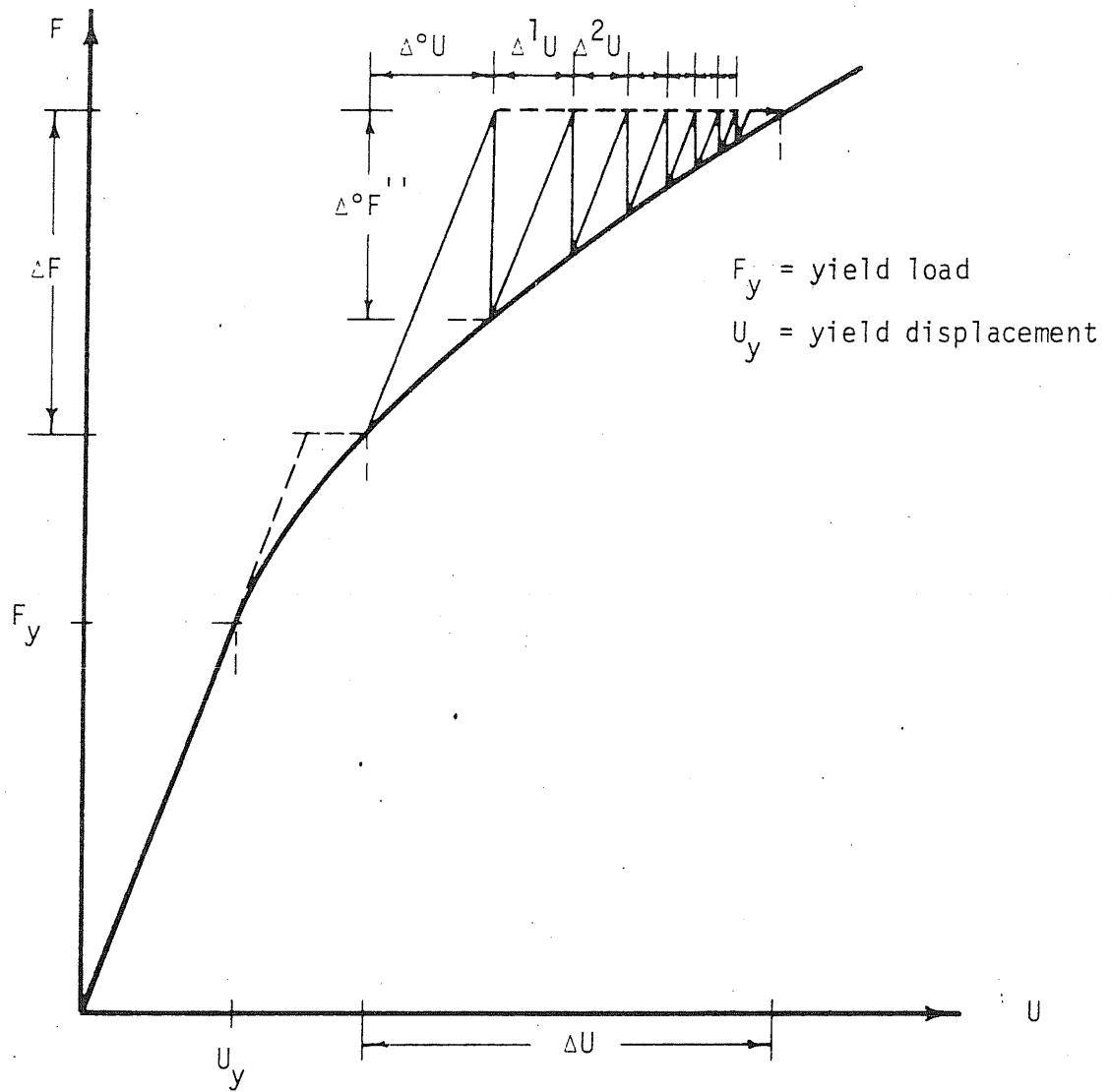
Figure 8.   Modified Newton-Raphson Approach for Elasto-Plastic
Analysis Under Uniaxial Loading

Poisson's Ratio = 0.0

10°

Radius 10"

1"
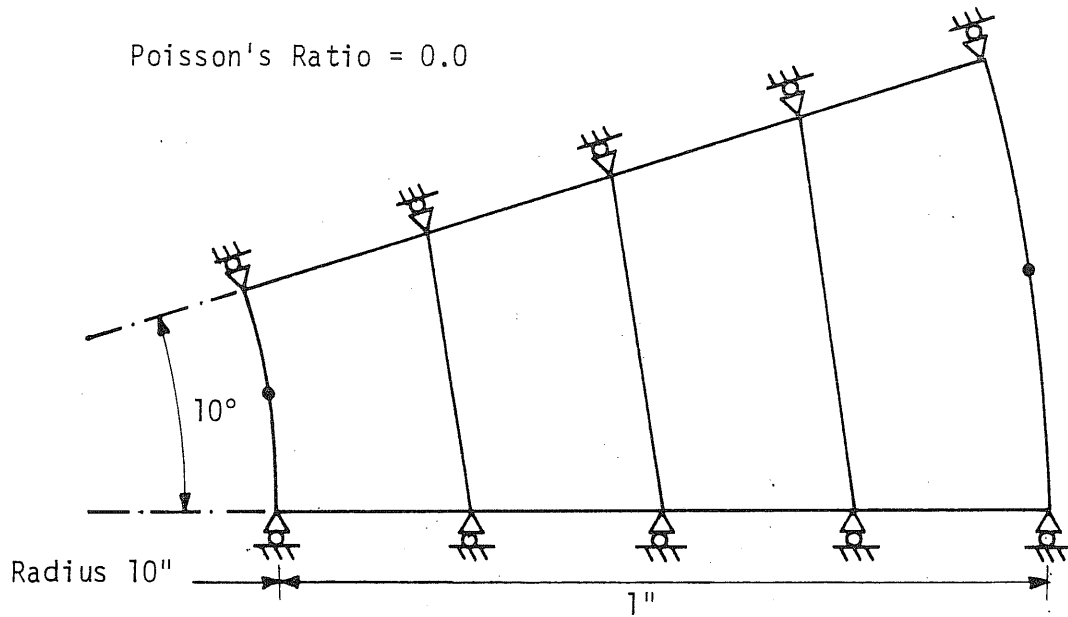
(a) Transverse Section

0.25" 0.25" 0.25" 0.25"
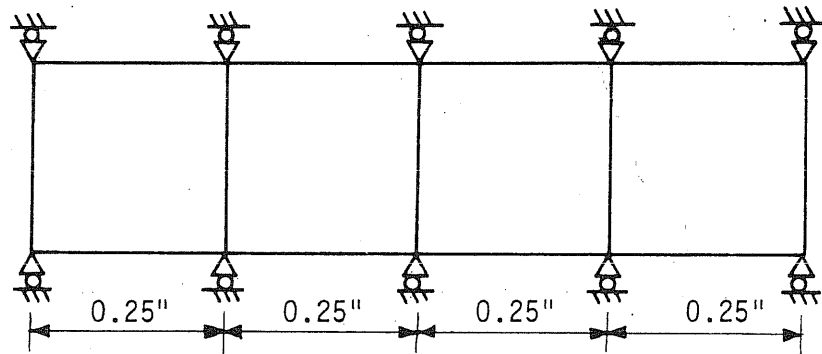
(b) Axial Section

Figure 9.   Finite Element Grid for the Hollow Circular
             Cylinder
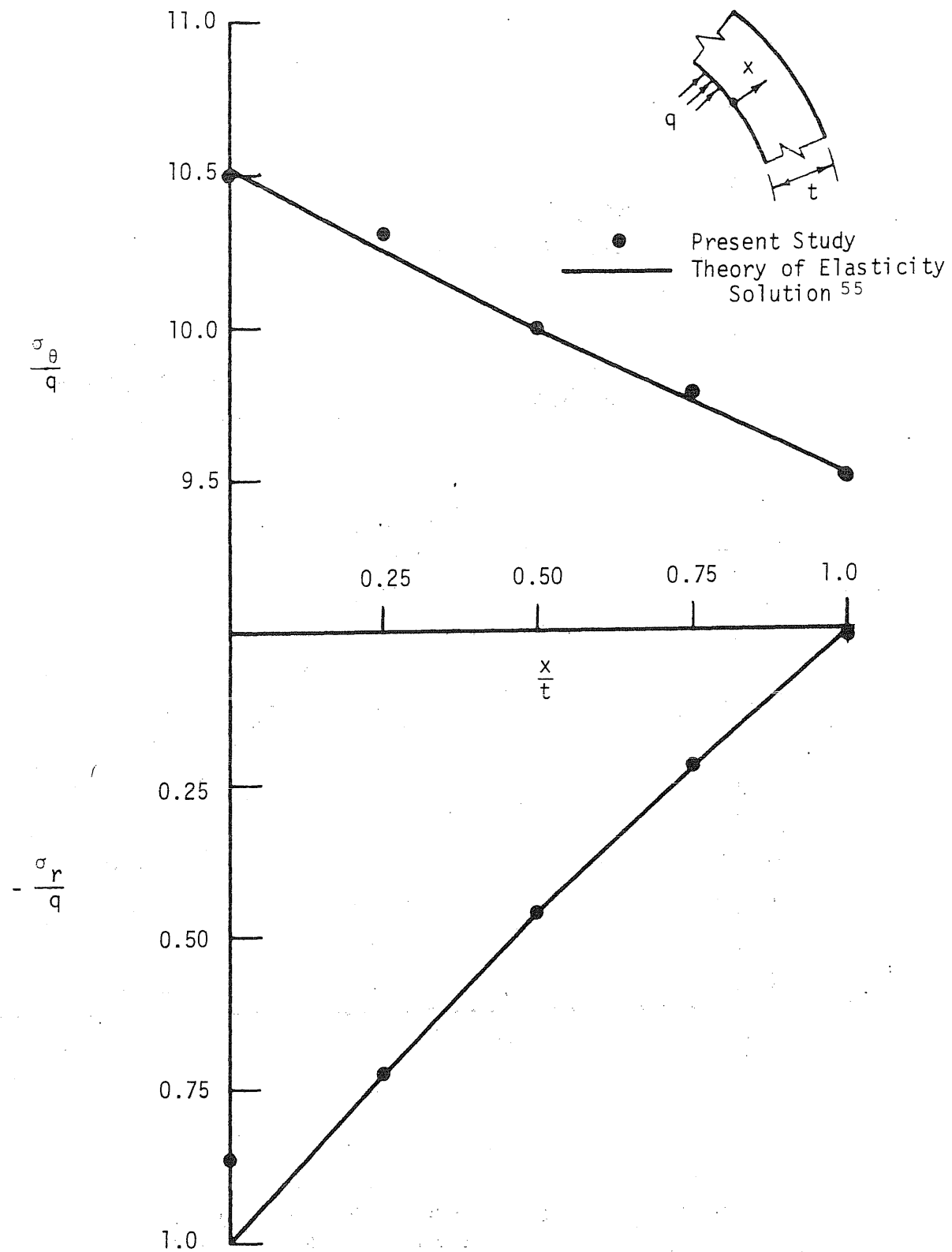
Figure 10. Distribution of Radial and Circumferential
Stresses in an Infinitely Long Hollow
Circular Cylinder
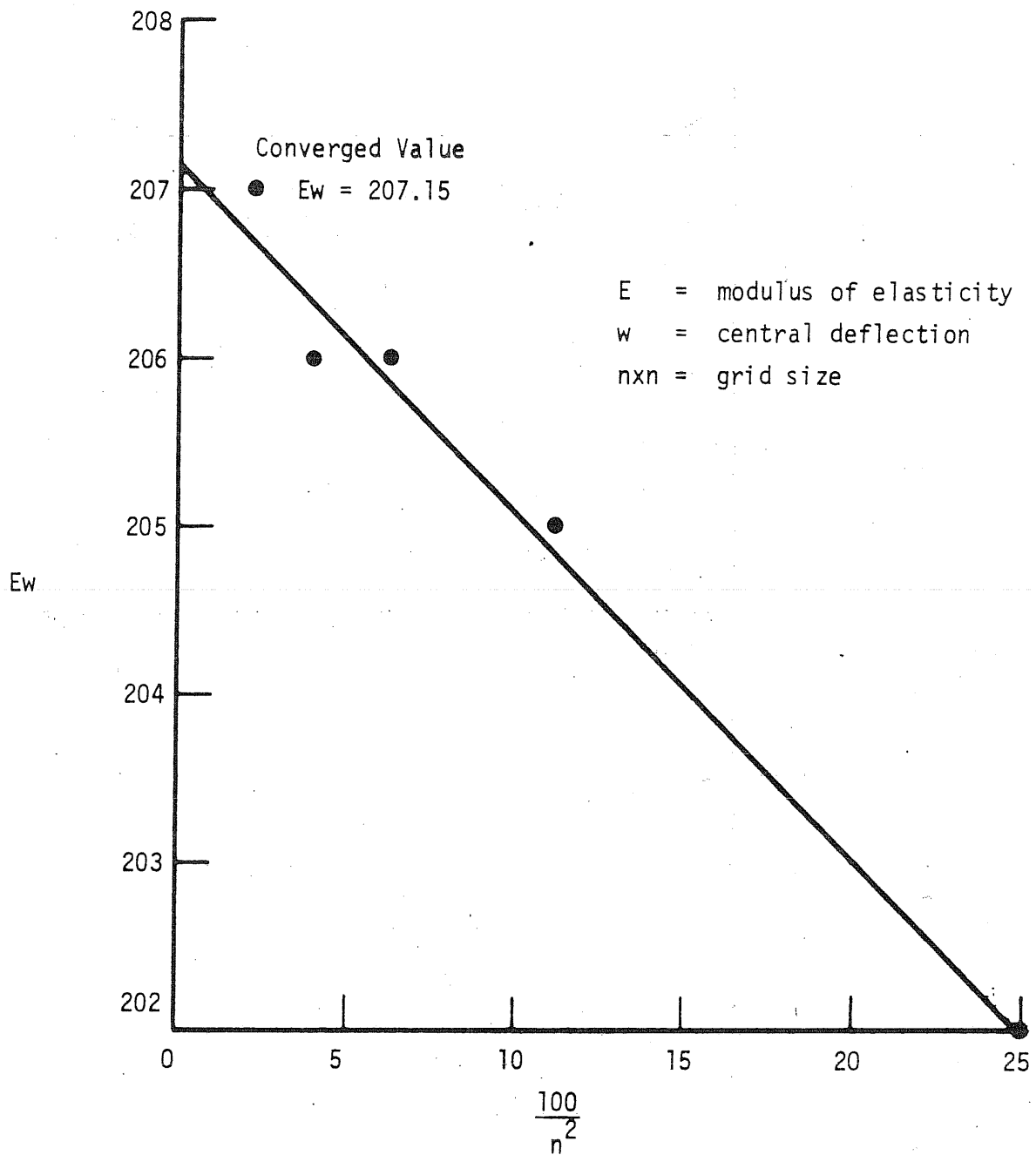
Figure 11. Convergence Study on the Center Deflection of a
Simply Supported Plate Under Uniformly Distri-
buted Lateral Load

P = 40 lbs
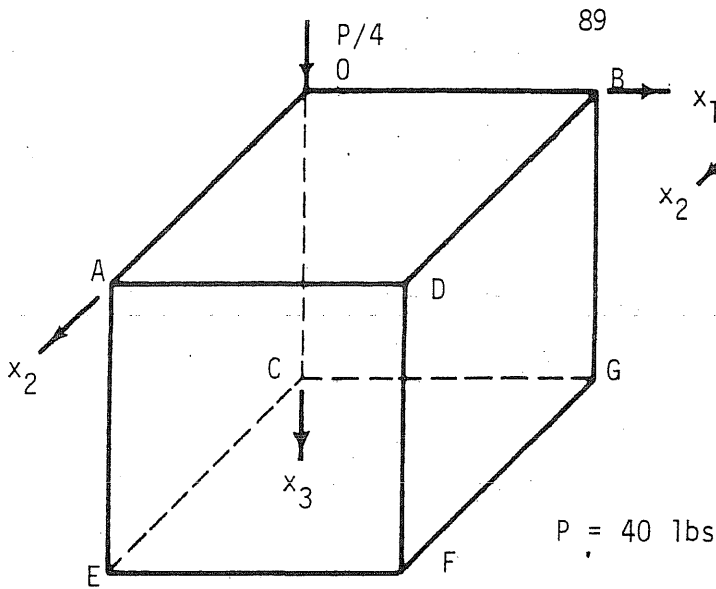
$u_1 = u_2 = u_3 = 0$, on EFGC

$u_1 = 0$ on OAEC   Symmetry

$u_2 = 0$ on OBGC
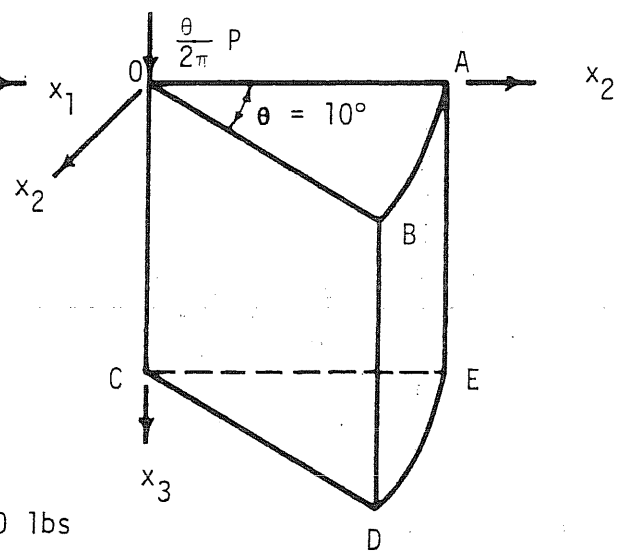
(a) Prism

$u_1 = u_2 = u_3 = 0$, on CDE

normal displacement = 0, on

OAEC and OBDC

(b) Circular Cylindrical
     Segment
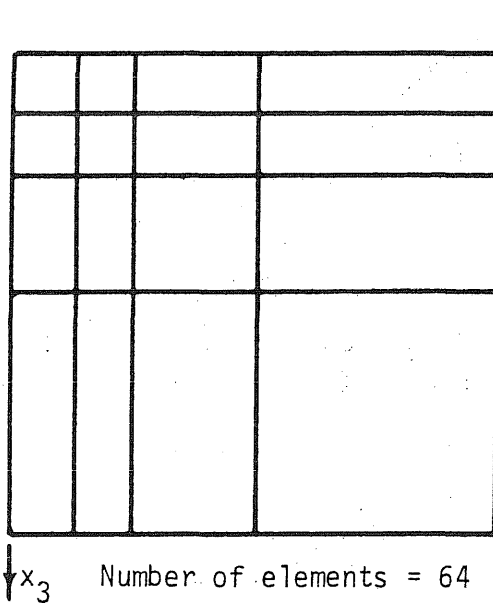
Number of elements = 64

Number of joints   = 125

Number of unknowns = 260

(c) Finite Element Grid for
     the Prism
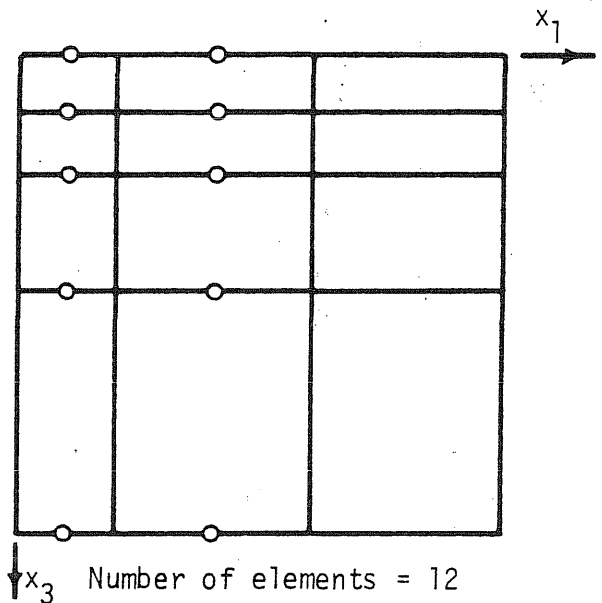
Number of elements = 12

Number of joints   = 65

Number of unknowns = 112

(b) Finite Element Grid for
     the Cylinder

Figure 12.   Finite Element Idealization of the Boussinesq Problem

Sec.	x_3
AA	0.625
BB	1.25
CC	1.875
DD	2.5
EE	3.75

● Prism Idealization
■ Cylinder Idealization
— Analytical[55]

Vertical Stress, psi

Horizontal Distance from the Axis of the Load, in.
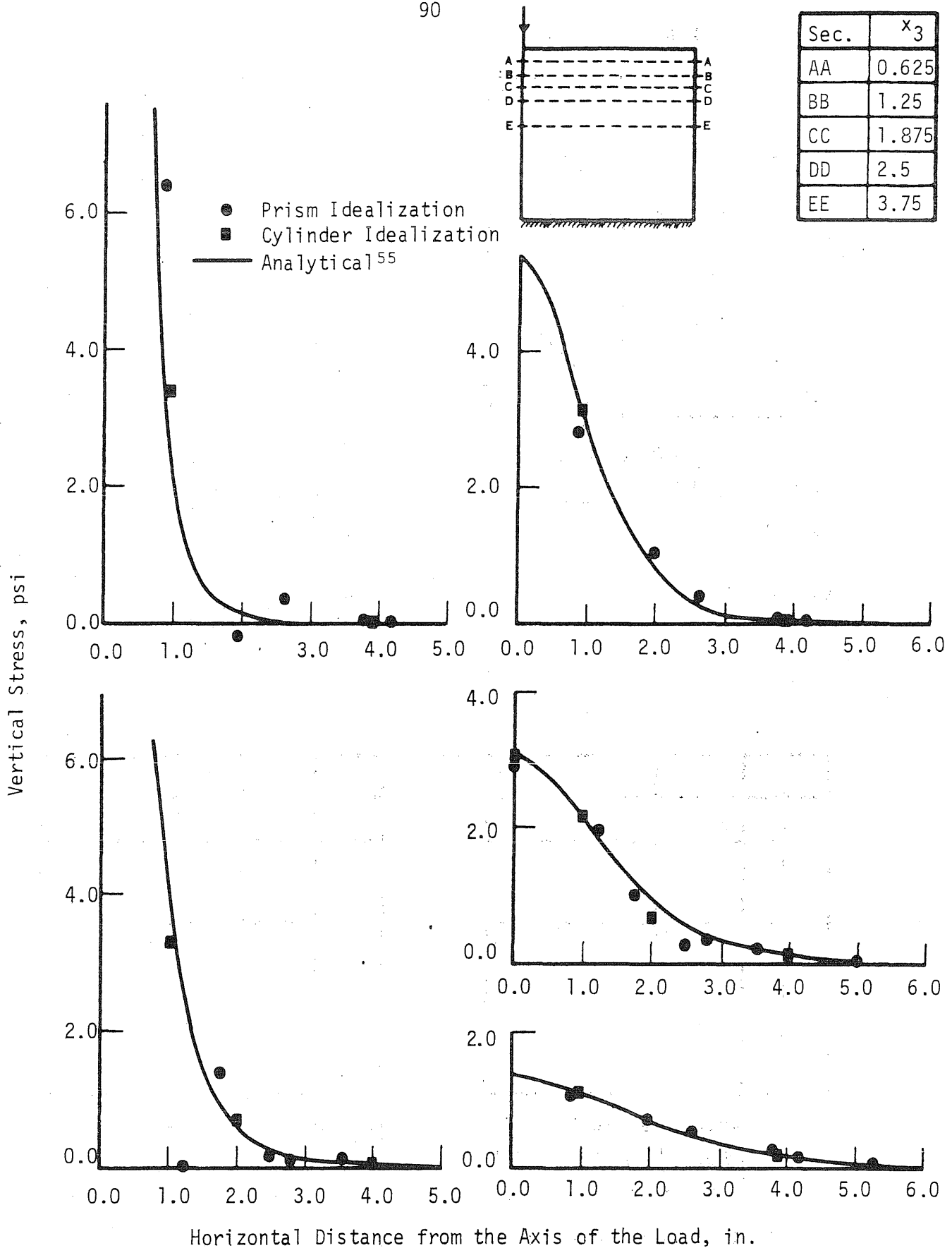
Figure 13. Distribution of Vertical Stresses in the Boussinesq Problem of a Semi-Infinite Body Subjected to a 40-lb Concentrated Load

$u_1 = u_2 = 0$

$E = 3 \times 10^6$ psi

$\nu = 0$

500
psi

6"

72"

6"

42"

(a) Axial Section

$u_3 = 0$

Number of elements = 52
Number of joints   = 172
Number of unknowns = 417
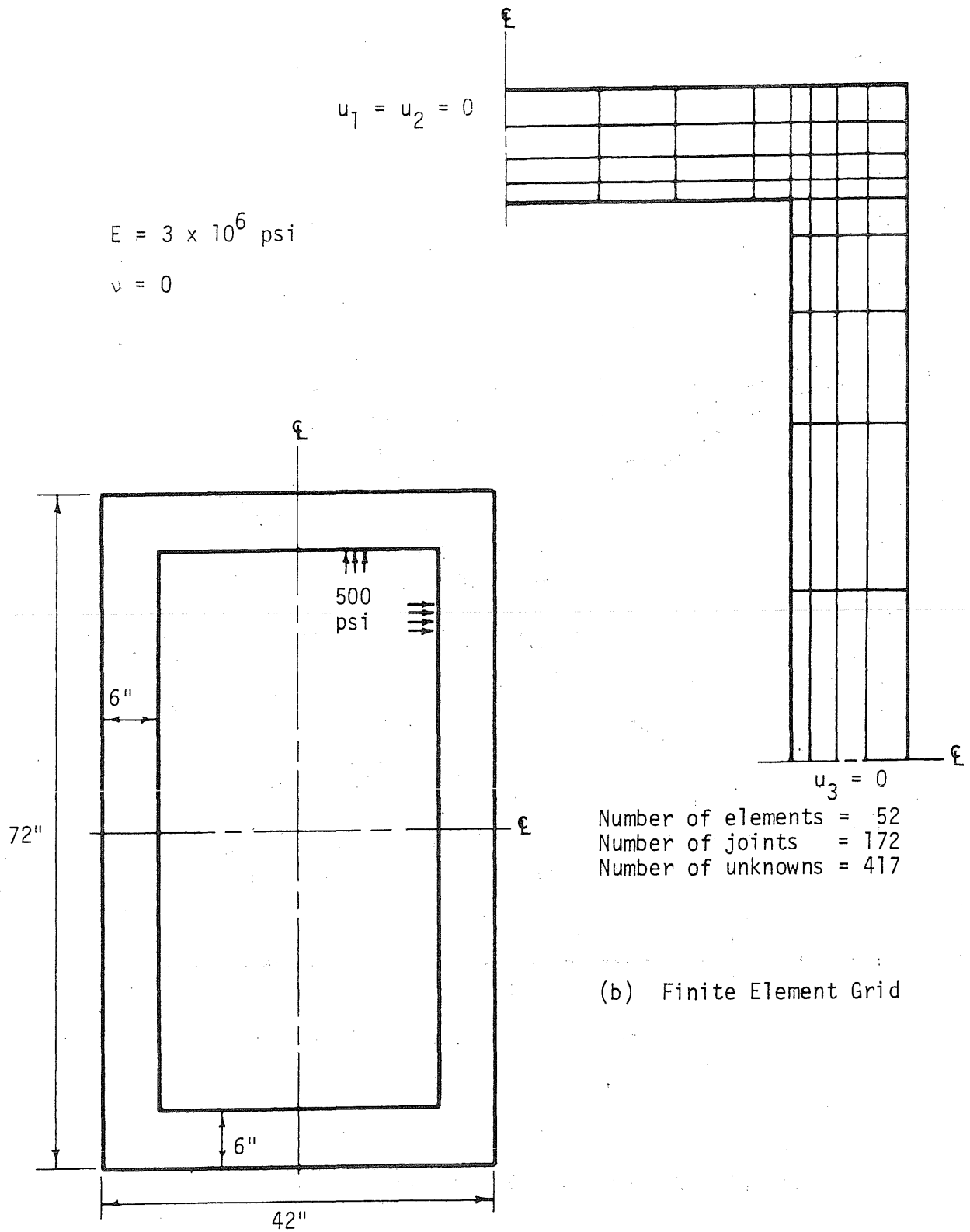
(b) Finite Element Grid

Figure 14. Axisymmetric Pressure Vessel
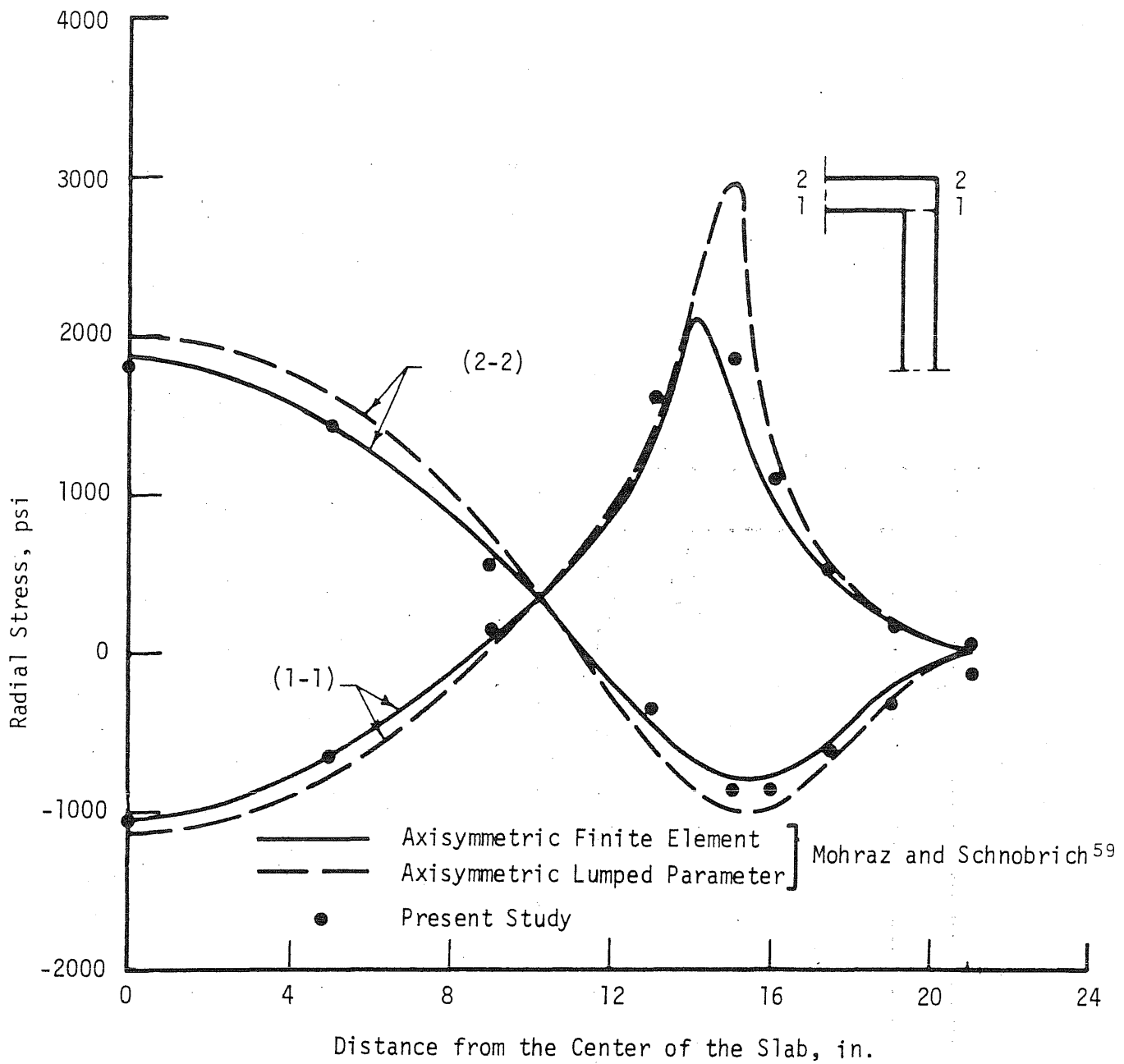
Figure 15. Distribution of Radial Stresses in the Slab of an Axisymmetric Pressure Vessel
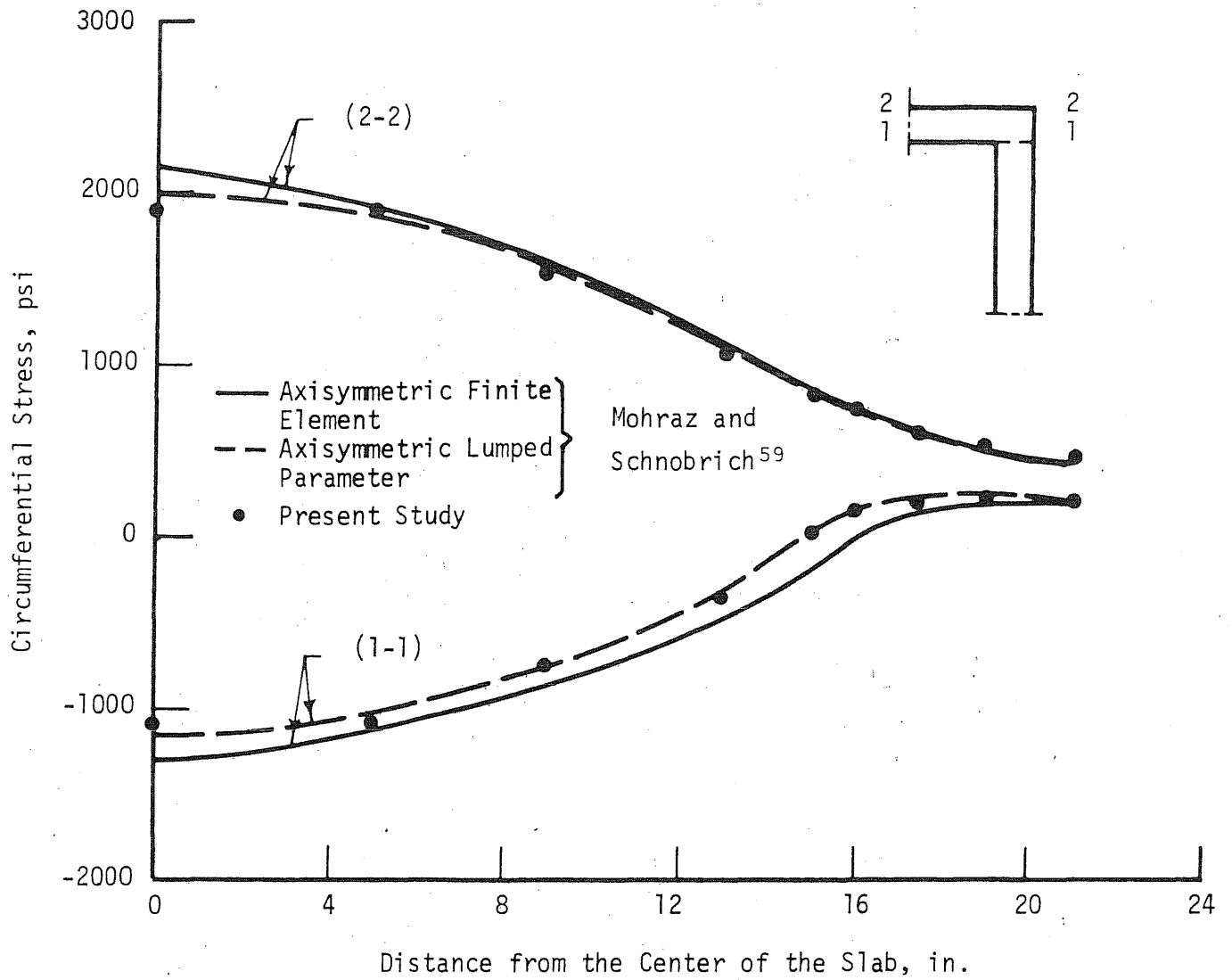
Figure 16. Distribution of Circumferential Stresses in the Slab of an Axisymmetric Pressure Vessel
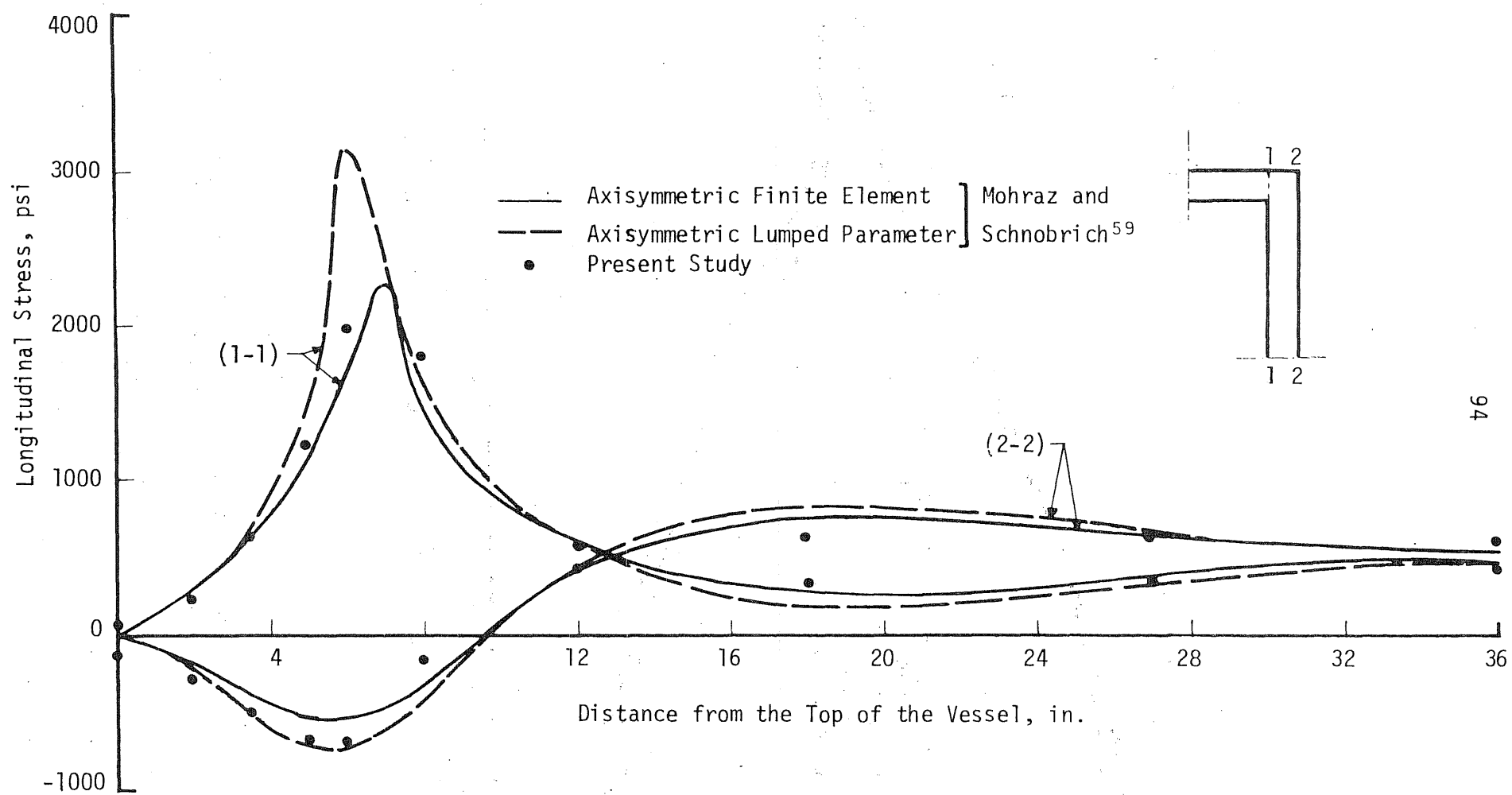
Figure 17. Distribution of Longitudinal Stresses along the Depth in the Cylinder of an Axisymmetric Pressure Vessel

Longitudinal Prestressing
26,000 psi

$u_1 = u_2 = 0$

10"

Radial
Prestressing
1200 psi

7.5"

3000 psi   40"

$u_3 = 0$
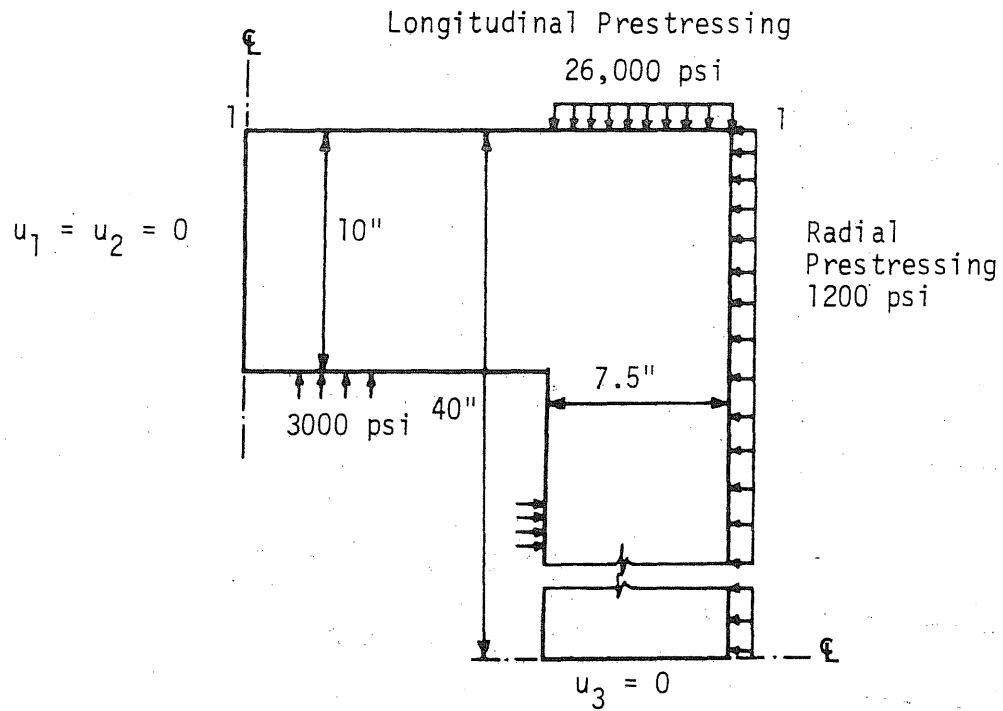
(a) Axial Section at OA

$E = 4 \times 10^6$ psi

$\nu = 0.15$

Displacements normal to OA
and OB = 0

20"

A

2"

0

8"

B
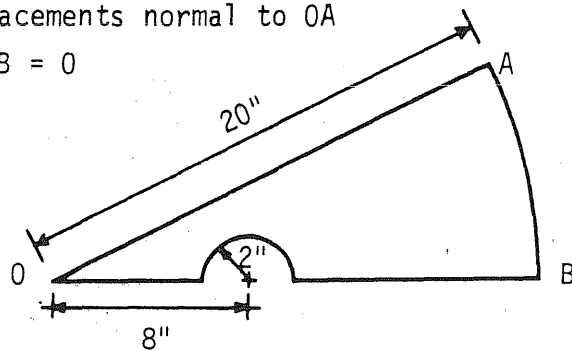
(b) Transverse Section at 1-1

Figure 18.   Prestressed Reactor Vessel with Circular Openings

Number of elements = 48
Number of joints = 173
Number of unknowns = 404

(b) Enlarged View of
     Element e

(a) Pie-Shaped Axial Segment
     with the Finite Element Grid
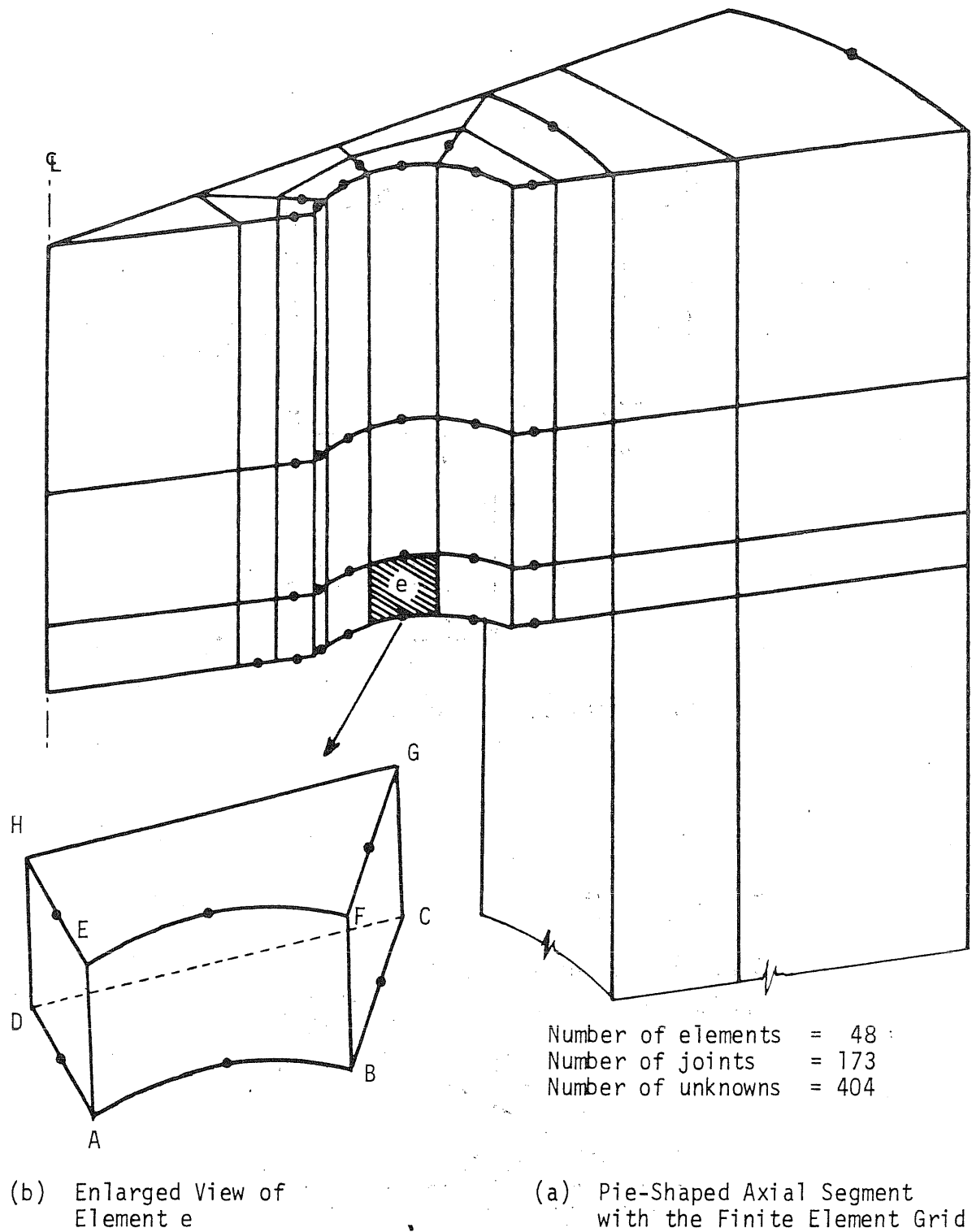
Figure 19. Finite Element Grid for the Prestressed Reactor
            Vessel with Circular Openings
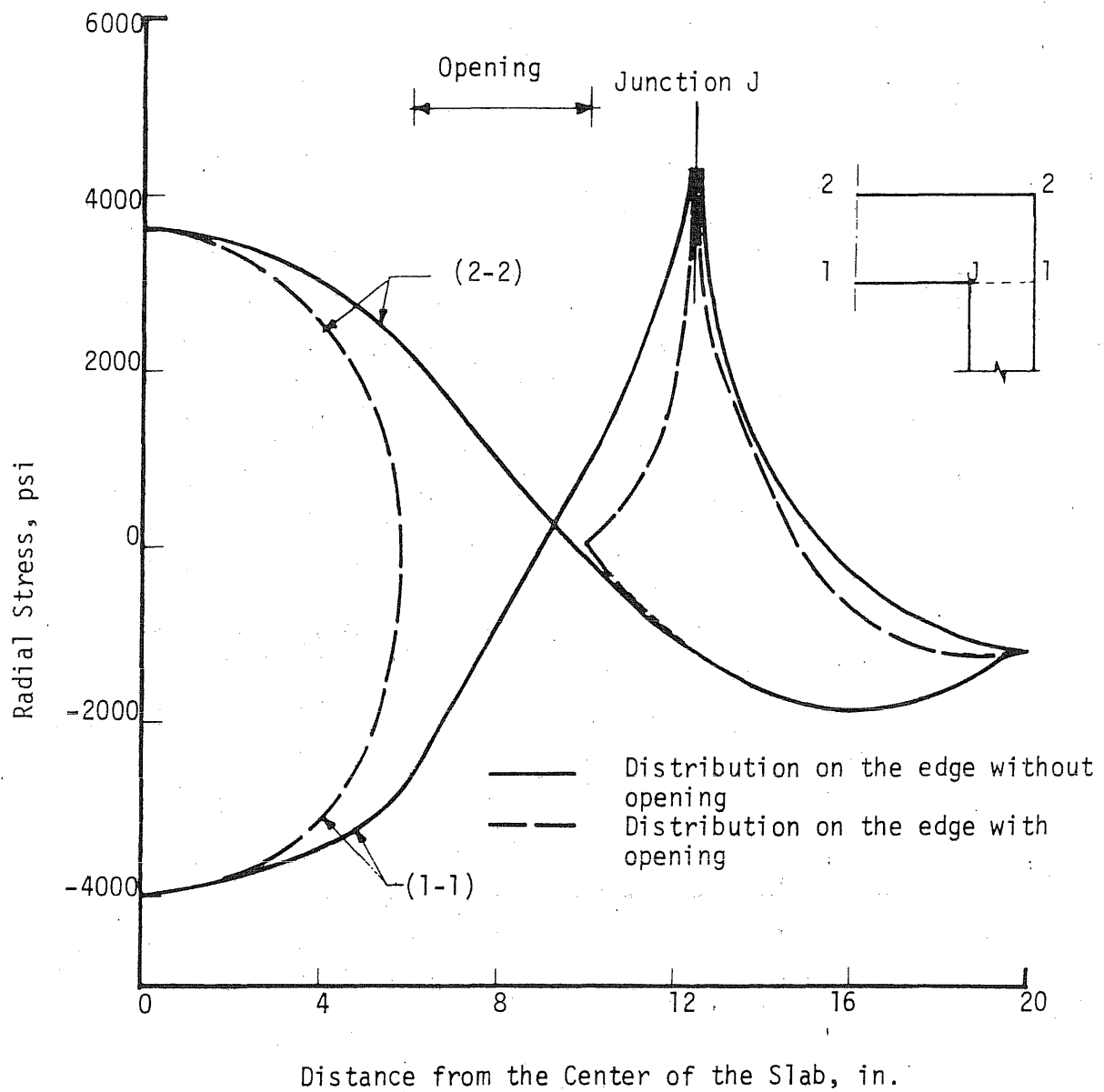
Figure 20. Distribution of Radial Stresses in the Slab
of the Prestressed Reactor Vessel with Openings
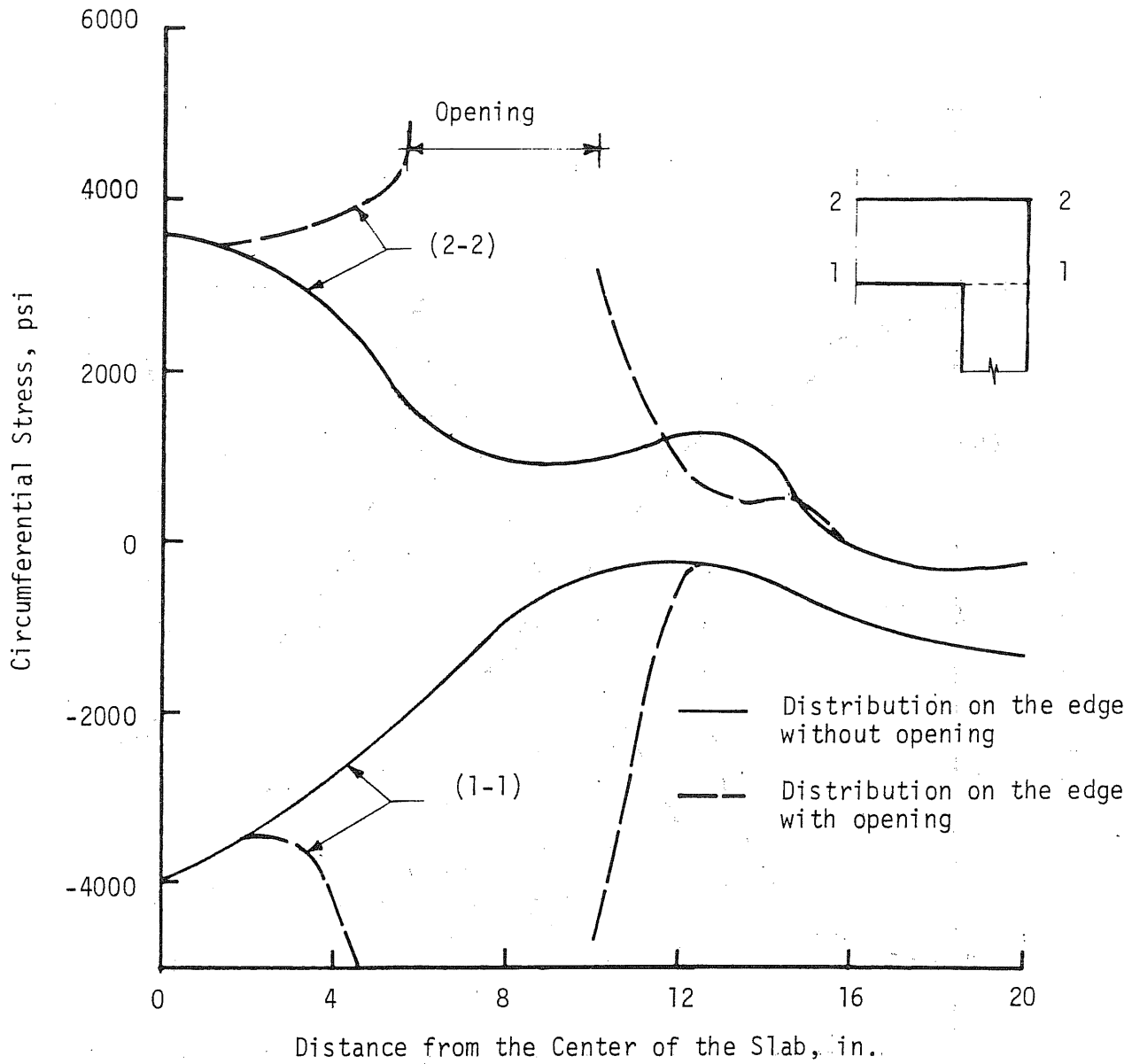
Figure 21. Distribution of Circumferential Stresses in the
Slab of the Prestressed Reactor Vessel with
Circular Openings
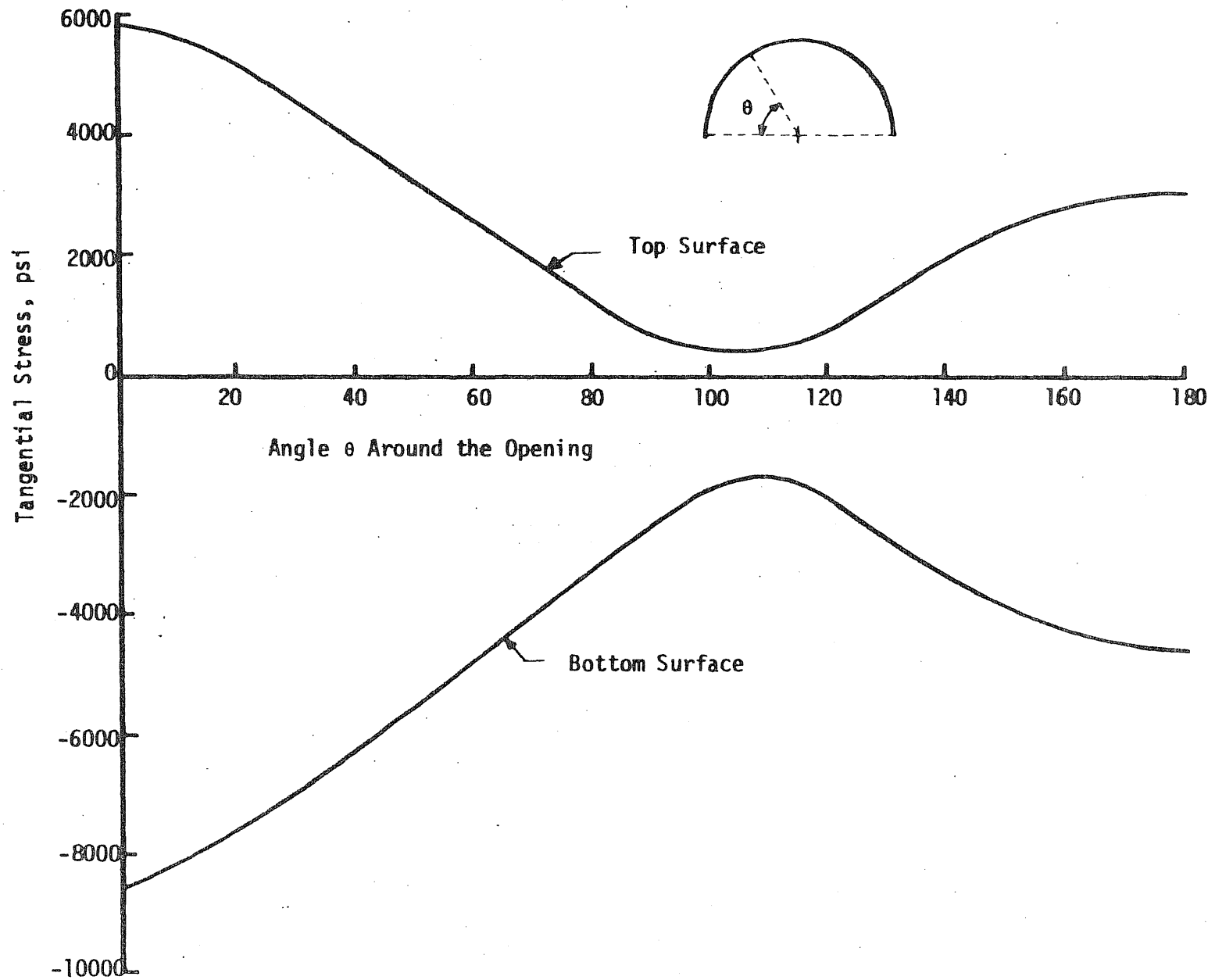
Figure 22.   Distribution of Tangential Stresses Around an Opening
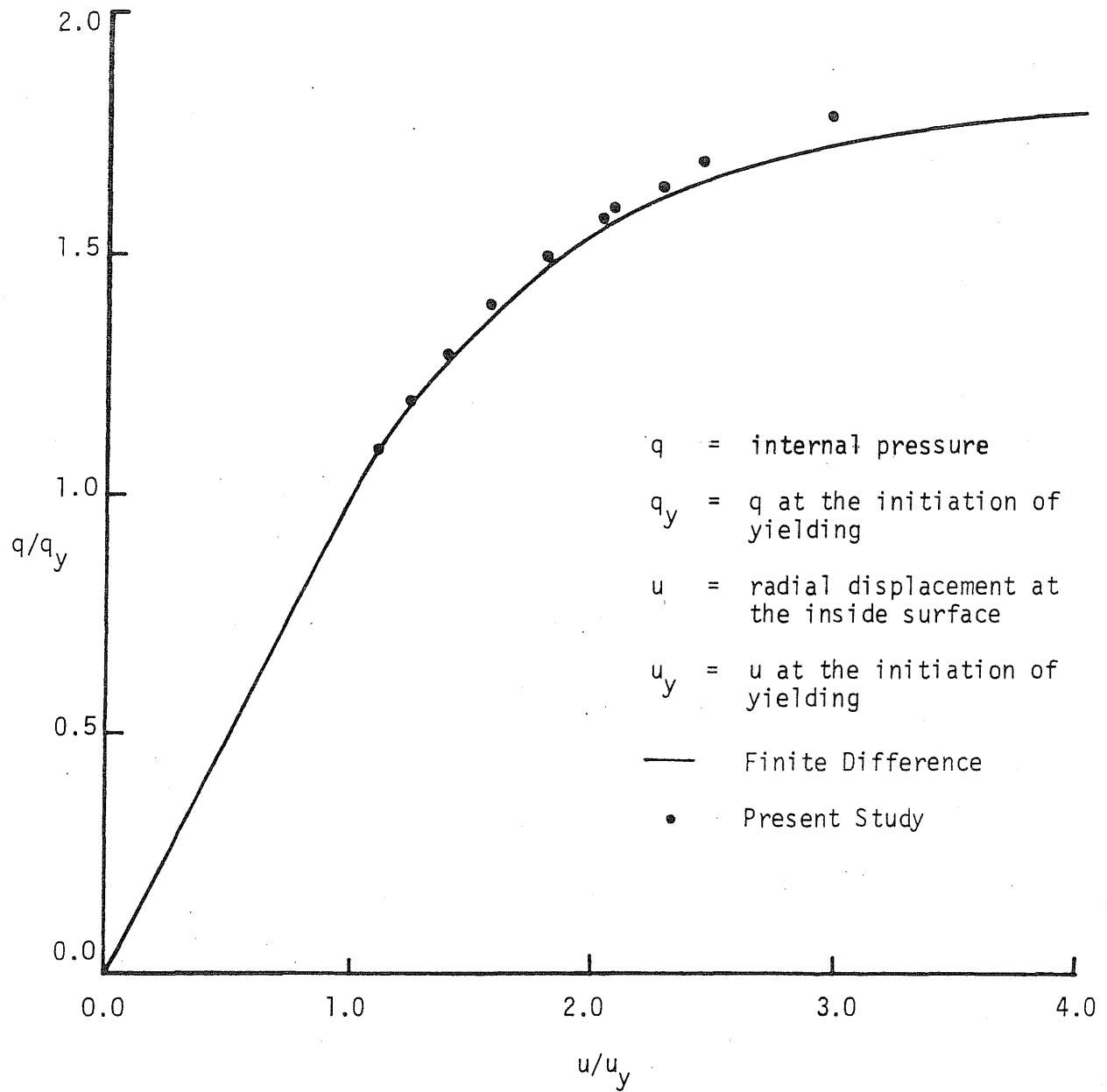
Figure 23. Load-Displacement Curve for the Thick Hollow
Circular Cylinder Subjected to a Uniform
Internal Pressure
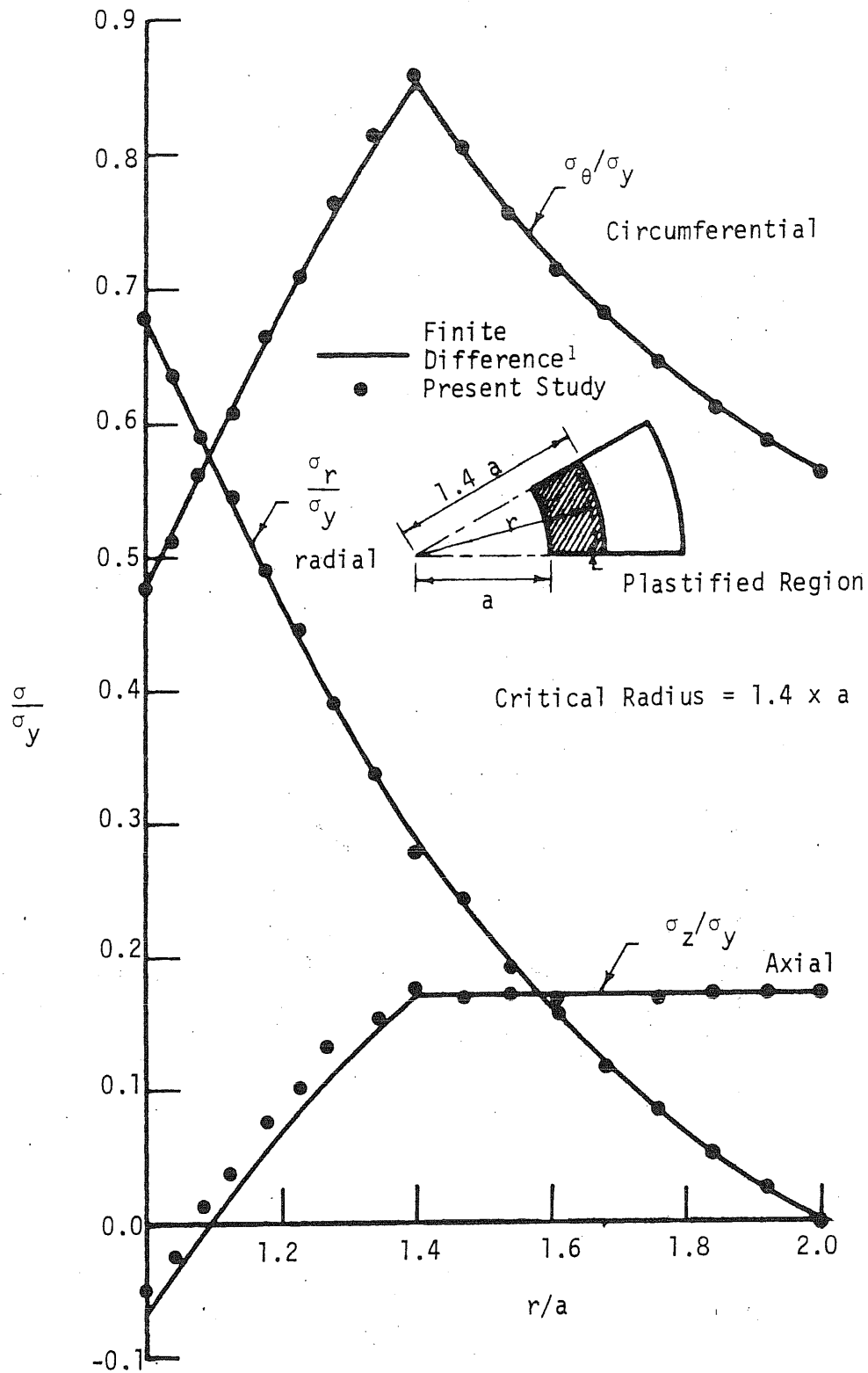
Figure 24. The Distribution of Radial, Circumferential and Axial Stresses in a Thick Hollow Circular Cylinder Subjected to Internal Pressure
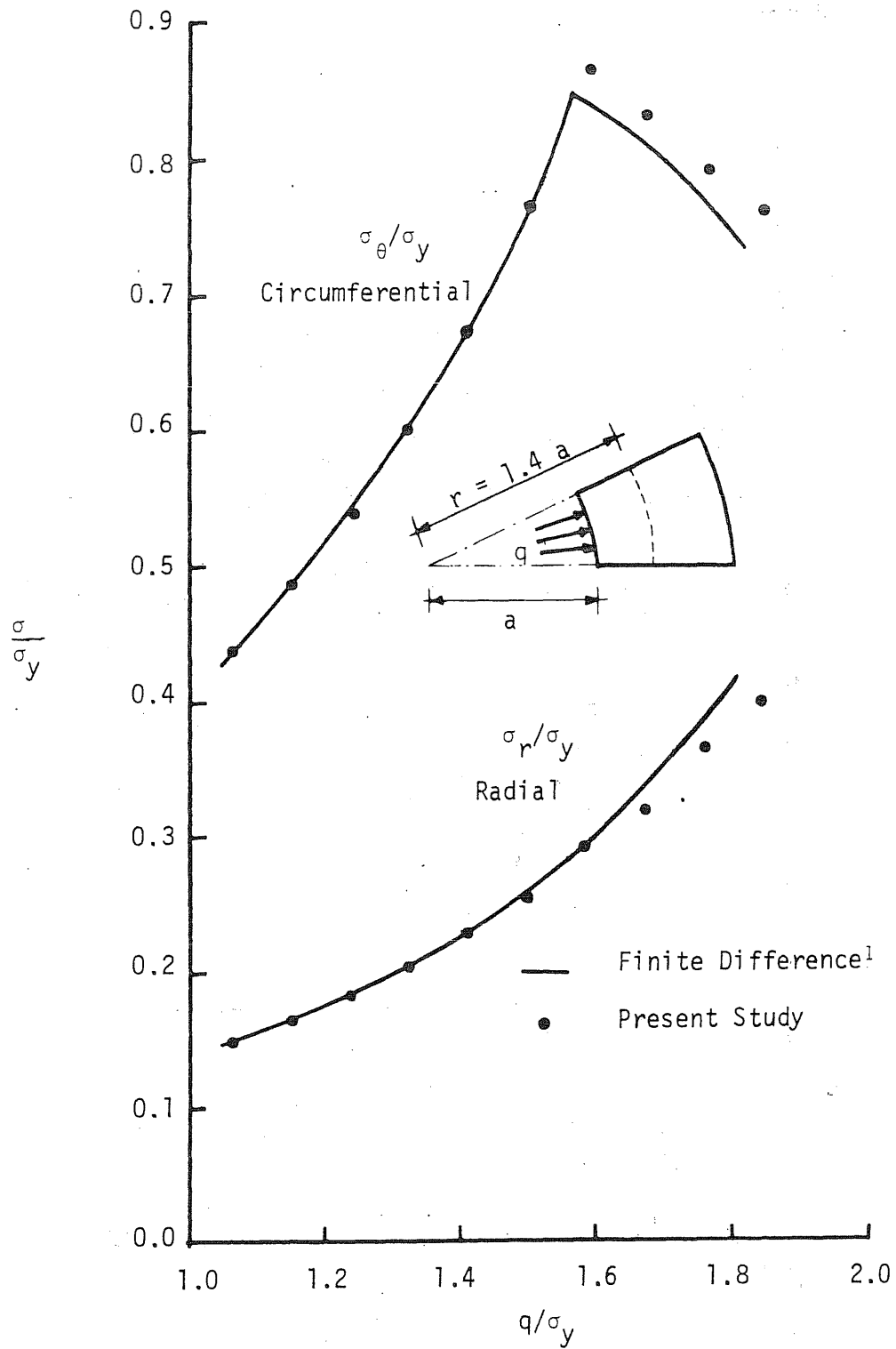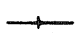
Figure 25. Variation of Radial and Circumferential Stresses at r/a = 1.4 for an Increasing Internal Pressure

(a) Beam
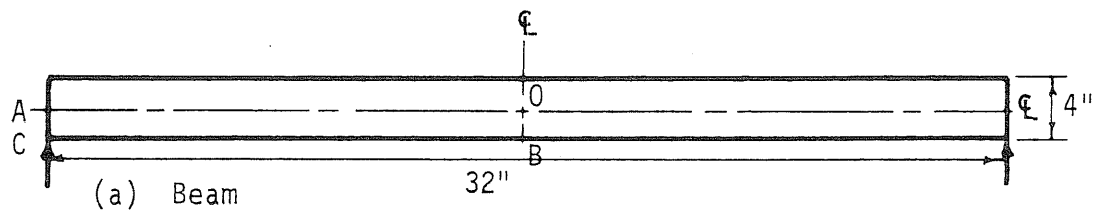
Theoretically Plastified Region
Plastified Nodes and Element Centroids (Present Study)
Nodes and Element Centroids in the Theoretically Plastified
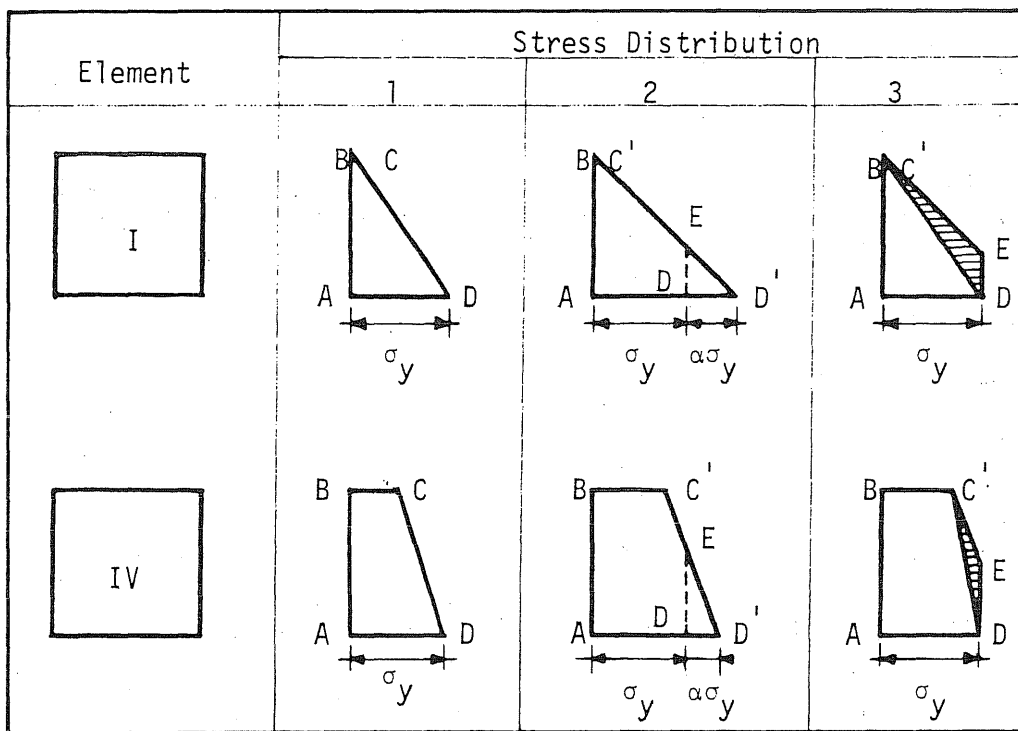Region, which did not Plastify Numerically
Intermediate Node

(b) Plastified Region at $q = 1.22\ q_y$

(c) Plastified Region at $q = 1.32\ q_y$

(d) Plastified Region at $q = 1.36\ q_y$
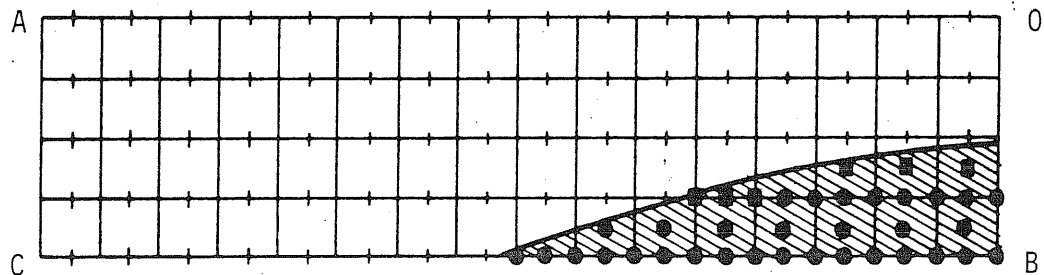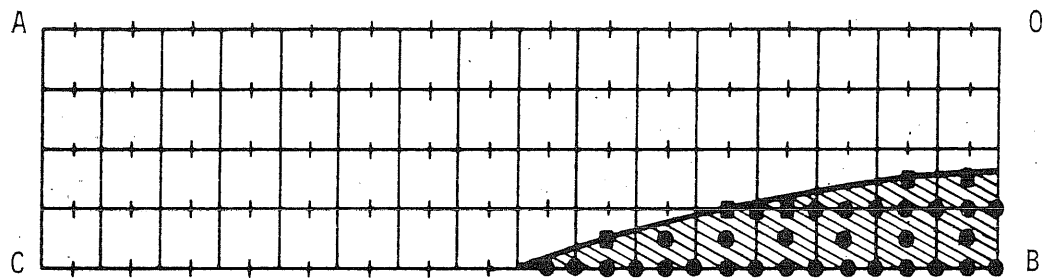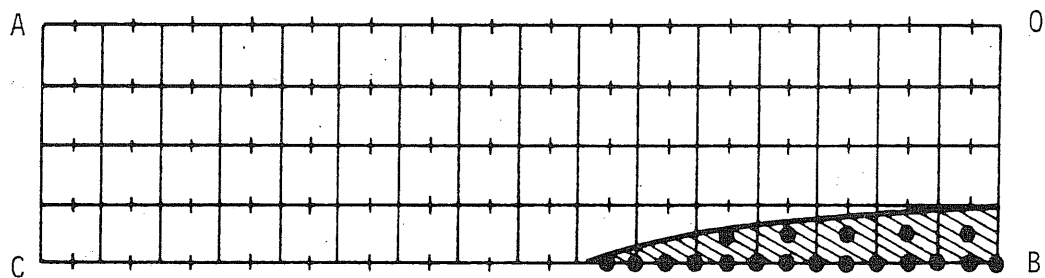
q = Lateral load on the beam
q_y = q at the initiation of yield

Figure 26. Comparison of Plastified Regions in a Simply
Supported Beam at Three Different Load Levels
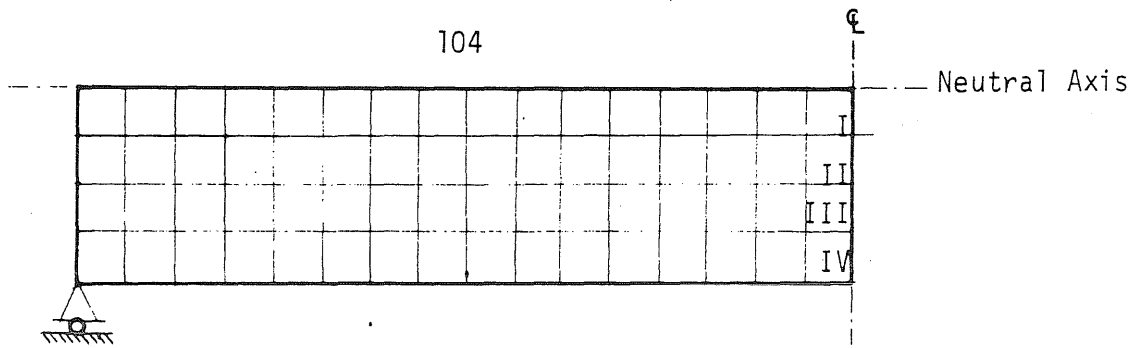
One-fourth of the Beam with the Finite Element Grid

Stress Distribution:

1. Beginning of the load increment

2. After elastic analysis for the load increment

3. After subtracting the initial stresses

◢ Stress loss

σ_y = Uniaxial yield stress

$\alpha\sigma_y$ = Elastic stress increment

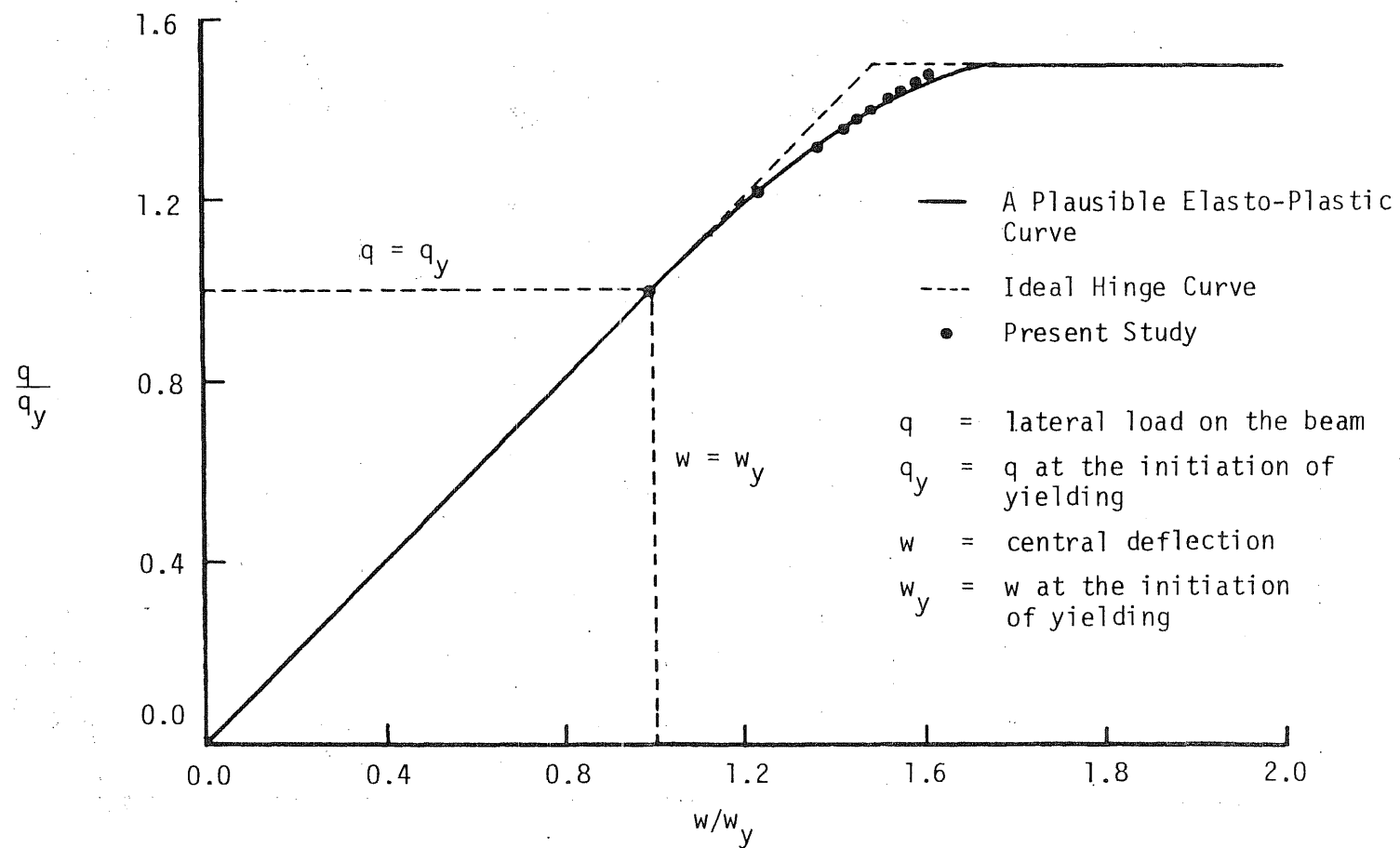Figure 27. The "Loss" of Stresses Due to Interpolation
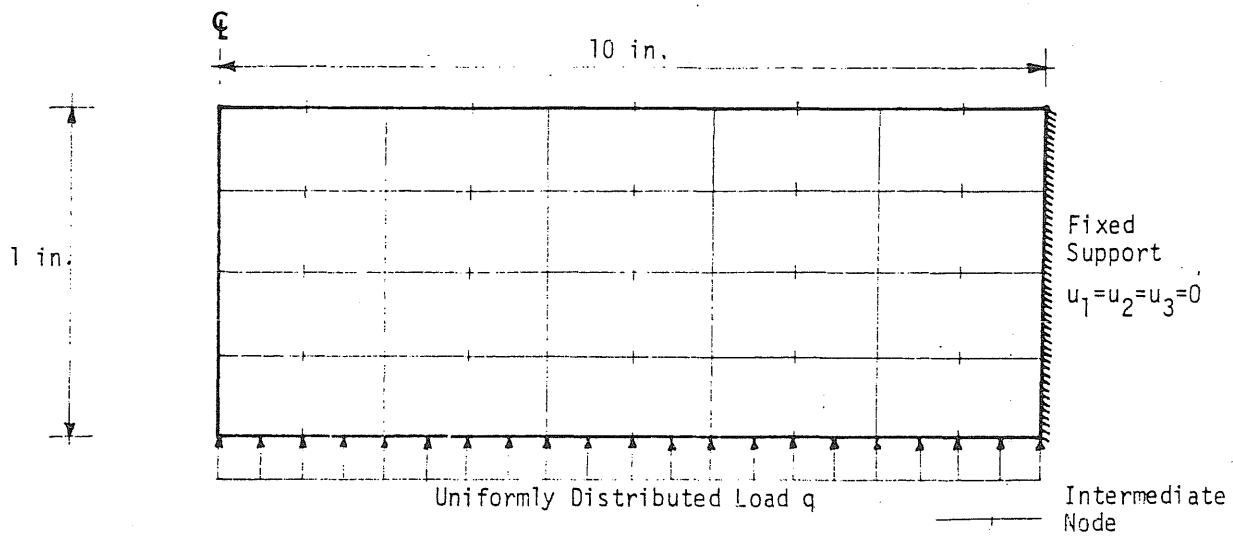
Figure 28. Load-Displacement Curve for the Beam

(a) Axial Section of the Plate
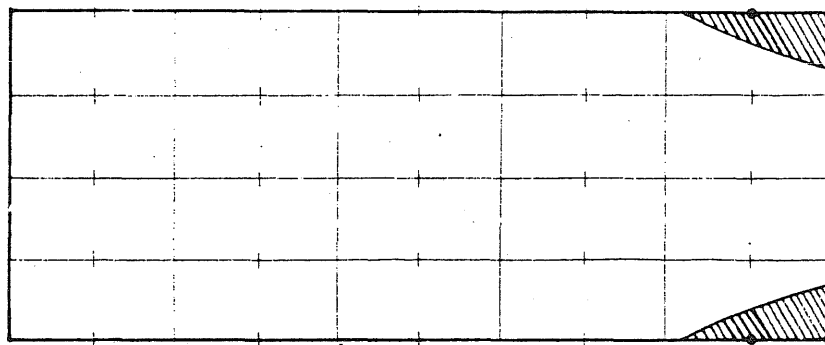
(b) Plastified Region at q = 1.3 q_y

(c) Plastified Region at q = 1.5 q_y

Figure 29. Elasto-Plastic Analysis of the Circular Plate
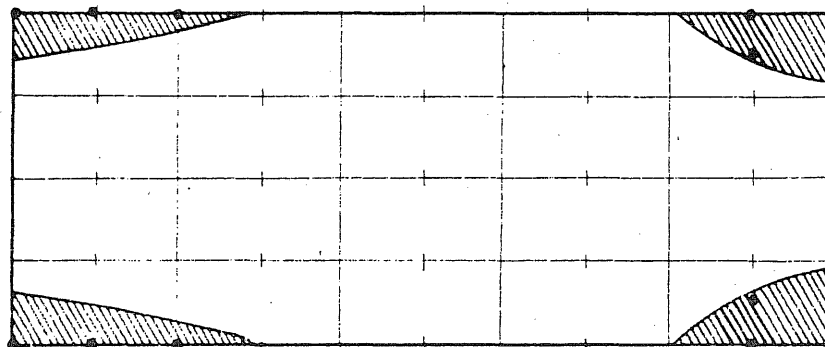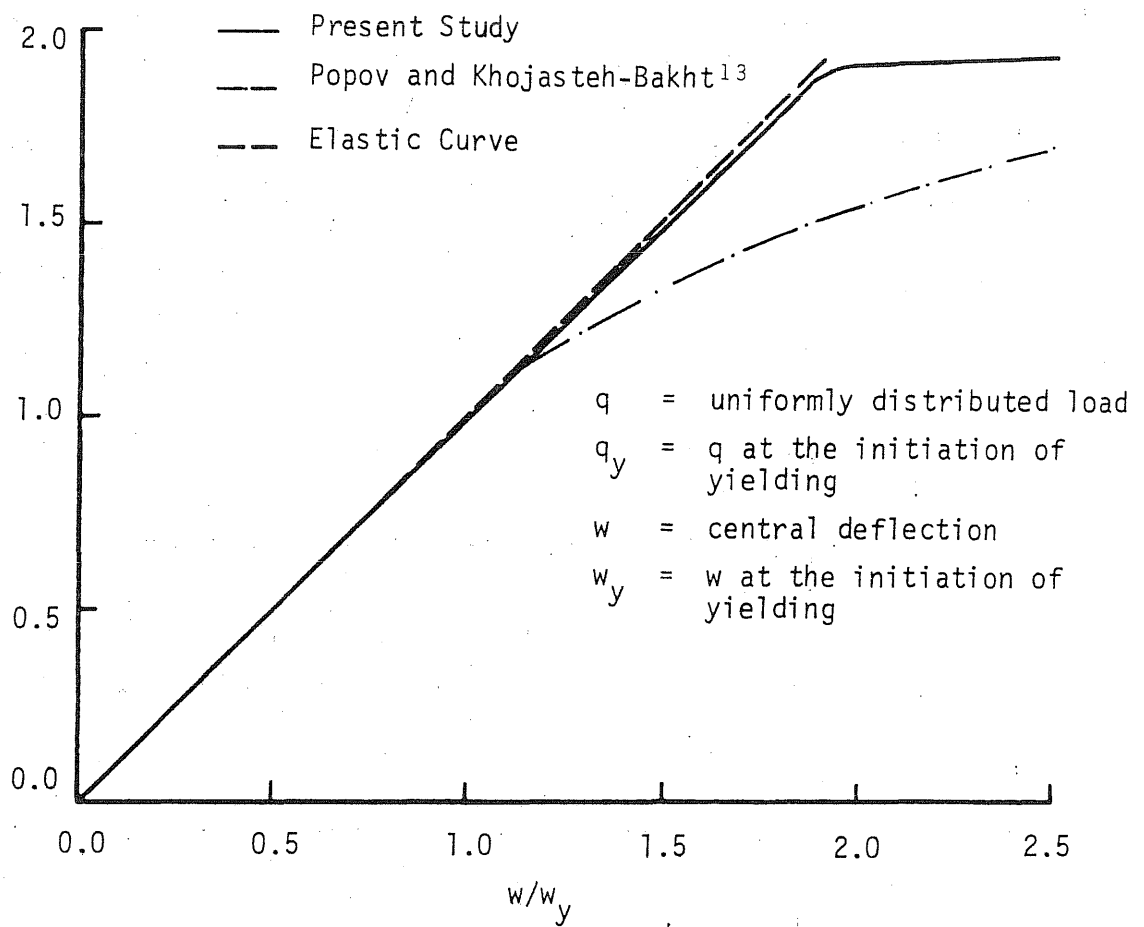
Figure 30. Load-Displacement Curve for the Elasto-Plastic Circular Plate

Poisson's Ratio = 0.3

Strain Hardening
Coefficient = 0

Fixed Support:

$u_1 = u_2 = u_3 = 0$

Symmetry Conditions:

$u_2 = 0$ on OB

$u_2' = 0$ on OA

(u_2' = displacement normal to OA)

(a) Circular Plate with the Pie-Shaped Axial Segment

Opening

4"

$u_1 = u_2 = 0$

6"

Uniformly Distributed Load q
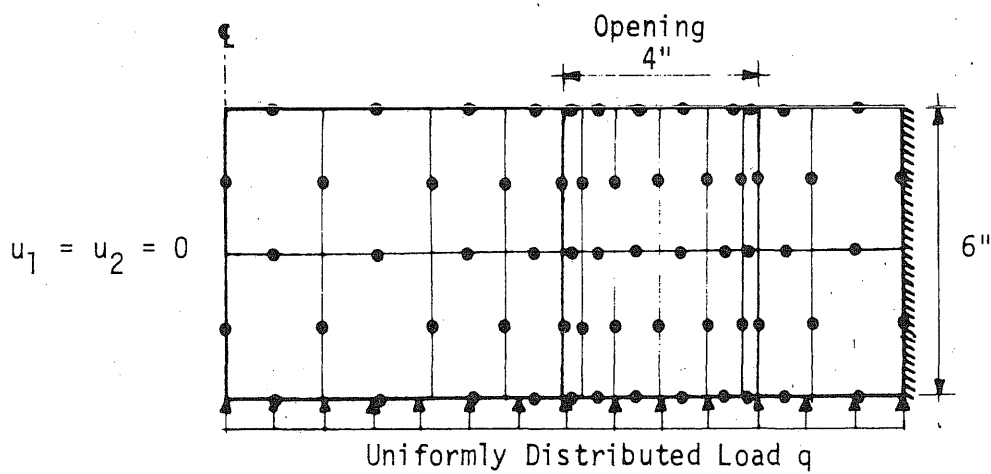
(b) Axial Section at OB

Figure 31.   Finite Element Grid for the Thick Circular
Plate With Openings

Section OA

Section OA

Section OB

Section OB

Section 1-1

Section 1-1

Section 2-2

Section 2-2

Section 3-3

Section 3-3
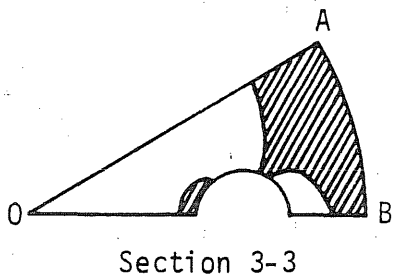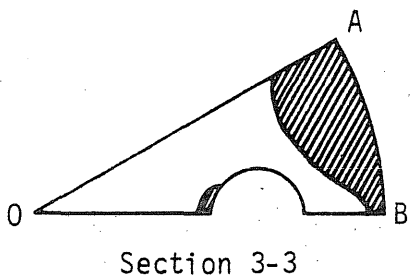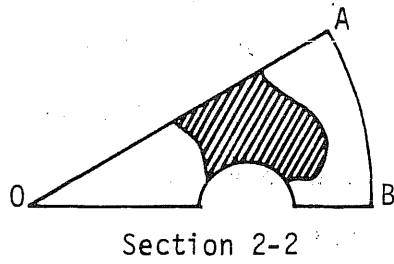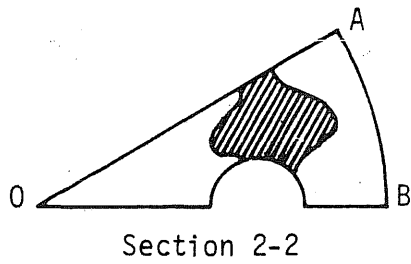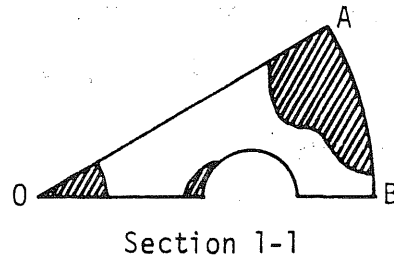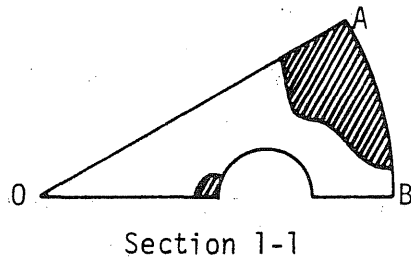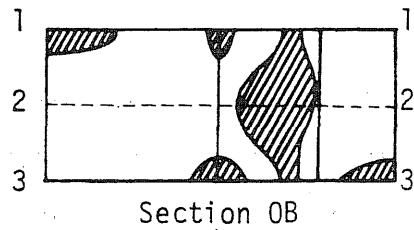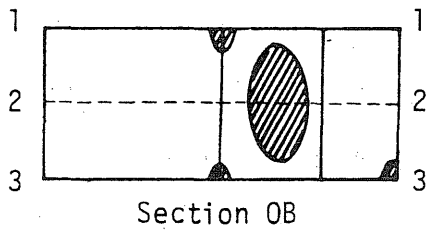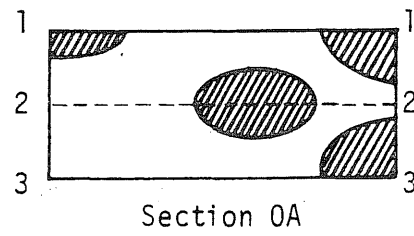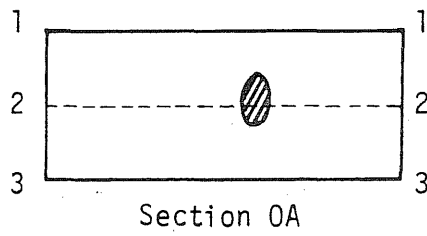
(a) 1.75 x Yield Load

(b) 1.95 x Yield Load

Plastified Region

Figure 32.   Plastified Regions in the Circular Plate with
Circular Openings at Two Load Levels

APPENDIX A

COMPUTATION OF THE NUMERICALLY INTEGRATED STIFFNESS MATRIX

A.1 General

It was indicated in Chapter 2 that the closed form integration
for the evaluation of the stiffness matrix of an isoparametric element is
a prohibitive task. In such cases, a numerical integration scheme is
employed. Although numerical integration for the evaluation of the
element stiffness matrix is both simple and adaptable to computer pro-
gramming, it increases the computations to be performed significantly.
The increase in computations presents an economic disadvantage, espec-
ially for large three-dimensional problems. For this reason, it is impor-
tant to employ efficient schemes for reducing the number of computations
within the computer.[62]

It was found during the course of this study that the formula-
tion of the element stiffness matrix in index notation results in a
better organization of computations. A method of computation is pre-
sented in the following section. Later a comparison between the proposed
method and the conventional method of computation is made in order to
ascertain their relative efficiencies.

A.2 Computational Procedure

In general, the element stiffness matrix can be evaluated by
numerically integrating Eq. 2.45 or Eq. 2.42 for isotropic and aniso-
tropic material properties, respectively. Since each set of computation
is repeated at every point of integration in the element, one can reduce
the number of operations significantly by taking the terms which are
not functions of the position coordinates outside of the integral sign

110

when possible. For homogeneous materials, the elements of the material property tensor $E_{ijk\ell}$ are not functions of the position coordinates. In such cases, an integration array W_{ij}^{mn} which is given by

$$W_{ij}^{mn} = \int_V \frac{\partial N^m}{\partial x_i} \frac{\partial N^n}{\partial x_j} \, dV \qquad (A.1)$$

is first evaluated. The result is then multiplied by the material property tensor to give the desired element stiffness matrix. For an isotropic elastic material,

$$k_{ij}^{mn} = \lambda W_{ij}^{mn} + \mu(W_{kk}^{mn} \delta_{ij} + W_{ji}^{mn}) \qquad (A.2)$$

and for an anisotropic elastic material

$$k_{ij}^{mn} = E_{ikj\ell} W_{k\ell}^{mn} \qquad (A.3)$$

For nonhomogeneous materials the elements of the material property tensor $E_{ijk\ell}$ are functions of the position coordinates. Therefore, the material property tensor cannot be taken outside of the integral sign and it must be included in the integration. For such cases the number of operations for evaluating the element stiffness matrix is significantly increased. However, as is shown in the next section, the amount of computation is still considerably less than that required by the conventional procedure.

A.3 Comparison of Numerical Computations

In the conventional approach, the formulation of the element stiffness matrix is given by

$$k = \int_V B^T D B \, dV \qquad (A.4)$$

where

$\quad$ B $\quad$ = $\quad$ a geometry matrix relating strains to displacements

$\quad$ D $\quad$ = $\quad$ material property matrix

For numerical integration the weight coefficient associated with every point of integration is first multiplied into the material property matrix. The product $B^T DB$ is then evaluated at the integration points through the element. The individual terms are added to give the elements of the stiffness matrix. The steps and the number of operations (additions and multiplications) for evaluating the stiffness matrix of a three-dimensional element are given in Table A.1. If Σ and Π denote the number of additions and multiplications, respectively, one obtains

$$\Sigma_1 = \frac{1}{2}(63r^2 + 237r)I$$

$$\text{(A.5)}$$

$$\Pi_1 = (27r^2 + 117r + 36)I$$

where

$\quad$ r $\quad$ = $\quad$ number of nodes in the element

$\quad$ I $\quad$ = $\quad$ number of integration points in the element

$\quad$ In the proposed procedure for the case in which the elements of the material property tensor $E_{ijk\ell}$ are not functions of position coordinates (anisotropic material property is considered for generality), the weight coefficients at every integration point through the element are first multiplied into the derivatives of shape functions. The individual terms of the integration array W_{ij}^{mn} are then added and the result is multiplied by the elasticity tensor to give the elements of the stiffness matrix. The steps and the number of additions and multiplications for a three-dimensional element are given in Table A.2. Thus,

$$\Sigma_2 = \frac{9}{2}(I + 9)(r^2 + r)$$

(A.6)

$$\Pi_2 = \frac{9}{2}(I + 9)(r^2 + r) + 3rI$$

For isotropic elastic material where the material property tensor can be expressed in terms of Lamé's constant and modulus of rigidity, Eq. 2.44, the number of operations can be somewhat decreased. However, the decrease is not very significant.

A similar procedure for the evaluation of the stiffness matrix in which the elements of the material property tensor are functions of position coordinates (nonhomogeneous material) is given in Table A.3. The number of additions and multiplications for a three-dimensional element are

$$\Sigma_3 = 18[r(r + 1)] I + 81rI$$

(A.7)

$$\Pi_3 = \frac{27}{2}[r(r + 1)] I + 81(1 + r) I$$

In order to obtain a measure for the amount of computation involved in various procedures, a simple three-dimensional element (eight nodes) and a high order three-dimensional element with two intermediate nodes on each side (thirty-two nodes) are considered. In both cases, it is assumed that fourth order Gaussian quadrature is used for the numerical integration (sixty-four integration points in the element). The number of additions and multiplications for various procedures are given in Table A.4.

The results presented in Table A.4 indicate that the number of operations for the evaluation of the stiffness matrix by the proposed

method is approximately one-sixth of that required by the conventional procedure. The computational ratio (the ratio of the addition or the multiplication in the proposed method to those of the conventional procedure) does not change significantly when the number of nodes in the element is increased. For cases in which the elements of the material property tensor are functions of position coordinates, the computational ratio is in order of 0.6, Table A.4, resulting in a 40 percent reduction in the computational effort.

A plot of the total computational ratio (addition and multiplication) versus the order of Gaussian quadrature integration for both the eight node and the thirty-two node elements is given in Fig. A.1. For the constant material properties, the ratio decreases as the order of Gaussian quadrature is increased. The total computational ratio is larger than unity for only the first order integration. This indicates that for such a case, where the integration is simply the volume of the element, no computational saving is achieved by the proposed procedure. However, the first order quadrature is seldom used for integration. The fourth order quadrature is the one usually recommended for the numerical integration of the element stiffness matrix. [37]

For the variable material properties, the total computational ratio remains constant regardless of the order of integration. Although, significantly more computational effort is needed for elements with variable material properties, the number of computations is still well below that of the conventional procedure.

No extra storage is needed for the evaluation of the integration array W_{ij}^{mn}, Eq. A.1, as it uses the same storage space as the stiffness

matrix k_{ij}^{mn}. A 3 x 3 array is the only space needed for the calculations contained in Eqs. A.2, A.3. In addition, W_{ij}^{mn} and K_{ij}^{mn} can be stored in a column array to avoid the unnecessary multiple indexing.

There are two factors which contribute to reduction in the number of computations in the proposed method. One is the organization of the formulation which is easily achieved by the index notation. The other is the realization that the material property tensor can be multiplied outside of the integral sign for cases in which the terms in the material property tensor are not functions of position coordinates.

Table A.1

Operations Required for the Evaluation of the Element Stiffness Matrix
Three-Dimensional Element (Conventional Procedure)

Computation Step	Number of Additions	Number of Multiplications
1. For each point of integration		
a. Product of weight coefficients and material property matrix D		6 x 6
b. Obtaining the product DB	6 x 6 x 3r	6 x 6 x 3r
c. Obtaining $B^T DB$ (upper triangular portion only)	$\frac{1}{2}[6 \times 3r(3r + 1)]$	$\frac{1}{2}[6 \times 3r(3r + 1)]$
Total for step 1	$27r^2 + 117r$	$27r^2 + 117r + 36$
2. Repeating the operations in step 1 for I integration points	$(27r^2 + 117r)I$	$(27r^2 + 117r + 36)I$
3. Summing up the individual elements of the stiffness matrix evaluated at I integration points	$\frac{1}{2}[3r(3r + 1)]I$	
4. Total number of operations to obtain the element stiffness matrix (steps 2 and 3)	$\frac{1}{2}(63r^2 + 237r)I$	$(27r^2 + 117r + 36)I$

r = number of nodes in the element

I = number of integration points in the element

Operations Required for the Evaluation of the Element Stiffness Matrix
Three-Dimensional Element (Proposed Procedure - Constant Material Properties)

Computation Step	Number of Additions	Number of Multiplications
1. For each point of integration		
a. Product of weight coefficients and $\frac{\partial N^m}{\partial x_i}$		$3r$
b. Obtaining the product $\frac{\partial N^m}{\partial x_i} \frac{\partial N^n}{\partial x_j}$ (n = m to r)		$\frac{1}{2}[r(r+1)](3 \times 3)$
Total for step 1		$\frac{1}{2}(9r^2 + 15r)$
2. Repeating the operations in step 1 for I integration points		$\frac{1}{2}(9r^2 + 15r)I$
3. Summing up the individual elements of the array W_{ij}^{mn} evaluated at I integration points	$\frac{9}{2}[r(r+1)]I$	
4. Multiplying $E_{ikj\ell} W_{k\ell}^{mn}$	$\frac{9}{2}[r(r+1)](3 \times 3)$	$\frac{9}{2}[r(r+1)](3 \times 3)$
5. Total number of operations to obtain the element stiffness matrix (steps 2, 3, and 4)	$\frac{9}{2}(I+9)(r^2+r)$	$\frac{9}{2}(I+9)(r^2+r) + 3rI$

r = number of nodes in the element

I = number of integration points in the element

Table A.3

Operations Required for the Evaluation of the Element Stiffness Matrix
Three-Dimensional Element (Proposed Procedure – Variable Material Properties)

Computation Step	Number of Additions	Number of Multiplications
1. For each point of integration		
a. Product of weight coefficients and $E_{ijk\ell}$		81
b. Obtaining the product $E_{ikj\ell} \frac{\partial N^m}{\partial x_k}$	$81r$	$81r$
c. Obtaining the product $E_{ikj\ell} \frac{\partial N^m}{\partial x_k} \frac{\partial N^n}{\partial x_\ell}$ $(n = m$ to $r)$	$\frac{9}{2}[r(r + 1)](3)$	$\frac{9}{2}[r(r + 1)](3)$
Total for step 1	$\frac{27}{2}[r(r + 1)] + 81r$	$\frac{27}{2}[r(r + 1)] + 81(1 + r)$
2. Repeating the operations in step 1 for I integration points	$\frac{27}{2}[r(r + 1)]I + 81rI$	$\frac{27}{2}[r(r + 1)]I + 81(1 + r)I$
3. Summing up the individual elements of the stiffness matrix evaluated at I integration points	$\frac{9}{2}[r(r + 1)]I$	
4. Total number of operations to obtain the element stiffness matrix (steps 2 and 3)	$18[r(r + 1)]I + 81rI$	$\frac{27}{2}[r(r + 1)]I + 81(1 + r)I$

r = number of nodes in the element

I = number of integration points in the element

Table A.4

Comparison of Computations for Determination of Element Stiffness Matrix
(Three-Dimensional Element with 64 Integration Points)

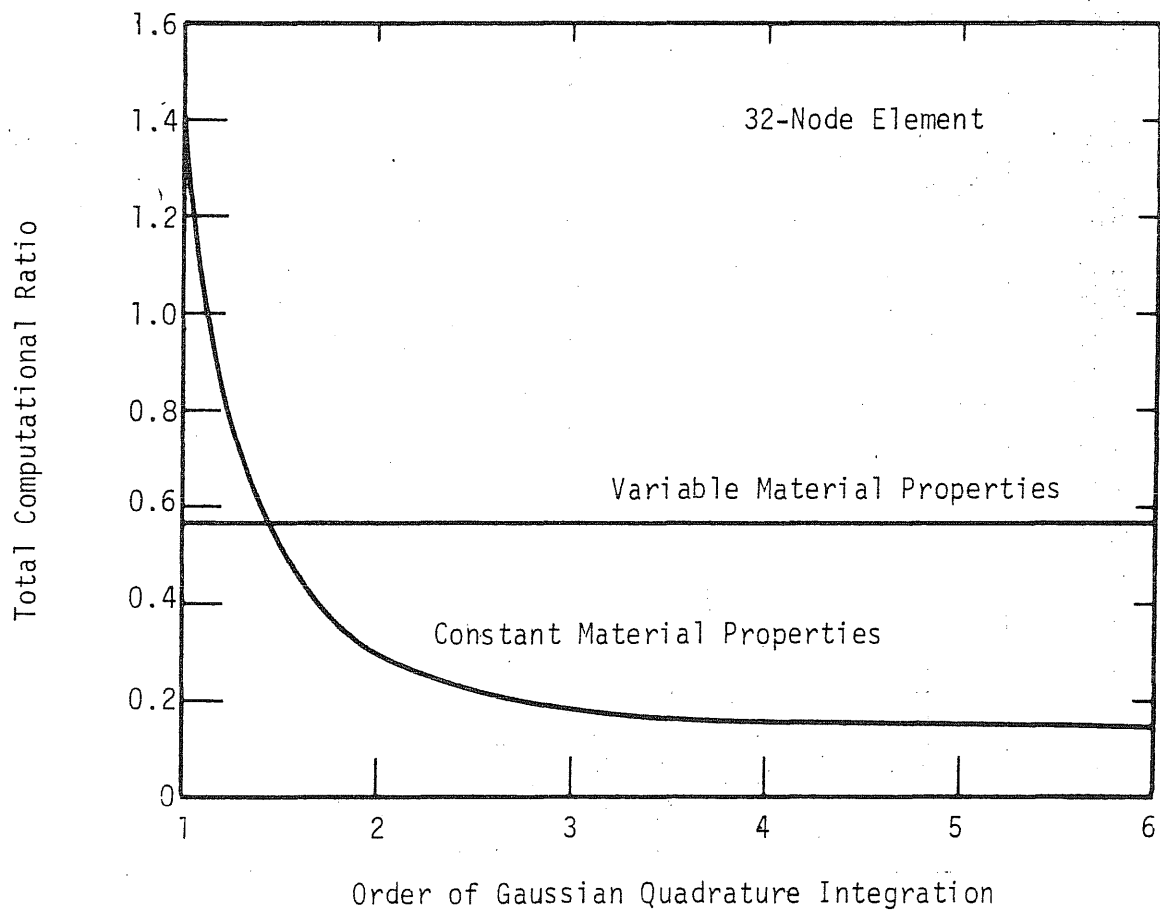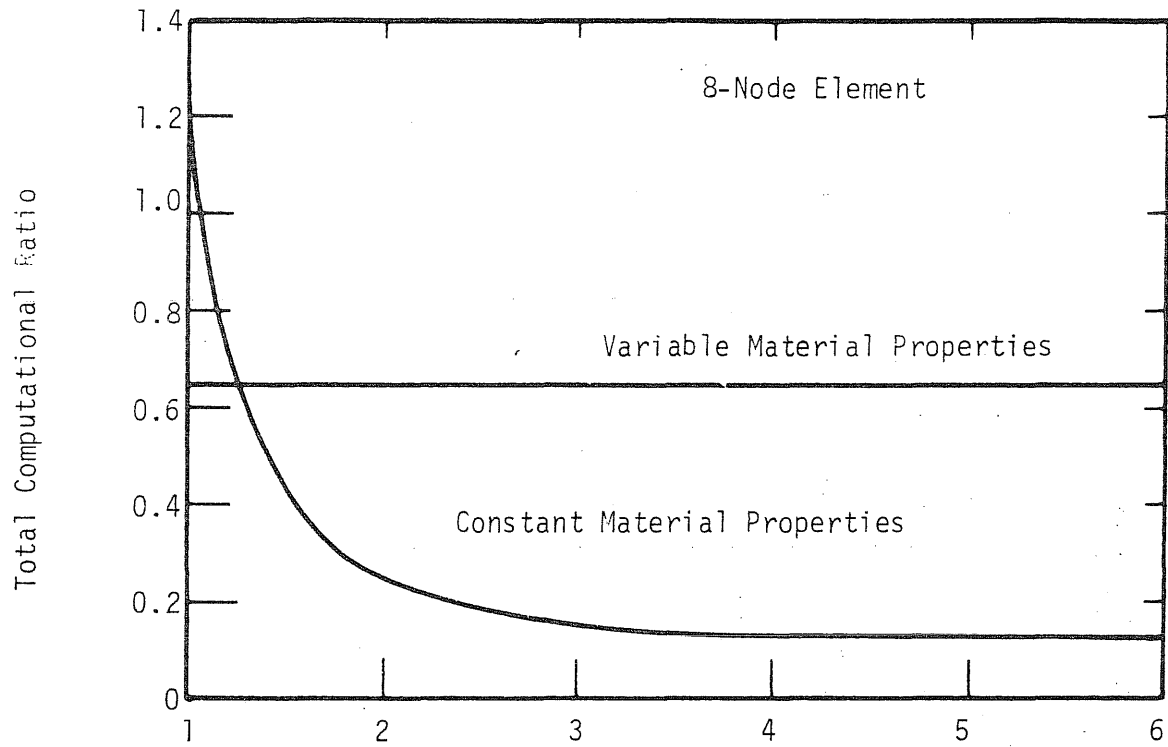| Procedure	8 nodes		32 nodes	
	Addition	Multiplication	Addition	Multiplication
Conventional	189,696	172,800	2,307,072	2,011,392
Proposed Constant $E_{ijk\ell}$	23,652	25,188	346,896	353,040
% Conventional	13	15	15	18
Proposed Variable $E_{ijk\ell}$	124,416	108,864	1,382,400	1,083,456
% Conventional	66	63	60	54

Figure A.1   Relationship Between Computational Ratio and
Order of Gaussian Quadrature Integration

Appendix B

THE ISOPARAMETRIC ELEMENT IN CURVILINEAR COORDINATES

B.1 General

The isoparametric element, as presented in Chapter 2, has been formulated in a cartesian coordinate system. The curved surfaces are idealized by defining intermediate nodes on appropriate edges. Intermediate nodes are also used if a higher order displacement field is desired. If a curvilinear coordinate system which defines the geometry of the structure can be selected, one need not use intermediate nodes for defining the geometry of the structure. For example, for cylindrical type structures, one can avoid intermediate nodes by using a cylindrical coordinate system. Similarly, spherical coordinates may be employed for sphere type structures.

B.2 Stiffness Matrix

In curvilinear coordinates, the strain tensor ε_{ij} is defined as

$$\varepsilon_{ij} = \frac{1}{2}(u_{i|j} + u_{j|i}) \tag{B.1}$$

where $u_{i|j}$ represents the covariant derivative of u_i with respect to x_j. It is implied that x_j represents the curvilinear system of coordinates under consideration. The covariant derivative $u_{i|j}$ is obtained from

$$u_{i|j} = \frac{\partial u_i}{\partial x_j} + R_{ijk} u_k \tag{B.2}$$

in which R_{ijk} denotes the Christoffel symbol of the second kind.[63]

Equations B.1, B.2 and 2.2 yield

$$\varepsilon_{ij} = Z^m_{ijk} u^m_k \tag{B.3}$$

121

where

$$Z^m_{ijk} = \frac{1}{2} (\delta_{ik} \delta_{j\ell} + \delta_{i\ell} \delta_{jk}) \frac{\partial N^m}{\partial x_\ell} + R_{ijk} N^m \qquad (B.4)$$

Using the principle of virtual displacement as in Chapter 2, the element stiffness matrix can be formulated. Thus,

$$k^{mn}_{ij} = \int_V E_{pqrs} Z^m_{pqi} Z^n_{rsj} \, dV \qquad (B.5)$$

B.3 Application to the Cylindrical Coordinate System

It is seen from the preceding section that in curvilinear coordinates the strain tensor is defined differently from that in the cartesian coordinates. The difference between the two is the additional term containing the Christoffel symbol in the geometric array Z^m_{ijk} (see Eqs. B.4 and B.5).

In cylindrical coordinates, Fig. B.1, the elements of the Christoffel symbol can be written as

$$R_{221} = \frac{1}{x_1} \qquad (B.6a)$$

$$R_{122} = R_{212} = -\frac{1}{2x_1} \qquad (B.6b)$$

and all other

$$R_{ijk} \equiv 0 \qquad (B.6c)$$

Once the elements of Christoffel symbol are known, the element stiffness matrix can be evaluated in a manner similar to that explained in Appendix A.

B.4 Numerical Result

An axisymmetric pressure vessel, identical to the one analyzed in Section 4.2.5 is solved in cylindrical coordinates. A similar grid spacing as the one in Section 4.2.5 is used, Fig. 14. Since intermediate nodes in the circumferential direction are not required for conforming to the cylindrical boundaries, they are omitted. The numerical results obtained using the cylindrical coordinates are identical to those obtained, using cartesian coordinates, Figs. 15 - 17.

B.5 Discussion

It may be advantageous to use the isoparametric element in curvilinear coordinates because it would largely eliminate the necessity of introducing intermediate nodes for conforming to the curved boundaries. This will, in turn, decrease the total number of unknown displacements.

There are two factors which may limit the usefulness of employing curvilinear coordinates. It can be shown that, in general, the displacement field in curvilinear coordinates does not satisfy the condition of rigid body motion nor does it provide for constant strain. Therefore, a great deal of care must be taken to use the element only for cases in which the error due to the violation of the above mentioned conditions is negligible or minimized. Another drawback of the curvilinear isoparametric element is that the expression for the element stiffness matrix, Eq. B.5, is relatively complex. This will tend to increase the number of computations in evaluating the stiffness matrix. On the other hand, since the decrease in the number of unknown displacements reduces the computational effort required for solving the equations, it is possible that for certain

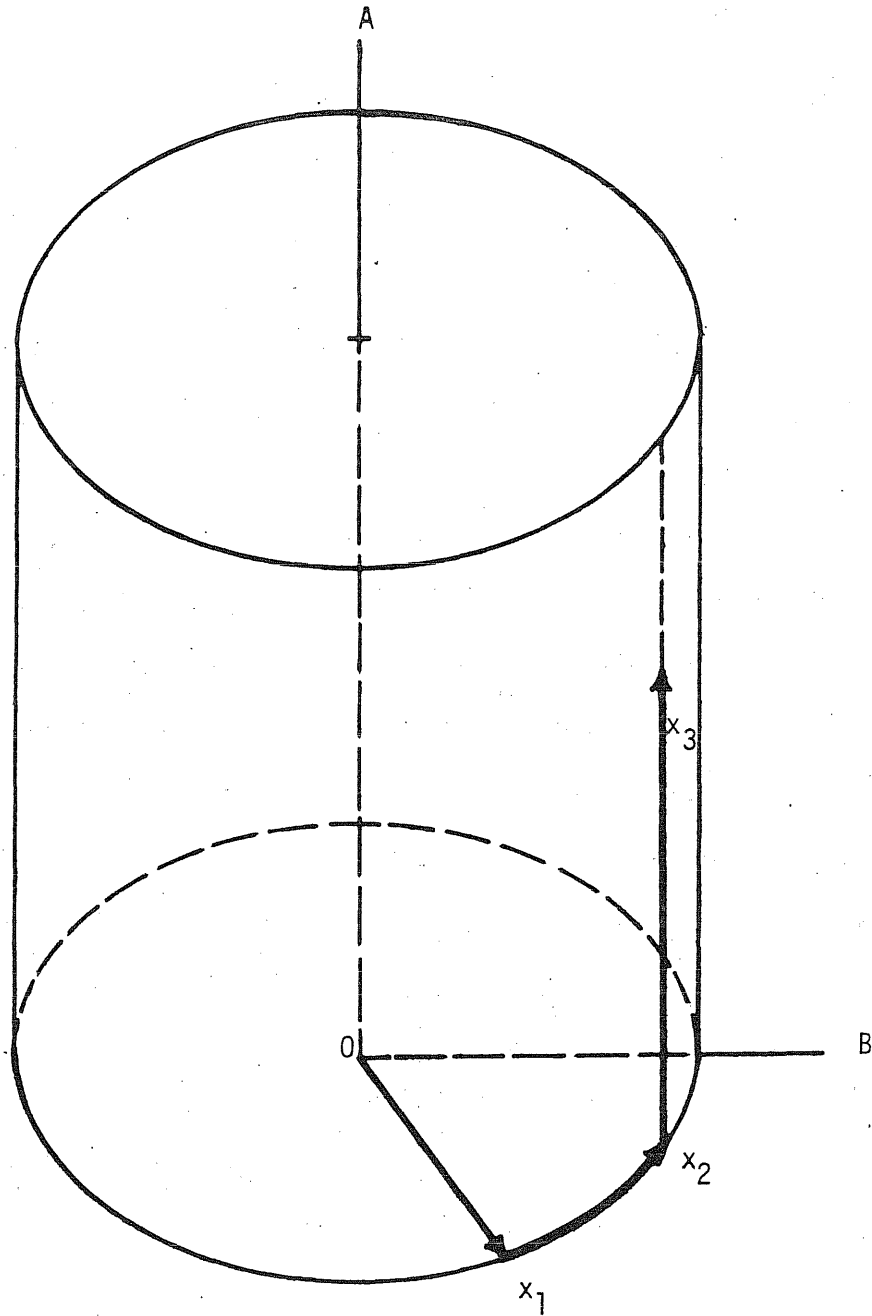problems the use of the curvilinear isoparametric element results in substantial saving in the computer time.

Figure B.1   Cylindrical Coordinates

Appendix C

TRANSCENDENTAL SHAPE FUNCTIONS

C.1 General

In the formulation of the isoparametric element, generally poly-
nomial shape functions have been used. The use of polynomial shape func-
tions assures the existence of the rigid body motion and the state of con-
stant strain in the displacement field, Section 2.3. For higher order
elements, Section 2.5, the displacement field is considered as consisting
of two parts, a linear displacement field as defined by the corner nodes,
and the departure from the linear field on individual edges as defined by
intermediate nodes. In this case, conditions of rigid body motion and
constant strain are satisfed by using polynomial shape functions for the
corner nodes alone, regardless of the variation of the departure from
linearity as defined by the intermediate nodes. This means that one has
freedom in the selection of the shape functions for the intermediate
nodes. Polynomial functions are one possibility and have been already
employed. Another possibility is the use of transcendental shape functions.
This selection is developed in the following section.

C.2 Development of the Transcendental Shape Functions

An individual edge AB of an element, Fig. 4d, with I intermediate
nodes is considered. As in Chapter 2, let ϕ denote a component of coordin-
ates or displacements. The value of ϕ on the edge AB is denoted by ϕ^{AB}.
The variation of ϕ^{AB} along the edge is defined by Eq. 2.16. The term $\Delta^{AB}\phi$
denotes the departure of ϕ^{AB} from the linear variation defined by the cor-
ner nodes A and B. In general, one can write

$$\Delta^{AB}\phi = \gamma^S g^S \qquad\qquad (C.1)$$

where

γ^S = a set of I unknown coefficients, and

g^S = I functions of the isoparametric coordinates along the edge AB, ξ_1 in this case.

The right-hand side of the Eq. C.1 can be looked upon as a truncated series. A polynomial series which resulted in polynomial shape functions was used in Chapter 2. Other series expansions may also be used. A Fourier series expansion, due to its rapid convergence property, is considered here. Again, as in Chapter 2, each of the individual functions g^S should satisfy the constraints imposed upon $\Delta^{AB}\phi$, namely they should vanish at the corner nodes A and B ($\xi_1 = \pm 1$). The sth term of the Fourier series which satisfy this constraint is given by

$$g^S = \sin\frac{s\pi (1 + \xi_1)}{2} \qquad\qquad (C.2)$$

Once the functions g^S have been defined, the steps used in Eqs. 2.26 - 2.31 can be followed in order to obtain the shape functions and the modified nodal values of ϕ.

C.3 Numerical Result

A simple problem has been solved in order to demonstrate the use of transcendental shape functions. A thick hollow circular cylinder (internal and external radii of 10 in. and 20 in., respectively) subjected to a uniform internal pressure is analyzed. Due to symmetry, a pie-shaped segment is considered and is divided into 5 elements with intermediate nodes in the radial and circumferential directions. The distributions of the

radial and circumferential stresses obtained by the present method and those obtained by the theory of elastiticy[55] are given in Fig. C.1. As can be seen, the agreement between the two is excellent.

C.4 Discussion

The application of transcendental shape functions in isoparametric element has been demonstrated. Its relative efficiency as compared to polynomial shape functions is a matter requiring more detailed investigation.

For a two-dimensional rectangular element with one intermediate node on each edge, the traces of the two element stiffness matrices obtained by using the polynomial and transcendental shape functions, respectively, were computed, and are in ratio of 1.273:1.0. This comparison, although limited to two-dimensional rectangular elements, indicates that the transcendental shape functions allow the element to be more flexible.
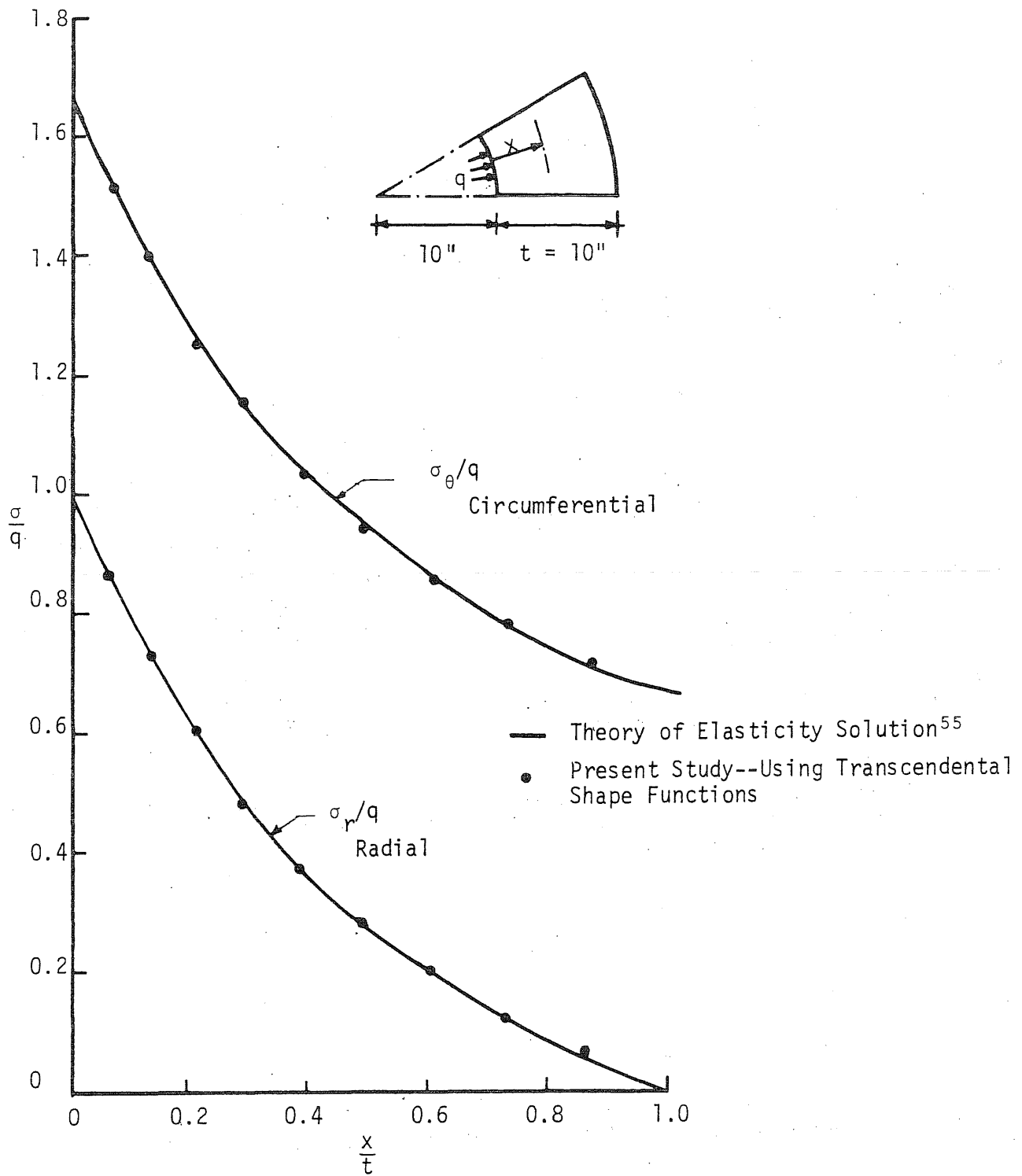
Figure C.1 Distribution of Radial and Circumferential Stresses
in a Thick Hollow Circular Cylinder

LIST OF REFERENCES

1. Hodge, P. G. and White, G. N., "A Quantitative Comparison of Flow and Deformation Theories of Plasticity," J. Appl. Mech., Vol. 17, 1950, pp. 180-184.

2. Koiter, W. T., "On Partially Plastic Thick-Walled Tubes," Biezeno Anniversary Volume in Applied Mechanics, N. V. De Technische Uitgeverij H. Stam, Haarlem, 1953, pp. 232-251.

3. Ilyshin, A. A., "Some Problems in the Theory of Plastic Deformation," RMB-12, Transaltion from Prikl. Math. Mech., Vol. 7, 1943, pp. 245-272, by Grad. Div. Appl. Math., Brown University, 1946.

4. Mendelson, A. and Manson, S. S., "Practical Solution of Plastic Deformation Problems in Elastic-Plastic Range," NASA, Technical Report R-28, 1959.

5. Mendelson, A. and Spero, S. W., "A General Solution for the Elastoplastic Thermal Stresses in a Strain Hardening Plate with Arbitrary Material Properties," J. Appl. Mech., Vol. 29, 1962, pp. 151-158.

6. Davis, E. A., "Extension of Iteration Method for Determining Strain Distribution to the Uniformly Stressed Plate with a Hole," J. Appl. Mech., Vol. 30, 1963, pp. 210-214; Discussions, ibid., Vol. 31, 1964, pp. 362-364.

7. Tuba, I. S., "Elastic-Plastic Stress and Strain Concentration Factors at a Circular Hole in a Uniformly Stressed Infinite Plate," J. Appl. Mech., Vol. 32, 1965, pp. 710-711.

8. Argyris, J. H., Kelsey, S. and Kamel, H., "Matrix Methods of Structural Analysis--A Precis of Recent Developments," Matrix Methods in Structural Analysis--AGARDograph 72, Ed., B. F. de Venbeke, Pergamon Press, Oxford, 1964.

9. Argyris, J. H., "Elasto-Plastic Analysis of Three Dimensional Continua," J. Royal Aero. Soc., Vol. 69, 1965.

10. Swedlow, T. L., Williams, M. L. and Yang, W. M., "Elasto-Plastic Stresses in Cracked Plates," Calcit Report SM 65-19, California Institute of Technology, 1965.

11. Marcal, P. V. and Pilgrim, W. R., "Stiffness Method for Elastic-Plastic Shells of Revolution," J. Strain Analysis, Vol. 1, 1966, p. 399.

12. Ueda, Y. and Matsuishi, M., "Analysis of Elastic Plastic Buckling of Plates by the Finite Element Method," Proc., Japan-U.S. Seminar on Matrix Methods in Structural Analysis and Design, Tokyo, 1969.

13. Popov, E. P., Khojesteh-Bakht, M. and Yaghmai, S., "Analysis of Elastic-Plastic Circular Plates," J. Eng. Mech. Div., ASCE, Vol. 93, 1967.

14. Popov, E. P., Khojasteh-Bakht, M. and Yaghmai, S., "Bending of Circular Plates of Hardening Material," Int. J. Solids Struct., Vol. 3, 1967, pp. 975-988.

15. Khojasteh-Bakht, M., "Analysis of Elastic-Plastic Shells of Revolution Under Axisymmetric Loading," Ph.D. Thesis, University of California, Berkeley, 1967.

16. Zienkiewicz, O. C., Valliappan, S. and King, I. P., "Stress Analysis of Rock as a 'No Tension' Material," Geotechnique, Vol. 18, No. 1, 1968, pp. 56-66.

17. Maier, G., "A Quadratic Programming Approach for Certain Nonlinear Structural Problems," Meccanica, Vol. 3, 1968, p. 121.

18. Maier, G., "Incremental Plastic Analysis in the Presence of Large Displacements and Physical Instabilizing Effects," Int. J. Solids Struct., Vol. 7, 1971, pp. 345-372.

19. Lopez, L. A. and Ang, A. H.-S., "Flexural Analysis of Elastic Plastic Rectangular Plates," Technical Report, Department of Civil Engineering, University of Illinois, Urbana, 1966.

20. Shoeb, N. A. and Schnobrich, W. C., "Analysis of Elastic-Plastic Shell Structures," Civil Engineering Studies, Structural Research Series No. 324, University of Illinois, Urbana, 1967.

21. Galloway, J. C. and Ang, A. H.-S., "A Generalized Lumped Parameter Model for Plane Problems of Solid Media," Civil Engineering Studies, Structural Research Series No. 341, University of Illinois, Urbana, 1968.

22. Mohraz, B., Schnobrich, W. C. and Echeverria Gomez, A., "Crack Development in a Prestressed Concrete Reactor Vessel as Determined by a Lumped Parameter Method," Nuclear Engineering and Design, Vol. 11, 1970, pp. 286-294.

23. Zienkiewicz, O. C. and Cheung, Y. K., "The Finite Element Method for Analysis of Elastic Isotropic and Orthotropic Slabs," Inst. Civ. Eng., Proc., Vol. 28, 1964, pp. 471-488.

24. Argyris, J. H., "The Lumina Element for the Matrix Displacement Method," Aero. J. Royal Aero. Soc., Vol 72, No. 690, 1968, p. 514.

25. Argyris, J. H., Fried, I. and Scharpf, D. W., "The Hermes 8 Element for the Matrix Displacement Method," Aero. J. Royal Aero. Soc., Vol. 72, No. 691, 1968, p. 613.

26. Martin, H. C., "Plane Elasticity Problems and the Direct Stiffness Method," Trend in Engineering, University of Washington, Seattle, Vol. 13, 1961.

27. Gallagher, R. H., Padlog, J. and Bijlaard, P. P., "Stress Analysis of Heated Complex Shapes," J. Am. Rocket Soc., 1962, p. 700.

28. Argyris, J. H., "Three Dimensional Anisotropic and Inhomogeneous Elastic Media, Matrix Analysis for Small and Large Displacements," Proc., 11th Int. Cong. Appl. Mech., Munich, 1964.

29. Argyris, J. H., "Three Dimensional Anisotropic and Inhomogeneous Elastic Media, Matrix Method for Small and Large Displacements," Ing. Archiv., Vol. 34, No. 1, 1965, pp. 35-55.

30. Argyris, J. H., "Matrix Analysis of Three Dimensional Elastic Media, Small and Large Displacements," AIAA Journal, Vol. 3, No. 1, 1965, pp. 45-51.

31. Argyris, J. H., "Continua and Discontinua," Proc., Conf. on Matrix Methods in Struct. Mech., Wright-Patterson AFB, Ohio, 1965.

32. Melosh, R. J., "Structural Analysis of Solids," J. Struct. Div., ASCE, Vol. 89, No. ST-4, 1963, pp. 205-223.

33. Ergatoudis, J., "Isoparametric Finite Element in Two and Three-Dimensional Stress Analysis," Ph.D. Thesis, Univeristy of Wales, 1968.

34. Ergatoudis, J. and Irons, B. M., "Curved, Isoparametric, 'Quadrilateral' Elements for Finite Element Analysis," Int. J. Solids Struct., Vol. 4, 1968.

35. Irons, B. M. and Zienkiewicz, O. C., "The Isoparametric Finite Element System--A New Concept in Finite Element Analysis," Conf. on Recent Advances in Stress Analysis, Aero. J. Royal Aero. Soc., 1968.

36. Zienkiewicz, O. C., Irons, B. M., Ergatoudis, J., Ahmad, S. and Scott, F. C., "Iso-Parametric and Associated Element Families for Two and Three Dimensional Analysis," Finite Element Methods in Stress Analysis, Ed., Ivar Holand and Kolbein Bell, TAPIR, Technical University of Norway, Trondheim, 1969.

37. Clough, R. W., "Comparison of Three Dimensional Finite Elements," Proc., Symp. on Application of Finite Element Methods in Civil Engineering, Nashville, Tennessee, 1969, pp. 1-26.

38. Argyris, J. H. and Scharpf, D. W., "The Curved Tetrahedron and Triangular Elements Tec and Tric for the Matrix Displacement Method," Aero. J. Royal Aero. Soc., Vol. 73, No. 697, 1969.

39. Kopal, Z., Numerical Analysis, John Wiley, 1955.

40. Stroud, A. H. and Secrest, D., Gaussian Quadrature Formulas, Prentice-Hall, 1966.

41. Zienkiewicz, O. C. and Cheung, Y. K., The Finite Element Method in Structural and Continuum Mechanics, McGraw-Hill, 1968.

42. Livesley, R. K., Matrix Methods of Structural Analysis, Pergamon Press/The Macmillan Company, 1964.

43. Brocci, R. A., Personal Communication, University of Illinois, 1969.

44. Irons, B. M., "A Frontal Solution Program for Finite Element Analysis," Int. J. Num. Meth. in Engng., Vol. 2, 1970, pp. 5-33.

45. Faddeeva, V. N., Computational Methods of Linear Algebra, Translated from Russian by Curtis D. Benster, Dover, 1959.

46. MacNeal, R. H., Ed., The NASTRAN Theoretical Manual, NASA, 1970.

47. Drucker, D. C., "Stress Strain Relations in the Plastic Range, A Survey of Theory and Experiments," Office of Naval Research, Contract N7, ONR-358, NR-041-032, 1950.

48. Mendelson, Alexander, Plasticity: Theory and Application, Macmillan/Collier-Macmillan, 1968.

49. Armen, H., Pifko, A. B., Levine, H. C. and Isakson, G., "Plasticity," Chap. 8, Finite Element Technique in Structural Mechanics, Ed., H. Tottenham and C. Brebbia, Southampton University Press, 1970.

50. Drucker, D. C., "Some Implications of Work Hardening and Ideal Plasticity," Quart. Appl. Math., Vol. 7, 1950, pp. 411-418.

51. Argyris, J. H., "Elasto-Plastic Matrix Displacement Analysis of Three Dimensional Continua," Aero J. Royal Aero. Soc., Vol. 69, 1965, pp. 633-635.

52. Pope, G. G., "A Discrete Element Method for Analysis of Plane Elasto-Plastic Strain Problems," R.A.F. Farnborough T. R. 65028, 1965.

53. Marcal, P. V. and King, I. P., "Elastic-Plastic Analysis of Two-Dimensional Stress Systems by the Finite Element Method," Int. J. Mech. Sci., Vol. 9, 1967, pp. 143-155.

54. Zienkiewicz, O. C., Valliappan, S. and King, I. P., "Elasto-Plastic Solutions of Engineering Problems: 'Initial Stress,' Finite Element Approach," Int. J. Num. Meth. Engng., Vol 1, 1969, pp. 75-100.

55. Timoshenko, S. and Goodier, J. N., Theory of Elasticity, McGraw-Hill/ Kogakusha, Second Edition, 1951.

56. Timoshenko, S. and Woinowsky-Krieger, S., Theory of Plates and Shells, McGraw-Hill/Kogakusha, Second Edition, 1959.

57. Salerno, V. L. and Goldberg, M. A., "Effect of Shear Deformations on the Bending of Rectangular Plates," J. Appl. Mech., Vol. 27, No. 1, 1960, pp. 54-58.

58. Ahmad, S., Irons, B. M. and Zienkiewicz, O. C., "Analysis of Thick and Thin Shell Structures by Curved Finite Elements," Int. J. Num. Meth. Engng., Vol. 2, 1970, pp. 419-451.

59. Mohraz, B. and Schnobrich, W. C., "A Lumped Parameter Element for the Analysis of Axisymmetric Solids of Revolution," Nuclear Eng. and Design, Vol. 11, 1970, pp. 333-334.

60. Karlsson, B. I., "Shear Strength of End Slabs with and without Penetrations in Prestressed Concrete Reactor Vessels," Ph.D. Thesis, University of Illinois at Urbana-Champaign, 1971.

61. Zienkiewicz, O. C., Taylor, R. L. and Too, J. M., "Reduced Integration Technique in General Analysis of Plates and Shells," Int. J. Num. Meth. Engng., Vol. 3, 1971, pp. 275-290.

62. Irons, B. M., "Economical Computer Techniques for Numerically Integrated Finite Elements," Int. J. Num. Meth. Engng., Vol. 1, 1969, pp. 201-203.

63. Synge, J. L. and Schild, A., Tensor Calculus, University of Toronto Press, 1949.